United States
Environmental Protection
Agency

Pilot Study on Coarse PM Monitoring

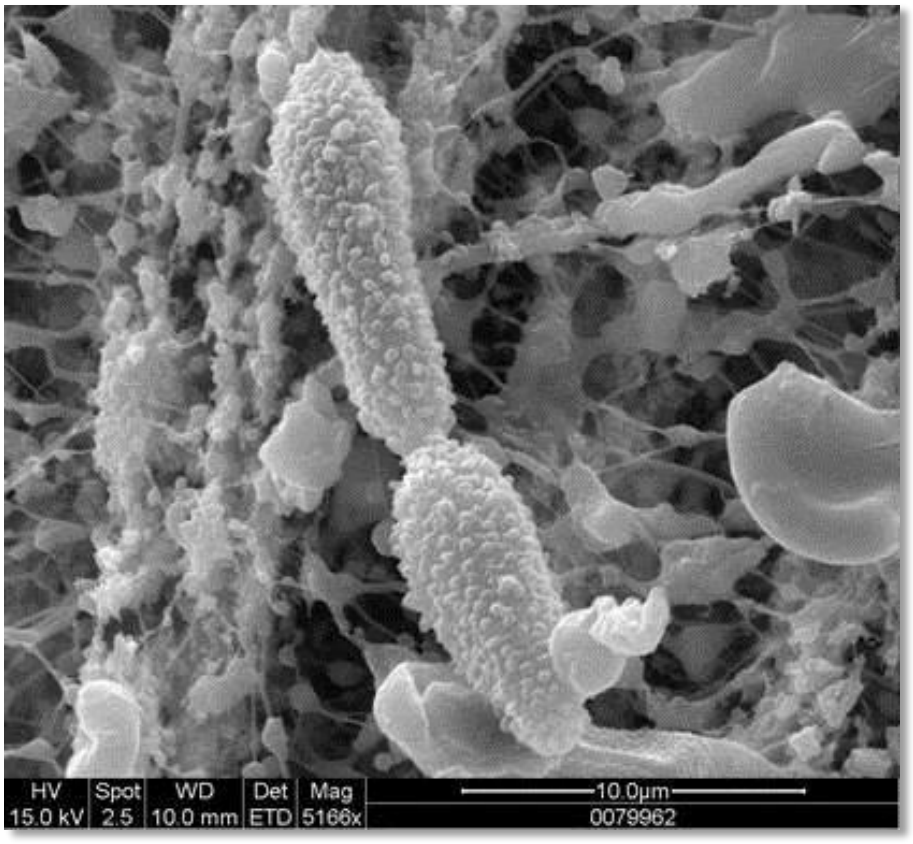

This document contains blank pages to accommodate two-sided printing.

EPA-454/R-15-001
February 2015

Pilot Study on Coarse PM Monitoring

Prepared by:
Jay R. Turner
Department of Energy, Environmental and Chemical Engineering
Washington University at St. Louis
1 Brookings Drive
St. Louis, MO 63130

Steven G. Brown
Hilary A. Minor
Sonoma Technology, Inc.
1455 N. McDowell Blvd., Suite D
Petaluma, CA 94954-6503

Prepared for:
Joann Rice
Office of Air Quality Planning and Standards
Air Quality Assessment Division

Contract No. EP-D-09-097

U.S. Environmental Protection Agency
Office of Air Quality Planning and Standards
Air Quality Assessment Division
Research Triangle Park, NC 27711

Acknowledgments

RTI performed laboratory analyses, overseen by James Flanagan with contributions by Karin Foarde and Frank Weber, and provided logistical support on instrumentation and maintenance, led by Jeff Nichol. Washington University in St. Louis students and field operators conducted the measurements in St. Louis. Maricopa County staff, led by Ben Davis, conducted the measurements in Phoenix. At Washington University, Varun Yadav led the field operations and Li Du led the analysis of St. Louis and Phoenix TEOM data. At Sonoma Technology, Inc., Adam Pasch and Theresa O'Brien assisted in data handling and quality control, Paul Roberts was the Principal Investigator, and Mary Jo Teplitz, Ron Teplitz, and Marina Michaels provided editorial support.

Disclosure: The St. Louis field operations were funded by EPA and were conducted by students and staff of the Jay Turner group at Washington University in St. Louis. Jay Turner was also a consultant to Sonoma Technology, Inc., on this project.

Table of Contents

Section **Page**

Section **Page**

List of Figures

Figure **Page**

Figure **Page**

List of Tables

Table **Page**

Executive Summary: Key Findings and Recommendations

The U.S. Environmental Protection Agency (EPA) conducted this field study in 2010 and 2011 to evaluate the challenges in sampling and analyzing coarse aerosol, the precision of coarse PM (PM_c) mass species measurements using dichotomous (dichot) samplers, and mass balance of PM_c. The study database is publicly available through the EPA Air Quality System (AQS) to EPA personnel, atmospheric scientists, and others concerned with the science of PM air pollution, related health effects, and human exposure to the coarse PM fraction of particulate matter. Additional samplers—including paired PM_{10} and $PM_{2.5}$ Federal Reference Method (FRM) samplers to calculate $PM_{10-2.5}$ mass and species concentrations by the difference method, and semi-continuous monitors—were operated to further characterize coarse PM and aid in the interpretation of any differences between dichot data and difference method data. The results of this study may be used to establish routine field operating procedures and laboratory standard operating procedures (SOPs) for use in PM_c speciation monitoring.

ES-1. Primary Objectives

The primary objectives of the coarse PM pilot speciation study were to:

1. develop the target species analyte list for routine speciation monitoring (what species need to be measured);
2. evaluate and define appropriate analysis methods for routine speciation monitoring and the necessary SOPs;
3. evaluate the field performance of the dichot samplers for routine speciation monitoring (e.g., comparing gravimetric mass and speciation to the FRM by difference data and assessing dichot collocated precision);
4. learn about sampling and operational issues regarding the use of dichots; and
5. evaluate data from the study to inform several issues related to coarse PM speciation measurements.

ES-2. Study Methods

The coarse PM pilot speciation study included one year of 1-in-3 day sampling at sites in Phoenix (Arizona) and East St. Louis (Illinois), from June 2010 through May 2011. At each site, two Thermo 2025D sequential dichot samplers, one Thermo 2025 sequential PM_{10} FRM sampler, one Thermo 2025 sequential $PM_{2.5}$ FRM sampler, and one Thermo 1405-DF Filter Dynamics Measurement Systems (FDMS) dichotomous Tapered Element Oscillating Microbalance (TEOM) monitor were used to make routine measurements. Samples were collected for laboratory analysis using Teflon®/nylon (T/N) and quartz/quartz (Q/Q) filter sandwiches.

Analytical methods adopted from the $PM_{2.5}$ Chemical Speciation Network (CSN) were used to characterize fine and coarse particle speciation for about half of the sampling events. The rest were archived for further study if needed. The analytical methods included gravimetric mass, elements by x-ray fluorescence (XRF), ions by ion chromatography (IC) from the Teflon

filter, and organic carbon (OC) and elemental carbon (EC) by thermal-optical analysis (TOA) from the quartz filter. Subsets of samples were analyzed for elements by inductively coupled plasma mass spectrometry (ICP-MS) and were analyzed for carbonate by TOA with sample acidification. Dichot PM_c and PM_{fine} (PM_f) concentrations were adjusted to correct for 10% PM_f intrusion into the PM_c channel; results in this report incorporate this correction. Coarse PM was thus measured directly both via the dichot (PM_c) and via the difference between FRM PM_{10} and $PM_{2.5}$ measurements (i.e., $PM_{10-2.5}$).

ES-3. Key Findings

The key study findings were as follows.

Sample completeness. The sample collection completeness objective of 80% was met for three of the four 2025D sequential dichot samplers. Sample collection completeness exceeded 90% for the two sequential dichot samplers at Phoenix and was 66% and 87% for the two sequential dichot samplers in St. Louis. Valid samples were collected from both sequential samplers on 92% of days at Phoenix, but only 52% of days in St. Louis. A major hardware failure required one St. Louis dichot sampler to be returned to the manufacturer, leading to low data completeness at that site. The most common field operations issues were filter exchange errors and pump failures in the sequential samplers.

Dichot versus FRM by difference. PM_c constituents measured on the Teflon filters (gravimetric mass, elements, and ions) were biased low for the dichot method compared to the FRM by difference method. In Phoenix, PM_c mass from the dichot was, on average, about 20% lower than the FRM difference method mass (dichot-on-FRM slope = 0.67-0.71, intercept = 2.2-2.7 $\mu g/m^3$ depending on the dichot sampler); in St. Louis, the dichot PM_c mass was 10% to 25% lower (dichot-on-FRM slope = 0.83-0.96, intercept statistically indistinguishable from zero [95% confidence level], depending on the dichot sampler). In contrast, PM_c total carbon and carbonate measured on the quartz filters showed no bias between the two methods, though the relationship for total carbon exhibited more scatter. The bias for constituents measured on the Teflon filters is attributed to particle losses from the dichot minor flow channel Teflon filter, which contains all of the coarse particles and 10% of the fine particles. Losses may occur during the automated filter exchange in the sequential dichot sampler, during handling, during shipping to the analytical laboratory, or during any combination of these events. Coarse particles collected on quartz filters are much less prone to losses because the particles are more deeply embedded into the filter matrix. Dichot Federal Equivalent Method (FEM) samplers with a modified shuttle mechanism and firmware to minimize particle loss due to filter exchange are now available, but were not available from the manufacturer for this study. After the dichots were modified to be FEM compliant, a follow-up study conducted at Research Triangle Park (North Carolina) by RTI and EPA resulted in better agreement between the dichot PM_c gravimetric mass and the FRM by difference ($PM_{10-2.5}$) gravimetric mass, with a dichot-on-FRM regression slope of 1.05 and an intercept statistically indistinguishable from zero (95% confidence level). Biases between the dichot method and the FRM by difference method prevented an evaluation of the potential measurement bias from mixing of PM_c and PM_f species components on the PM_{10} filter.

Dichot precision. Dichot collocated precision for PM_c gravimetric mass and major soil constituents (aluminum [Al], calcium [Ca], iron [Fe], silicon [Si], and titanium [Ti]) was in the 8% to 15% range. In contrast, the collocated precision of organic carbon, which was about 15% of the mass at both sites, was 19% in Phoenix and 34% in St. Louis. The OC data in St. Louis are less precise in part from having lower concentrations. Dichot collocated precision for PM_f gravimetric mass was 10% in Phoenix—consistent with the precision for PM_f major crustal species—and 2% in St. Louis.

Acid gas denuders. Ambient nitric acid can adsorb onto filters and cause a positive artifact for PM nitrate measurements. Sampling conducted in the summertime with collocated samplers, with and without acid gas denuders, showed insignificant differences in PM_f and PM_c nitrate. It appears the sampler inlets can efficiently remove nitric acid and suppress a nitrate measurement bias.

Organic Carbon. OC mass loadings on the dichot PM_c channel backup filters were statistically indistinguishable from the trip blanks and field blanks OC mass loadings. This is consistent with very little volatile OC in the PM_c size fraction.

Carbonate fraction. Carbonate (CO_3) was measured from the dichot PM_c quartz filters on 69 selected sampling events (43 in Phoenix, 26 in St. Louis). Carbonate was also measured on the dichot PMf quartz filter for 15 of these sampling events. PM_f carbonate was below the 3-sigma minimum detection limit (MDL) of 0.52 $\mu gC/m^3$ for all samples. However, PM_c carbonate was consistently detected with mean concentrations of approximately 1.2 $\mu g/m^3$ and 75^{th} percentile concentrations of approximately 1.6 $\mu g/m^3$ in both Phoenix and St. Louis. The mean carbonate concentrations correspond to 6% and 12% of the PM_c mass in Phoenix and St. Louis, respectively. PM_c carbonate was highly correlated with PM_c calcium at both sites. Assuming all carbonate is present as calcium carbonate, about half of the PM_c calcium in Phoenix and two-thirds of the PM_c calcium in St. Louis can be explained as being calcium carbonate.

Biomarker concentrations. Biomarkers (proteins, (1,3)-β-D-glucans, and endotoxin) were measured from Teflon filters in the dichot coarse particle channel for 54 sampling events (28 in Phoenix and 26 in St. Louis). These samples were collected from February through May 2011. In both Phoenix and St. Louis, median PM_c glucan concentration was approximately 0.2 ng/m^3, and protein concentration was about 0.08 $\mu g/m^3$. However, relatively high blank corrections caused large uncertainties in the proteins data. PM_c endotoxin concentrations were suspect in Phoenix because of dramatic differences in concentrations between analysis batches, although the batches correspond to adjacent but not overlapping time periods. Median endotoxin concentration was 0.07 EU/m^3 St. Louis.

Mass closure via dichot. Closure between the gravimetric mass and sum-of-species mass was evaluated for the dichot Teflon filters. The analysis ignored OC artifacts and assumed that EC and OC loadings on the quartz filters were representative of EC and OC loadings on the Teflon filters (it is possible that carbonaceous particulate matter is also lost from the dichot PM_c channel filters as reported above for mass, elements, and ions). The analysis also assumed that the equation commonly used to estimate PM_f crustal mass concentration from the major crustal elements (Al, Ca, Fe, Si, and Ti) is valid for estimating PM_c crustal mass concentrations.

Assuming an organic-matter-(OM)-to-OC ratio of 1.6, both PM_f and PM_c mass concentrations reconstructed from the speciation data at Phoenix were, on average, about 13% higher than the gravimetric mass. For the St. Louis data, the reconstructed mass was 6% lower for PM_f and 1% higher for PM_c compared to the gravimetric mass. Additional analyses were performed using the OM/OC ratio as an adjustable parameter to obtain best-fit mass balance closure. For PM_f, the best-fit OM/OC ratios were about 1.2 in Phoenix and 1.8 in St. Louis; these ratios are consistent with estimates reported in the literature, e.g., Simon et al. (2011). For PM_c, the best-fit OM/OC ratio for St. Louis was about 1.5, but subject to large uncertainty; for Phoenix, the ratio was 0.6, which is physically unrealistic (the ratio cannot be less than unity). This finding that the PM_c reconstructed mass is biased high, especially in Phoenix, suggests systematic errors in the estimation methodology, such as improper multipliers for estimating crustal PM_c from elemental concentrations, or corrections for X-ray attenuation during XRF analysis of light elements (e.g., Al, Si, Ca) that are too large. Two additional confounders are the assumption that EC and OC are not lost from the Teflon filter (accounting for such losses may improve mass closure, though it may lead to an overestimate of mass collected on the Teflon filter), and the exclusion of carbonate from the reconstructed mass calculation (accounting for carbonate would increase the reconstructed mass concentrations and thus lead to even larger overestimation of the gravimetric mass).

XRF measurements. Corrections for X-ray attenuation during XRF analysis (self-attenuation) were evaluated by analyzing Teflon filters from 18 sampling events (10 in Phoenix, 8 in St. Louis) using both XRF and ICP-MS. Dichot PM_f and PM_c channel filters were analyzed for all 18 events, and PM_{10} and $PM_{2.5}$ FRM filters were analyzed for 10 of the events. For light elements associated with crustal material (Al, Ca), the coarse particle concentrations by blank-corrected ICP-MS were greater than the concentrations by XRF. This pattern does suggest that the corrections for self-attenuation for these constituents are too large. However, quantitative comparisons were confounded by large ICP-MS blank values for elements such as Al and Ca, which are present in the membrane filter support ring, the adhesive, and the ink used to stamp the filter ID number. Smaller corrections for self-attenuation will yield lower PM_c concentrations for these elements and a lower estimate for the crustal PM_c mass concentration.

Dichot FDMS TEOM measurements. Hourly $PM_{2.5}$ and $PM_{10-2.5}$ concentrations from the Thermo 1405-DF FDMS TEOM instruments revealed appreciable volatile $PM_{2.5}$ mass, but volatile $PM_{10-2.5}$ mass was too small to be reliably distinguished from measurement error. This is consistent with expectations that ammonium nitrate and particle-phase semivolatile organic compounds tend to be in the fine size fraction.

ES-4. Recommendations

The recommendations presented here are based on experiences from the one-year pilot study with sampling in Phoenix and St. Louis. There are limitations when basing recommendations on the operations and data for only two sites, and care should be taken to adapt the recommendations as appropriate for other environmental settings.

Sequential dichot sampling is an attractive approach to particle collection for PM_c measurement. The dichot sampler segregates fine and coarse particles onto separate filters,

thus minimizing the potential for measurement artifacts from the mixing of these particles. With sequential sampling, the instrument can be programmed for multiple sampling events, reducing the manpower burden for field operations. Care must be taken to maintain the setpoint fine and coarse channel flowrates to achieve the design $PM_{2.5}$ cutpoint and to appropriately correct the coarse channel data for fine particle intrusion.

On the basis of this study, paired dichotomous samplers are recommended, with one sampler collecting particles onto Teflon filters and the other sampler collecting particles onto Q/Q filters (see note below). If high concentrations of coarse particle nitrate are expected, e.g., at sites where atmospheric processes have converted sea salt into sodium nitrate, a T/N filter and Q/Q filter combination should also be used during the first year of operations, with analysis of ions on the T and N filters to assess coarse particle nitrate concentrations. In environments similar to St. Louis or Phoenix, a denuder does not appear to be necessary; in environments where there may be significant nitric acid that could absorb onto the Teflon filter and be quantified as aerosol nitrate, it may be useful to conduct a series of test days to determine whether a denuder is needed as part of routine sampling. Specific recommendations and caveats regarding field operations and chemical analyses are discussed below.

Post pilot study note: since the completion of this pilot study, EPA has determined that backup quartz filters are not necessary for OC artifact correction; therefore, the recommendation for a paired dichot with Q/Q filters is revised to recommend a paired dichot with a Q filter only.

Sampling and Field Operations

At both sites, dichot PM_c constituents measured on Teflon filters (gravimetric mass, XRF elements, and ions) were biased low compared to $PM_{10-2.5}$ data collected under the FRM by difference method. In contrast, such bias was not observed for PM_c constituents measured on quartz filters in the dichot PM_c channel (carbon). It is likely that coarse particles become dislodged from the dichot PM_c channel Teflon filter during the automated filter exchange, but it is also possible that the particles are dislodged during shipping from the field sites to the analytical laboratory or during filter handling. Although a shipping protocol recommended by the EPA's Office of Research and Development (ORD) was used to minimize particle loss, this study did not conclusively determine which mechanism was responsible (filter exchange or shipping) for particle loss.

Hardware failures were more frequent than anticipated, especially in St. Louis, with the most common problem being errors during the automated filter exchanges and pump failures, together accounting for 8% of dichot sampling events being invalid. Although the Thermo 2025D sequential dichotomous sampler has since been designated a FEM for PM_c, the 2025D samplers used for this study were not FEM-compliant. The aforementioned issues with particle losses and field robustness of the sampler may be specific to the non-FEM version of the 2025D, and users should ensure they are using FEM-compliant samplers. Given that a complete speciation sample requires valid data be collected by two independently operating samplers, it may be necessary to maintain an inventory of backup hardware to minimize sampler downtimes.

Low-volume (16.7 liter per minute [LPM]) dichot samplers were used in this study. Detectability and precision were deemed adequate for the constituents of primary interest.

Standard operating procedures (SOPs) for the analytical methods used were included in the pilot study's Quality Assurance Project Plan (QAPP). These SOPs are appropriate for use in PM_c speciation measurement except for the analysis of elements by XRF (where attenuation correction factors would need to be revised) and ICP-MS (where a stronger digestion method is required for the crustal species).

Sample Analyses

Based on experiences in Phoenix and St. Louis, the following baseline measurements are recommended for PM_c speciation.

1. *Gravimetric mass concentrations* using Teflon filters and following the $PM_{2.5}$ CSN method. Analysis must be performed on both the PM_f and PM_c channel filters. This study used the filter handling and shipping protocols developed by the EPA's ORD and are presumed to be adequate for mass and chemical speciation. However, these protocols should be verified by conducting a specific study to assess potential filter handling and shipping effects on PM_c once a routine network is operational.
2. *Elemental mass concentrations* by XRF using Teflon filters and following the $PM_{2.5}$ CSN method. Analysis must be performed on both the PM_f and PM_c channel filters. At both sites, coarse PM mass was dominated by crustal material, so it is important to quantify the major crustal constituents. However, the corrections for self-attenuation applied to XRF results for light elements such as Al, Ca, and Si in PM_c appear to be too high. Examination of PM_c mass balance closure and comparisons of PM_c constituents measured by XRF and ICP-MS suggest that the corrections for self-attenuation are necessary, but that the current corrections overestimate the actual concentrations. Additional work is needed to establish corrections for use with PM_c data. The best-fit corrections determined in this study are subject to confounders that may bias the estimates. Numerous factors that influence the corrections, such as the particle size distribution, should be taken into consideration to generate robust corrections. The comparison should be made using a larger data set, with samples collected at sites that have high crustal loadings, and ideally including coarse PM from different sources, such as desert dust and agricultural dust.
3. *Elemental and organic carbon concentrations* by TOA using quartz filters and following the $PM_{2.5}$ CSN method with the Interagency Monitoring of Protected Visual Environments (IMPROVE) analysis protocol IMPROVE_A. Both the PM_f and PM_c channel filters must be analyzed. The IMPROVE_A protocol is recommended because it would be consistent with the $PM_{2.5}$ CSN network. Also, the maximum temperature during analysis by the IMPROVE_A protocol is below the decomposition temperature for calcium carbonate. However, carbonate might decompose at lower temperatures because of matrix interactions among particle constituents, and more work should be done to evaluate whether carbonate, which was observed in PM_c at both sites, interferes with the measurement of EC and OC.

4. *Carbonate mass concentration* by TOA with acidification and using quartz filters. Carbonate was measured for a subset of the collected samples. PM_f carbonate concentrations were all below the 3-sigma minimum detection limit and did not contribute to PM_f mass. However, PM_c carbonate concentrations were, on average, about 6% of the PM_c gravimetric mass at Phoenix and 12% of the PM_c gravimetric mass at St. Louis. PM_f carbonate is expected to be low at virtually all sites; therefore, the measurement should be performed on the PM_c channel filter only, because the correction for fine particle carbonate will be negligible. While carbonate concentrations were similar at Phoenix and St. Louis despite the dramatically different environments, it is possible that PM_c carbonate might be negligible at some sites and could be dropped from the analysis plan for such sites after a period of sampling that demonstrates persistently low carbonate concentrations.

In addition to the above baseline measurements, the following analyses are recommended depending on site-specific conditions.

1. *Anion species mass concentrations* by water extraction and IC using Teflon and nylon filters and following the $PM_{2.5}$ CSN analysis method. PM_c sulfate and nitrate concentrations were persistently low at both Phoenix and St. Louis. XRF measurement of total sulfur (S) includes sulfate, and for PM_c speciation it is likely unnecessary to discriminate the sulfate contribution to total sulfur. In contrast to Phoenix and St. Louis, some locations—particularly sites near coastlines—may have significant concentrations of PM_c nitrate, which should be measured on the Teflon filter. PM_c nitrate is expected to be nonvolatile, and in the absence of fine particle ammonium nitrate, it is possible to analyze only the Teflon filter. However, in some locations with PM_c nitrate, there may be considerable fine particle ammonium nitrate—in such cases, it will be necessary to also measure nitrate on a nylon filter placed immediately downstream of the PM_f Teflon filter to properly correct the PM_c data for fine particle intrusion in the dichot PM_c channel. In locations where there is abundant nitric acid, a denuder may also be necessary to ensure that nitric acid is not quantified as aerosol nitrate. As part of a site-specific assessment of the abundance of coarse particle nitrate, collocated samplers with and without a denuder should be run for a limited period to assess the need for a denuder as part of the site's routine operations.
2. *Cation species mass concentrations* by water extraction and IC using Teflon filters and following the $PM_{2.5}$ CSN analysis method. PM_c ammonium concentrations were very low in Phoenix and St. Louis and are expected to be low at most locations. PM_c sodium concentrations were higher than PM_f sodium concentrations and were present predominantly as the monovalent cation (Na^+). PM_c potassium concentrations were similar to PM_f potassium concentrations, and were present predominantly in forms other than the monovalent cation (K^+). The limited utility from measuring PM_c ammonium, ionic sodium, and ionic potassium does not justify the additional cost for routine operations at most sites.

The following analyses may be considered for special cases, but are not warranted as routine measurements for PM_c speciation.

- Scanning electron microscopy (SEM) can provide substantial insights into particle sources by classifying particle shape and/or composition. However, Teflon and quartz filters cannot be used for quantitative analysis by SEM. An additional sampler would be needed to collect particles onto a suitable substrate, such as polycarbonate membrane filters. The extra sampling requirement and analytical costs relegate SEM to special studies rather than routine measurements.
- Biological material—both intact and fragmented—can be a significant contributor to PM_c. Biomarker concentrations for glucans (an indicator for spores) and proteins can provide insights into spatial and temporal patterns, but to be most valuable to PM_c speciation, multipliers are needed to convert the biomarker concentrations to mass concentrations of the corresponding biologic material (i.e., mass biologic material per mass of biomarker). This issue and the extra analytical costs relegate biomarkers to special studies rather than routine measurements.
- For many elements, ICP-MS provides better sensitivity than XRF. However, this study demonstrates that detectability and precision using XRF are adequate for the primary elements of interest. ICP-MS may be attractive for special cases where higher-quality trace elements data are desired or to confirm that appropriate corrections for self-attenuation are being used for XRF analysis. EPA's current $PM_{2.5}$ ICP-MS SOP would need to be optimized for the specific elements targeted for ICP-MS analysis of PM_c elements. For example, the ICP-MS analyses conducted for this project required the use of microwave and mixed acid (nitric, hydrochloric, and hydrofluoric) digestion process because crustal elements were the primary target of the analysis.

1. Introduction

In 1997, the U.S. Environmental Protection Agency (EPA) promulgated revisions to the National Ambient Air Quality Standards (NAAQS) for particulate matter (PM) and added a standard for fine particulate matter ($PM_{2.5}$). In 2006, the EPA issued a final monitoring rule for thoracic coarse particles. Coarse particles have aerodynamic diameters between 2.5 µm and 10 µm; here coarse PM is referred to as PM_c, if measured from dichot samplers, or termed $PM_{10\text{-}2.5}$ if from FRM by difference method. The promulgated monitoring requirements specified the placement of coarse PM speciation samplers at National Core (NCore) monitoring sites. In 2013, the requirement for coarse PM speciation at NCore was revoked because of technical issues related to the development of appropriate monitoring methods. Sample collection procedures and analysis methods for coarse PM speciation measurements were explored as part of the small-scale pilot monitoring study presented here.

In 2009, the Clean Air Scientific Advisory Committee (CASAC) Ambient Air Monitoring and Methods (AAMM) Subcommittee provided input on sampling and analysis issues for coarse PM speciation. For coarse PM speciation, the CASAC AAMM strongly recommended the use of dichotomous samplers (dichots), where coarse particles are directly sampled, rather than Federal Reference Method (FRM) samplers, where coarse PM is derived from a difference of PM_{10} and $PM_{2.5}$ measurements, i.e., $PM_{10\text{-}2.5}$.

To address concerns of the EPA and CASAC AAMM, a small-scale pilot monitoring study was deployed, the results of which are presented in this report. This pilot study is important from several perspectives.

One reason why this study is important is the need to assess whether chemical and physical characterization of coarse PM differ when the values are determined using the PM_{10} minus $PM_{2.5}$ method (termed $PM_{10\text{-}2.5}$ in this report) as compared with characterization of the PM_c fraction derived from the dichotomous sampler. Dichots directly sample the coarse particles, with 10% of the fine particles drawn through the inlet also present in the sample stream. There was concern that "mixing" of the PM_c fraction with the $PM_{2.5}$ fraction on a filter from the PM_{10} sampler (in the difference method) could lead to changes in aerosol composition that are different from the changes that occur on the coarse particle filter in the dichot (which contains only 10% of the $PM_{2.5}$ mass).

A second important reason for conducting the pilot study was to assess the robustness of commercial samplers and the training and skills required of the field operator and supporting laboratory to produce quality data with a high percentage of data capture.

A third reason for the pilot study was to compile a database of coarse PM chemical and physical information, supplemented by information from measurements not normally made in the $PM_{2.5}$ Chemical Speciation Network (CSN) (e.g., protein content, metals determination by inductively coupled plasma mass spectrometry [ICP-MS], organics speciation by gas chromatography–mass spectrometry [GC-MS]) and by information derived from collocated instruments, including a dichotomous tapered element oscillating microbalance (TEOM) monitor for hourly $PM_{10\text{-}2.5}$ and $PM_{2.5}$ volatile and nonvolatile mass measurements.

1.1 Study Objectives

The primary pilot study objectives were to develop the target species analyte list for routine speciation monitoring (what species need to be measured); evaluate and define analysis methods and the necessary SOPs; evaluate the appropriateness of using a dichot sampler; learn about sampling and operational issues regarding the use of dichots; and evaluate data from the study to inform other issues (e.g., closure between gravimetric mass and sum-of-species mass). The coarse PM measurement system includes media preparation, media shipping, sample handling, routine sampling operations, and laboratory analyses. A list of species and appropriate measurements needed to reasonably characterize PM_c using the low-volume dichot measurement system is recommended.

The main objectives of the study were as follows:

- **Objective 1: Develop the target species analyte list for routine speciation monitoring.** This objective was addressed by starting with the speciate analyte list for the $PM_{2.5}$ Chemical Speciation Network and supplementing with additional measurements such as PM_c carbonate.
- **Objective 2: Evaluate and define analysis methods for routine speciation monitoring and the necessary SOPs.** Again, the $PM_{2.5}$ Chemical Speciation Network was used as a starting point with supplemental measurements added to evaluate the conventional methods.
- **Objective 3: Evaluate the field performance of the dichot samplers for routine speciation monitoring.** To meet project objectives, the PM_c dichot and associated comparison samplers and monitors were operated for one year to provide sufficient comparison data over a range of atmospheric and seasonal conditions. This information was needed for the major components of the PM_c aerosol, including elements, ions, and carbon. The needed information was obtained from collocated measurements, trip blanks, and field blanks. Primary and collocated dichot samplers were used to collect eight collocated samples of each substrate type per sampling season (with three sampling seasons per year). In order to accomplish this objective, both dichots were run with a Teflon/nylon filter pair for eight events per season, and with quartz filters for eight events per season. Both trip and field blank filters were collected, and four times each season, field blanks were collected that mimicked a sampling event (but with no air pulled through the sampler).
- **Objective 4: Learn about sampling and operational issues regarding the use of dichots.** Again, the PM_c dichot and associated comparison samplers and monitors were operated for one year to provide information on sampling and operational issues.
- **Objective 5: Evaluate data from the study to inform several issues related to coarse PM speciation measurements.** Data analyses were conducted to inform sampling measurement performance including precision, comparability, and representativeness. Mass balance closure was examined to identify potential issues in the speciation measurements.

1.2 Study Design

For this pilot study, two monitoring sites were chosen representing different environmental concentrations and aerosol mixes to operate for nominally one year (May 2010 to May 2011). The pilot study included sites in Phoenix, Arizona (abbreviated as PHX in tables and figures), and East St. Louis, Illinois (abbreviated as STL in tables and figures).

At both sites coarse PM was likely to be dominated by crustal elements, but as Phoenix is in the arid Southwest, concentrations were likely to be higher there. Primarily, two methods were used to collect coarse PM samples for analysis:

- dichotomous samplers to directly measure PM_{fine} (PM_f) and PM_c, and
- paired PM_{10} and $PM_{2.5}$ FRM samplers to determine $PM_{10-2.5}$ (difference method).

All samples were collected for 24 hours from midnight to midnight local time. Laboratory analysis methods consistent with $PM_{2.5}$ CSN processes (i.e., gravimetric mass, ions by ion chromatography [IC], elements by XRF, carbon by thermal-optical analysis) were used to analyze about 50% of the filter samples. The remaining samples were archived for future analyses.

Sampling commenced in May 2010, with four weeks of nearly daily sampling to refine the field operations and provide a data set for preliminary evaluation of certain sampling configurations (e.g., whether the presence of a denuder affected the PM_c mass measurements). Sampling was conducted on a one-in-three day schedule from June 1, 2010, through May 31, 2011, using various sampling configurations to address the technical objectives of the project. For details, see the $PM_{10-2.5}$ Speciation Pilot Monitoring Quality Assurance Project Plan (abbreviated as QAPP and approved in 2010). Additional sampling was conducted periodically during the study to provide samples for biological content analyses. Under contract EP-D-08-047, RTI International personnel and subcontractors who regularly serve the EPA/Office of Air Quality Planning and Standards (OAQPS) $PM_{2.5}$ CSN provided support for integrated sampler installation and operation, necessary training, initial equipment audits and flow checks. Filter preparation and laboratory sample processing and analyses were provided under contract EP-D-09-010. Under EPA contract EP-D-09-097, Sonoma Technology, Inc. (STI) personnel and Dr. Jay Turner (Washington University, St. Louis) analyzed the data.

The Phoenix site (**Figure 1-1**) is at 43rd Avenue and Broadway Road in Phoenix, Arizona (AQS ID 04-013-4009). The Maricopa County Air Quality Department in Phoenix managed the day-to-day operations.

The East St. Louis, Illinois, coarse PM speciation pilot site (**Figure 1-2**) is the PM Supersite location used previously for PM research (AQS ID 17-163-9010). The St. Louis-Midwest Supersite is located at 13th Street and Tudor Avenue in East St. Louis, Illinois, which is about 3 km east of the City of St. Louis, Missouri, central business district. The Air Quality Laboratory at Washington University in St. Louis managed the day-to-day operations. The physical footprint managed by Washington University is immediately adjacent to the East St. Louis compliance monitoring site operated by the Illinois EPA (AQS ID 17-163-0010).

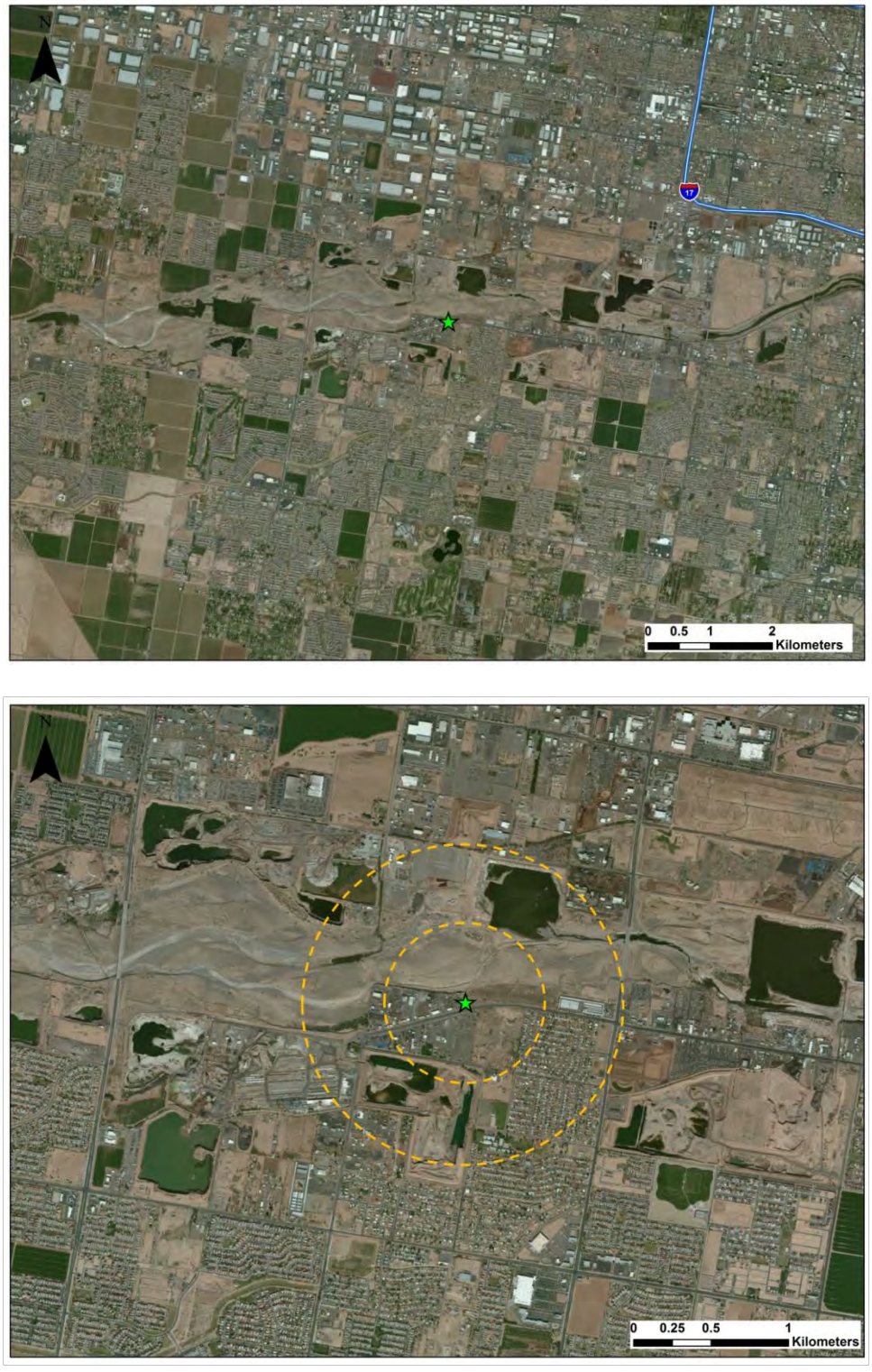

Figure 1-1. Site maps for W 43rd Ave, Phoenix monitoring site. Concentric circles in the bottom map are 500 m and 1,000 m radii from the site.

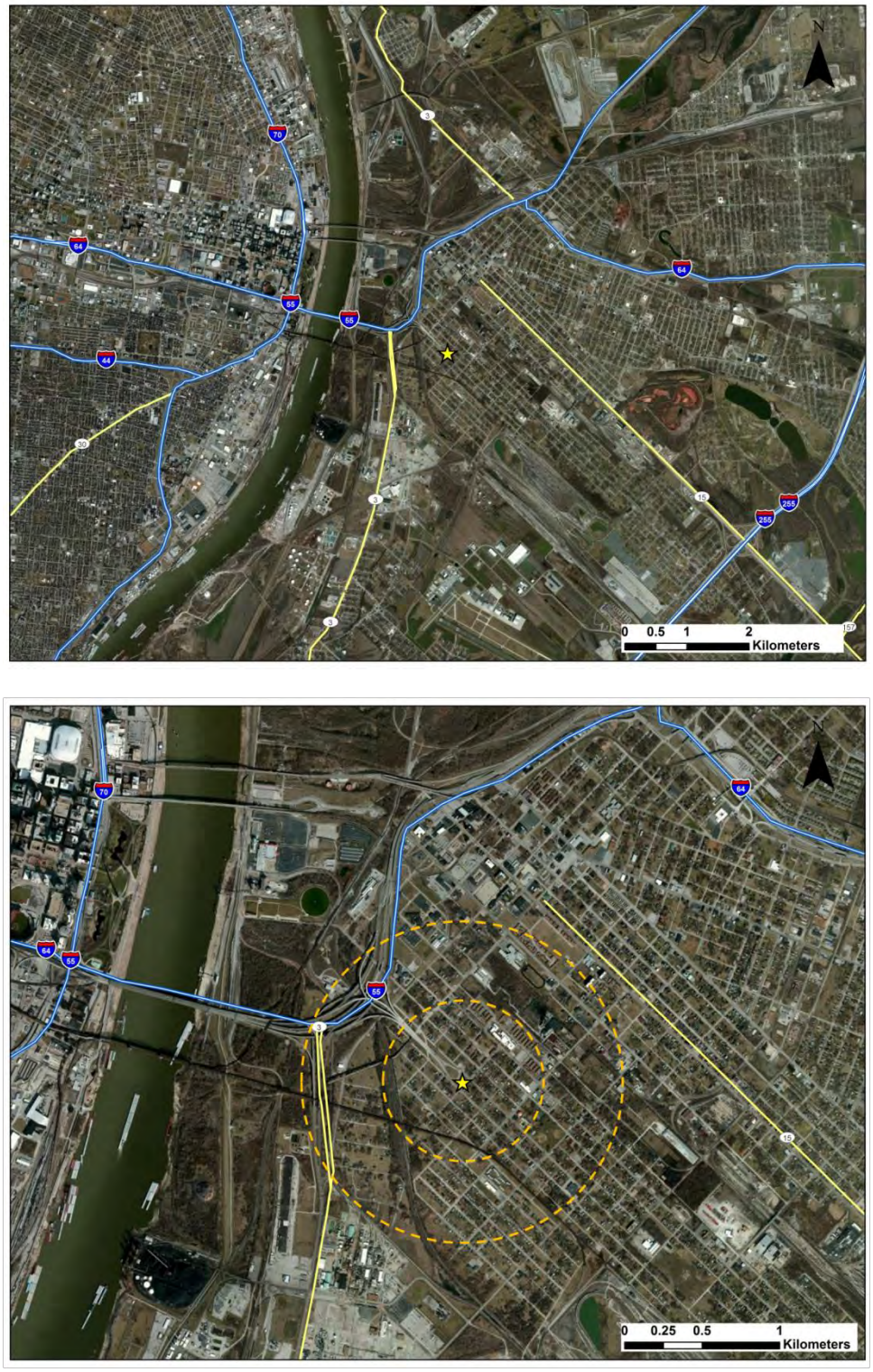

Figure 1-2. Site maps for 13th and Tudor, East St. Louis monitoring site. Concentric circles in the bottom map are 500 m and 1,000 m radii from the site.

1.3 Technical Approach

Each dichot had two channels, one for coarse PM and one for fine PM. To collect data for the calculation of mass balance, at a minimum, a Teflon filter (for ions and elements) and a quartz fiber filter (for carbon) had to be collected for each size fraction; this means data from two collocated dichots were needed to achieve mass balance on any given day. To understand collocated dichot precision, two dichots were run with the same filter media, i.e., either Teflon or quartz fiber. In addition, the sampling schedule was harmonious with the field work already occurring on site, which was typically one-in-three day sampling. Filter blanks were also collected at a regular interval.

To best achieve these goals, a six-day cycle was implemented that alternated between collocated, mass balance, and field blank collection days for a four-month period, as shown in **Figure 1-3**. This cycle was repeated twice more to complete a year of sampling. This sampling approach resulted in filters for mass balance every sixth day, while the other every-sixth-day pattern resulted in a series of collocated filters or field blanks. In addition, $PM_{2.5}$ and PM_{10} FRM samples were also collected on Teflon filters in parallel with the dichot measurements. Thus, at each site there were two dichots plus collocated $PM_{2.5}$ and PM_{10} FRM samplers. In addition, a Thermo 1405-DF Filter Dynamics Measurement Systems (FDMS) dichotomous TEOM – which is a Federal Equivalent Method (FEM) for $PM_{2.5}$ but not $PM_{10-2.5}$ – was operated to obtain hourly $PM_{2.5}$ and $PM_{10-2.5}$ data.

6-day cycle	1	2	3	4	5	6
01	(T/N,Q)01			(T/N,Q)FB01		
02	(T/N,Q)02			(T/N,T/N)01		
03	(T/N,Q)03			(Q,Q)01		
04	(T/N,Q)04			(T/N,T/N)02		
05	(T/N,Q)05			(Q,Q)02		
06	(T/N,Q)06			(T/N,Q)FB02		
07	(T/N,Q)07			(T/N,T/N)03		
08	(T/N,Q)08			(Q,Q)03		
09	(T/N,Q)09			(T/N,T/N)04		
10	(T/N,Q)10			(Q,Q)04		
11	(T/N,Q)11			(T/N,Q)FB03		
12	(T/N,Q)12			(T/N,T/N)05		
13	(T/N,Q)13			(Q,Q)05		
14	(T/N,Q)14			(T/N,T/N)06		
15	(T/N,Q)15			(Q,Q)06		
16	(T/N,Q)16			(T/N,Q)FB4		
17	(T/N,Q)17			(T/N,T/N)07		
18	(T/N,Q)18			(Q,Q)07		
19	(T/N,Q)19			(T/N,T/N)08		
20	(T/N,Q)20			(Q,Q)08		

Figure 1-3. Four-month sampling schedule for collocated dichots. In Column 1, green indicates a "mass balance" day with Teflon (T) filters and nylon (N) backup filters on one dichot and quartz fiber (Q) filters on the other dichot. Field blanks were collected four times in this cycle, as indicated by blue in Column 4. Gold indicates the days when collocated Teflon/nylon filters were collected, and yellow indicates the days when collocated quartz fiber filters were collected.

1.3.1 Instrumentation

The following equipment was installed and operated at each of the two sites:

- Two (2) sequential dichotomous samplers (Thermo 2025D);
- Two (2) sequential Thermo 2025 FRM samplers of the same make and model, one for PM_{10} and the other for $PM_{2.5}$ (for the $PM_{10-2.5}$ "difference method" measurements);
- One (1) dichotomous semi-continuous mass monitor (Thermo 1405-DF FDMS TEOM); and
- One (1) eight-stage (0.18, 0.32, 0.56, 1.0, 1.8, 2.5, 5.6, and 10 μm) MOUDI impactor (MSP Corporation).

While the Thermo 2025D sequential dichotomous samplers were designated as an FEM prior to this study, the samplers provided by Thermo were older models that were not FEM-compliant. Thus, it will be important to obtain additional field operations experience with the FEM-compliant version of the sampler.

1.3.2 Sample Analysis

Routine sample handling and analysis protocols followed the Standard Operating Procedures (SOP) used by RTI for the $PM_{2.5}$ CSN. Details on sample handling and analysis are provided in the Pilot Study QAPP (U.S. EPA, 2010). The following Whatman® 47 mm filters (GE Healthcare, Pittsburgh, PA) were used: Teflon membrane (Part Number 7592-304); nylon membrane (Part Number 7410-004), and quartz fiber (Part Number 1851-047). Teflon filters were analyzed for mass by gravimetric weighing, for elements by XRF, and for water-soluble ions by IC. The backup nylon filters were analyzed for ions by IC. Quartz fiber filters were analyzed for carbon using the IMPROVE_A thermal-optical analysis (TOA) protocol currently used in the CSN network. Mass and speciation data from these measurements have been uploaded to the EPA Air Quality System (AQS) database. Additional filters were selected for analysis of carbonate, biologicals, metals by ICP-MS, microscopy, and speciated organics.

1.3.3 Nomenclature and Dichot Sampling Concentration Equations

Table 1-1 defines the different types of particulate matter referenced in this document. $PM_{2.5}$ from the FRM is termed PM_{fine} (PM_f) in some cases when the distinction is unambiguous.

Table 1-1. Definitions of the different types of PM referenced in this document.

Abbreviation	Description
$PM_{10-2.5}$	Coarse PM by difference method FRM-measured PM_{10} minus FRM-measured $PM_{2.5}$
PM_{10}	FRM-measured PM_{10}
$PM_{2.5}$	FRM-measured $PM_{2.5}$
PM_f	Fine PM measured by a dichotomous sampler
PM_c	Coarse PM measured by a dichotomous sampler

The dichot samplers used in this study include a 16.7 liters-per-minute (LPM) standard PM_{10} inlet followed by a virtual impactor that splits the sample stream into major (15.0 LPM) and minor (1.67 LPM) flows. The major flow includes only fine particles, whereas the minor flow includes all of the coarse particles and 10% of the fine particles. PM_f mass concentrations are calculated directly from the major flow, and PM_c mass concentrations are calculated by correcting the minor flow for fine particle intrusion. For a nonvolatile species *j* collected on the front filter of the two-filter (routine/backup) sandwiches, the governing equations for species mass concentration are

$$\begin{aligned} PM_{j,f} &= \frac{m_{\text{j, front major}}}{V_{\text{major}}} \\ PM_{j,c} &= \frac{1}{V_{\text{total}}}\left(m_{\text{j, front minor}} - \frac{V_{\text{minor}}}{V_{\text{major}}} m_{\text{j, front major}} \right) \\ &= \frac{m_{\text{j, front minor}}}{V_{\text{total}}} - \frac{V_{\text{minor}}}{V_{\text{total}}} PM_{j,f} \end{aligned} \qquad \textbf{(Eq. 1-1)}$$

where $PM_{j,k}$ is the mass concentration of species *j* in size fraction *k* (*f* = fine, *c* = coarse), $m_{j,p}$ is the species *j* mass loading on the front filter in the specified flow channel *p* (major or minor); and V_p is the total air volume sampled by flow channel *p* (major, minor, or total = major + minor). For operation with the setpoint flow rates, V_{minor}/V_{total} = 0.10; thus, the correction to the coarse particle concentration for fine particle intrusion is 10% of the fine particle concentration (Dzubay and Stevens, 1975).

For species such as nitrate that are collected on both the front (Teflon) filter and back (nylon) filter, the governing equations are

$$\begin{aligned} PM'_{j,f} &= \frac{m_{\text{j, front major}} + m_{\text{j, back major}}}{V_{\text{major}}} \\ PM'_{j,c} &= \frac{1}{V_{\text{total}}}\left[\left(m_{\text{j, front minor}} + m_{\text{j, back minor}} \right) - \frac{V_{\text{minor}}}{V_{\text{major}}} \left(m_{\text{j, front major}} + m_{\text{j, back major}} \right) \right] \\ &= PM_{j,c} + \frac{m_{\text{j, back minor}}}{V_{\text{total}}} - \frac{V_{\text{minor}}}{V_{\text{total}}} \left(\frac{m_{\text{j, back major}}}{V_{\text{major}}} \right) \end{aligned} \qquad \textbf{(Eq. 1-2)}$$

where the prime species mass concentration includes mass on both the front and back filters.

1.4 Field Operations Overview

1.4.1 Methods

Field operations methods are detailed in the Pilot Study QAPP (U.S. EPA, 2010). All work performed and data collected at the Pilot Monitoring Program site locations were based on the following quality objectives:

- Multiple samplers were installed at each pilot site with inlets as close to the same height as possible and within a 1- to 4-meter separation from each other.
- All routine field sampling information (start time, end time, average flow rate, temperature and pressure data, meteorological conditions, etc.) and verification quality assurance (QA) checks were recorded on hard-copy field data forms prepared for use with each sampler.
- All integrated sampler field data were verified and placed in the RTI database and periodically provided to EPA/STI. These data were also posted to the EPA AQS database. The TEOM mass monitor data was submitted to STI via the AirNow-Tech website. RTI was the central repository for all integrated sampler data (including raw data) and related field information.
- All sampler parameters (flow rate, ambient and filter temperature, and barometric pressure) were verified against NIST-traceable standards prior to beginning and at the completion of the study, or after any sampler maintenance.
- For this project, the target completeness objective (completeness being the percentage of valid data compared to the total expected data) for all species and measurements was 80% of all scheduled measurements. In addition to individual measurement completeness, the program completeness (sampling events with all attempted measurements having valid data) was tracked, because program completeness dictates the robustness of the data set across the entire measurement strategy.

The $PM_{10-2.5}$ Pilot Study QAPP details audit procedures and routine operations, as well as sample handling and laboratory procedures.

1.4.2 Field Operations Summary

Table 1-2 summarizes the study sample collection completeness for June 1, 2010, through May 31, 2011, excluding the extra sampling days programmed to collect samples for biological content analysis. At each site, the two dichotomous samplers were distinguished by the designations "A" and "B," or primary (P) and collocated (C). Sampler hardware failures were the most common reasons for invalid samples. Sampling completeness for the Phoenix operations was above 90% for all samplers, and each sampler met the 80% completeness target. For St. Louis, the sampling completeness was much lower because of issues with the 2025D (dichotomous) samplers, and one sampler failed to meet the 80% completeness target. The low sample collection completeness in St. Louis was particularly problematic for this methods evaluation study, which places high value on the number of days with valid sample collection for all four samplers (only 44% of all sampling days for St. Louis).

Table 1-2. Sample completeness by site and sampler type for operations from June 1, 2010, through May 31, 2011, excluding sampling days for biological aerosols analysis. About half of valid samples were archived by RTI rather than analyzed. The total number of possible sample days is 122.

Sample Type	Phoenix		St. Louis	
	Valid Sample Days	% of Total Possible Sample Days	Valid Sample Days	% of Total Possible Sample Days
$PM_{2.5}$ FRM (2025)	115	94%	101	83%
PM_{10} FRM (2025)	114	93%	112	92%
Dichot A (2025D)	113	93%	80	66%
Dichot B (2025D)	120	98%	106	87%
Both Dichots	112	92%	71	58%
All Samplers[a]	105	86%	54	44%

[a] Sampling events with all four samplers ($PM_{2.5}$ and PM_{10} FRMs, Dichots A and B) having valid sample collection.

At both sites, there were sampler issues in the beginning of the study. These issues were most often due to issues with the filter exchange mechanism. Overall, there were fewer valid dichot measurements in St. Louis than in Phoenix.

At Phoenix, one sample from Dichot B and four samples from Dichot A were lost because of issues with the filter exchange mechanism. In addition, Dichot A sampling events were lost because of a short run time (one), a flow rate problem (one), and operator error (two); one sample from each dichot was lost because of non-operational events (e.g., filter mishandling).

At St. Louis, for Dichot A, 28 samples were not collected because an electronic board failure required the sampler to be returned to the manufacturer for repairs, and there was a delay in receiving a functioning replacement. Other samples were lost or not collected because of filter exchange errors (five samples), operator error (four samples, two due to a denuder installed for quartz/quartz [Q/Q] sampling), pump failure (four), and laboratory technician error (one). Once the original Dichot A was replaced in mid-January, data completeness for the remaining 45 sampling events was 96%, indicating that the majority of lost samples were due to the malfunctioning unit. Dichot B samples were lost because of a pump failure that was initially misdiagnosed as a filter exchange mechanism error (six), a second/replacement pump failure (six), filter exchange errors (three), and operator error (one). One problem with the pump failures is that they often initially manifest as a filter exchange error when the actuator line pressure drops too low to properly advance the filter shuttle mechanism. $PM_{2.5}$ FRM sampling issues were predominantly limited to filter exchange errors.

While the Thermo 2025D sequential dichotomous air sampler was designated as a FEM prior to this study, FEM-compliant samplers were not available and therefore, not provided by Thermo. Given the sampler delivery lead time and time constraints, only the two dichotomous and two FRM samplers sent to the Phoenix site were verified operational at RTI prior to

deployment. These four samplers were evaluated for flow rate, leaks, temperature, barometric pressure, and filter exchange. Double quartz (Q/Q) filter cassettes required modification in thickness to reduce filter cassette jamming. Samplers deployed in St. Louis were also newly purchased but were not verified operational at RTI; minimal sampler testing was performed at St. Louis due to time constraints, likely contributing to equipment problems during the study.

1.5 Guide to This Report

Section 1 provides an overview of the pilot study and field operations.

Section 2 compares dichot and FRM samplers for gravimetric mass in order to gauge precision and bias. In this section, to put analyses presented in later sections in context, the overall composition of the fine and coarse aerosol at each site is discussed. The order in which the results of the study are presented here builds up to the question of mass balance closure.

As crustal elements are the largest contributor to coarse aerosol mass, Section 3 provides details on the collocated precision of these measurements, a discussion of potential biases regarding the correction in for X-ray attenuation in XRF measurements, and a description of how the XRF measurements compared to ICP-MS measurements.

Section 4 presents details on carbonaceous aerosol, OC/EC splits, and the influence of biological material on OC.

Section 5 examines ions, including an analysis of nitrate loss on Teflon filters and an assessment of the usefulness of ion measurements as part of a long-term monitoring network.

Building on the results in Sections 2 through 5, Section 6 then presents mass balance results for dichot measurements, i.e., an examination of how well the measured species reconstruct the measured gravimetric mass, including exploration of "best fit" OM/OC ratios to achieve mass closure.

Section 7 provides additional collocated measurement comparisons using hourly FDMS TEOM data, and examines volatile versus non-volatile coarse PM.

The appendices provide supporting information as follows.

- **Appendix A** provides tables of summary statistics (concentrations and minimum detection limits [MDLs] by species and size fraction) for the samplers in St. Louis and Phoenix.
- **Appendix B** is a table of the summary ratios of collocated dichot measurements.
- **Appendix C** is a table summarizing the dichot-to-FRM comparisons.
- **Appendix D** provides information on quartz fiber filter carbon blanks.
- **Appendix E** is a table showing nitrate correlations with other species.

2. Gravimetric Mass and Composition Overview

PM_c constituents measured on the Teflon filters (gravimetric mass, elements, and ions) were biased low for the dichot compared to the FRM by difference method (Section 2.1). In Phoenix, PM_c mass from the dichot was on average about 20% lower than the FRM difference method mass, and in St. Louis, the dichot PM_c mass was 10% to 25% lower, depending on the dichot sampler. These findings are consistent with those found for pre-FEM 2025D sequential dichots evaluated during a multi-site evaluation of candidate methodologies for $PM_{10-2.5}$ (U.S. EPA, 2011). In contrast, PM_c total carbon measured on the quartz filters showed no bias between the two methods, though the relationship exhibited more scatter. The bias for constituents measured on the Teflon filters is attributed to particle losses from the dichot minor flow channel Teflon filter, which contains all of the coarse particles and only 10% of the fine particles. On average, PM_c was predominantly composed of crustal oxides at both sites, with 15% of the mass attributed to OC and less than 5% of the mass from other species, such as sulfate and nitrate (Section 2.2). As shown in Section 2.3, dichot collocated precision for PM_c constituents was typically in the 8% to 15% range for species with high rates of detectability. An exception was organic carbon, which had a collocated precision of 19% in Phoenix and 34% in St. Louis. The relatively less precise OC results in St. Louis arise in part from lower OC concentrations than in Phoenix. Organic carbon is further discussed in Section 4.

2.1 Gravimetric Mass Comparisons Between Dichot and FRM Samplers

Figure 2-1 shows scatter plots of the gravimetric mass measured by the dichotomous samplers at Phoenix and St. Louis compared to the FRM measurements for $PM_{2.5}$, $PM_{10-2.5}$, and PM_{10}. Using the FRM samplers, the $PM_{10-2.5}$ concentration is not directly measured, but instead is calculated from the difference between PM_{10} and $PM_{2.5}$ measurements.

Similarly, dichot PM_c is not directly measured, but instead must be corrected for fine PM particle intrusion into the dichot minor flow channel; dichot PM_{10} is not directly measured, but is rather the sum of the PM_f and PM_c measurements. At each site, there were two dichotomous samplers, labeled "primary" and "collocated." Summary statistics for gravimetric mass comparisons are presented in **Table 2-1**. For PM_f gravimetric mass, excellent agreement was observed at St. Louis for both the primary and collocated dichot samplers compared to the $PM_{2.5}$ FRM (Figure 2-1a). The mean value of the daily dichot-to-FRM mass ratio was 1.01 for both dichots, with mean absolute relative differences of 4% to 5%. In contrast, Figure 2-1d shows that at Phoenix, the dichot PM_f gravimetric mass was biased low with respect to the FRM, with mean ratios of 0.91 for both dichots. The mean absolute relative differences of 11% to 13% were worse than observed in St. Louis. Samples at high concentrations and outside the ±20% envelope (i.e., below the lower dashed line in Figure 2-1d) all correspond to samples collected in February and early March 2011. Dichot PM_c agreed reasonably well with $FRM_{10-2.5}$ on these days, so it is the dichot PM_f measurement that is suspect. The reason for the discrepancies on these sample days is not known.

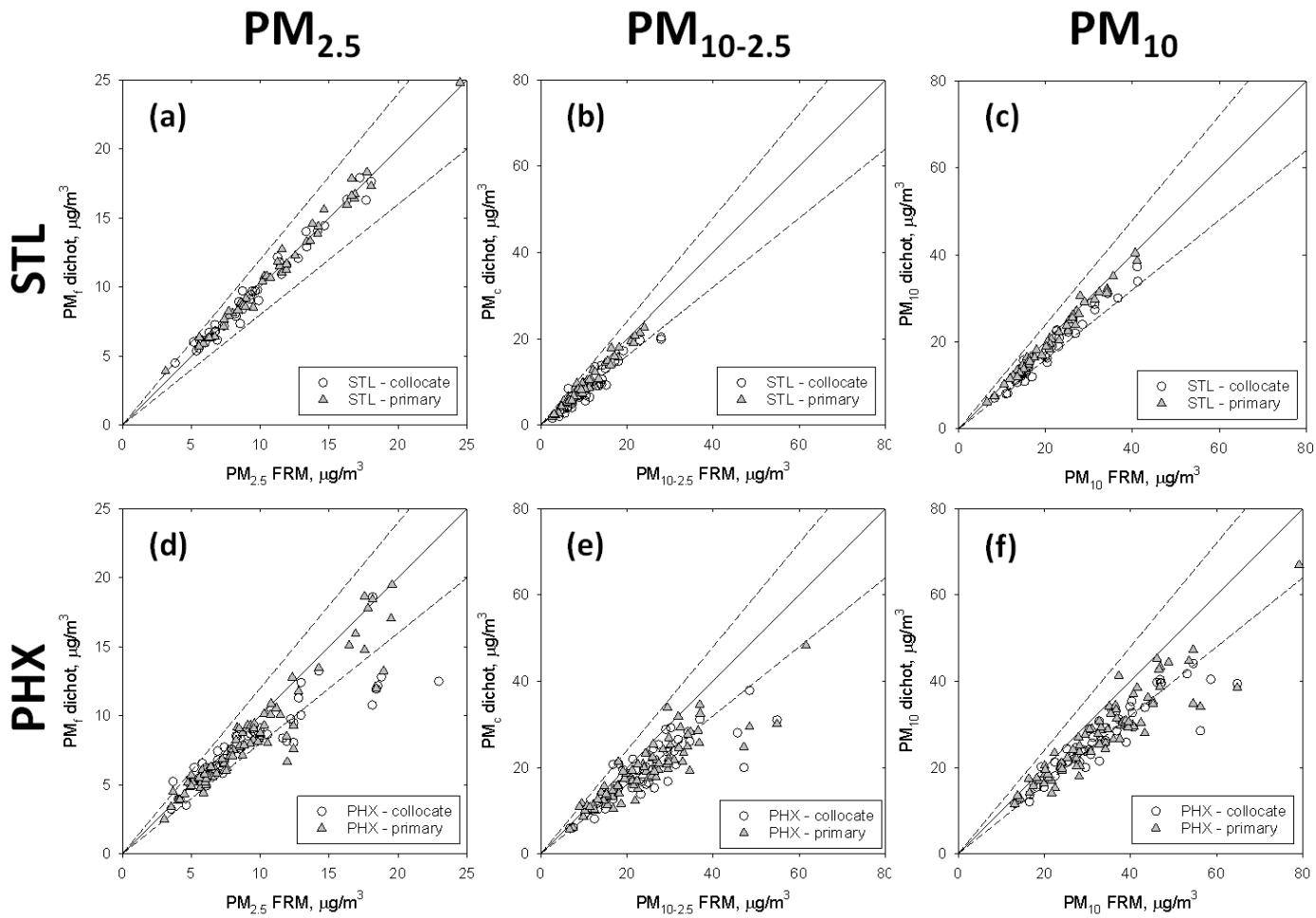

Figure 2-1. Dichot versus FRM mass concentrations for St. Louis (top row) and Phoenix (bottom row) for $PM_{2.5}$ (left), $PM_{10\text{-}2.5}$ (center), and PM_{10} (right). Triangles are data from the primary dichot sampler and circles are data from the collocated dichot sampler. Diagonal lines are 1:1 (solid) and ±20% of 1:1 (dashed).

Dichot PM_c gravimetric mass was consistently biased low compared to $FRM_{10\text{-}2.5}$ for both dichots at both sites (Figures 2-1b, e). At St. Louis, the dichot-to-FRM mean ratio for the primary dichot was 0.90 while for the collocated dichot it was only 0.76. At Phoenix, the two dichots show quite similar performances, with dichot-to-FRM mean ratios of approximately 0.82. Overall, the mean absolute relative differences of 12-26% across the sites and four samplers is driven more by systematic bias than random measurement error, as demonstrated by regression slopes significantly different from unity.

Dichot PM_{10} gravimetric mass comparison metrics[1] (Table 2-1) fall between the PM_f and PM_c results. For St. Louis, the PM_{10} values are near the midpoint of PM_f and PM_c values, which

[1] These metrics include a reduced major axis (RMA) regression, which is a type of orthogonal regression. Ordinary least squares (OLS) regression minimizes the sum of square differences between the reported and predicted y-values (i.e. the vertical distance between the best-fit line and measured values) and assumes the x-values are exact. In contrast, RMA minimizes the sum of square differences between the reported and the predicted values based on the distance perpendicular to the best-fit line and the measured values. Thus, RMA takes into consideration uncertainty in both the x- and y-values.

reflects the similar contributions from fine and coarse PM mass to PM_{10} mass. For Phoenix, the PM_{10} values are close to the PM_c values, since PM_{10} in Phoenix is generally dominated by coarse PM. The dichot-to-FRM bias observed for PM_{10} demonstrates that the PM_f and PM_c biases do not arise from poor cutpoint performance of the dichot virtual impactor. There must be other sources of significant bias, such as functional differences in the standard PM_{10} inlet performance (e.g., from differences in the cleaning protocol and frequency), particle losses during filter exchanges within the dichot sequential samplers, or particle losses from the filters during shipping and handling.

Table 2-1. Gravimetric mass comparisons between the dichot and FRM samplers. P = primary dichot and C = collocated dichot. Mean and median absolute relative differences were calculated using the FRM as the reference sampler. Mean and median ratios have been calculated for dichot-to-FRM comparisons. Regression statistics are from reduced major axis (RMA) regressions of dichot mass on FRM mass.

Total Samples➔	PHX-P 80	PHX-C 55	STL-P 45	STL-C 40
PM_f ($PM_{2.5}$)				
Mean Absolute Relative Difference (Median Absolute Relative Diff.)	11% (9%)	13% (7%)	4% (2%)	5% (4%)
Mean Ratio (Median Ratio)	0.91 (0.92)	0.91 (0.94)	1.01 (1.01)	1.01 (1.00)
Regression Slope, μg/m^3	0.91 ± 0.07	0.65 ± 0.08	1.00 ± 0.03	0.97 ± 0.05
Regression Intercept	-0.1 ± 0.7	2.0 ± 0.8	0.1 ± 0.4	0.3 ± 0.5
r^2	0.893	0.798	0.987	0.978
PM_c ($PM_{10-2.5}$)				
Mean Absolute Relative Difference (Median Absolute Relative Diff.)	19% (19%)	20% (19%)	12% (10%)	26% (27%)
Mean Ratio (Median Ratio)	0.83 (0.83)	0.81 (0.81)	0.90 (0.92)	0.76 (0.74)
Regression Slope, μg/m^3	0.71 ± 0.07	0.67 ± 0.10	0.96 ± 0.05	0.83 ± 0.08
Regression Intercept	2.2 ± 1.9	2.7 ± 2.5	-0.6 ± 0.6	-0.6 ± 1.1
r^2	0.787	0.719	0.971	0.904
PM_{10}				
Mean Absolute Relative Difference (Median Absolute Relative Diff.)	17% (16%)	18% (17%)	5% (4%)	13% (12%)
Mean Ratio (Median Ratio)	0.84 (0.84)	0.82 (0.83)	0.96 (0.96)	0.87 (0.88)
Regression Slope, μg/m^3	0.79 ± 0.07	0.71 ± 0.08	0.97 ± 0.04	0.91 ± 0.06
Regression Intercept	1.1 ± 2.5	3.2 ± 2.7	-0.3 ± 0.9	-0.7 ± 1.3
r^2	0.845	0.839	0.983	0.960

2.2 Distribution of Species Between Fine and Coarse Mode

Next, the average composition was examined at Phoenix and St. Louis for PM_c and PM_f, shown in **Figure 2-2**. At this stage, the objective was not to determine mass balance closure but rather to examine which classes of species dominate each size fraction. The PM_f composition was similar to the composition observed with longer-term measurements at both sites, where Phoenix PM_f is predominantly crustal oxides and carbonaceous aerosol, while St. Louis is mostly ammonium sulfate and carbonaceous aerosol. For PM_c, both sites were dominated by crustal oxides; OC was about 15% of the mass, and other species, including sulfate and nitrate, made up less than 5% of the average mass. Appendix A shows summaries of average concentration and MDL, the fraction of samples above MDL and 3×MDL, and the average uncertainty greater than MDL by species, site, and size (fine or coarse) for species analyzed from the Teflon and quartz filters.

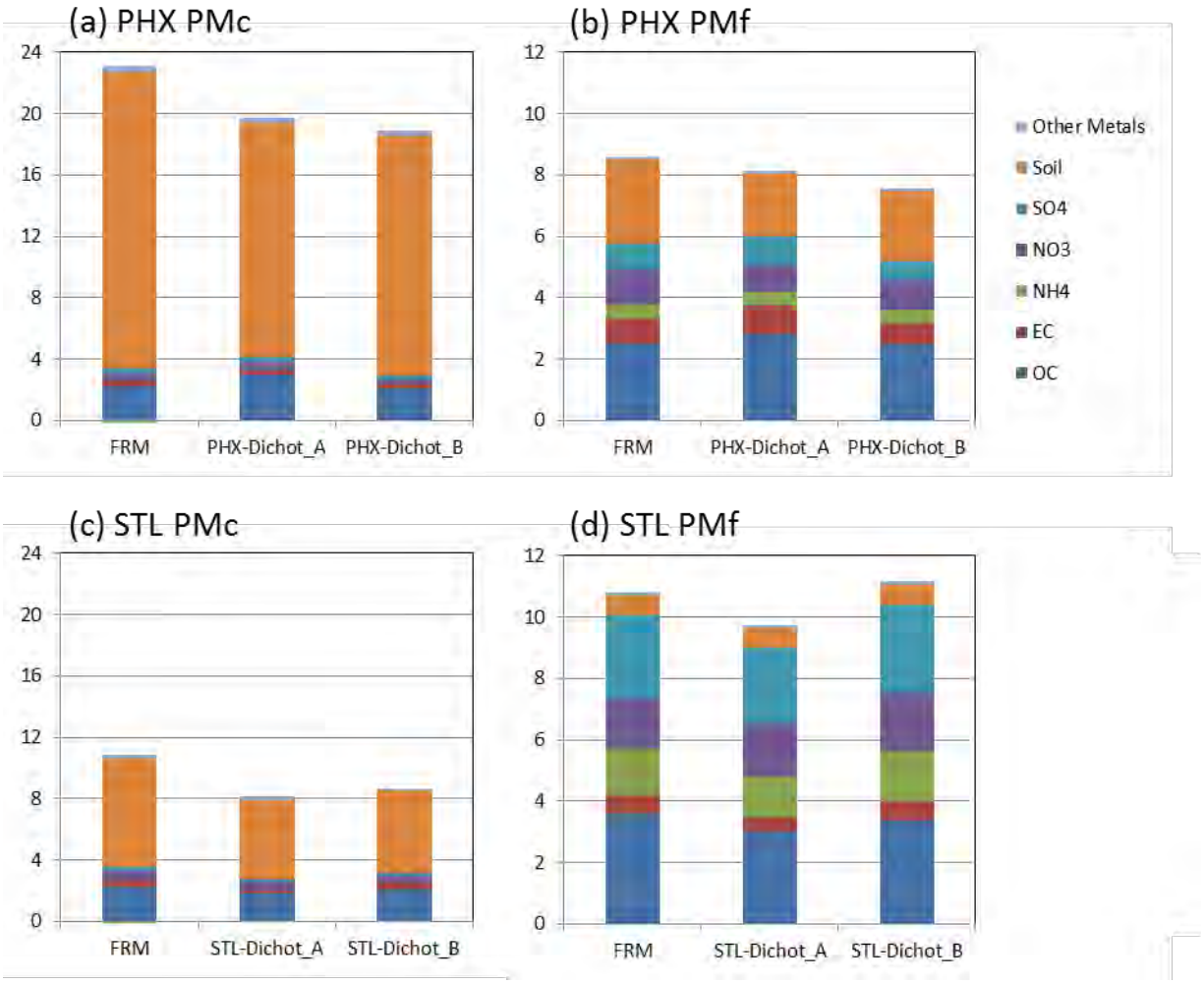

Figure 2-2. Stacked bar plots of average composition for (a) PM_c at Phoenix; (b) PM_f at Phoenix; (c) PM_c at St. Louis; and (d) PM_f at St. Louis. All concentrations are in $\mu g/m^3$.

As seen in **Figure 2-3** and detailed in Appendix A, the $PM_{10}/PM_{2.5}$ ratio from FRM measurements is typically much greater than unity, with values greater than two representing an enhancement in coarse PM species abundance relative to fine PM. Ammonium, sulfate (both by IC and by XRF sulfur), bromine, and rubidium are almost exclusively in the fine fraction. Because the $PM_{10-2.5}$ concentration will be the difference between two very similar values, measurement of these species in $PM_{10-2.5}$ using the FRM-by-difference method can result in large relative uncertainties. However, from a mass balance perspective, these species contribute little to $PM_{10-2.5}$ mass. EC, OC, soluble potassium (by IC), lead, and zinc are, on average, nearly evenly distributed between the fine and coarse fractions. The remaining elements tend to be more abundant in the coarse fraction, with the species commonly associated with crustal material (e.g., aluminum [Al], calcium [Ca], magnesium [Mg], and silicon [Si]) enhanced in $PM_{10-2.5}$ by more than a factor of five (i.e., a $PM_{10}/PM_{2.5}$ ratio greater than ten).

Based on these coarse PM concentration and relative abundance patterns, the analysis of measurement precision focuses primarily on crustal species and secondarily on OC.

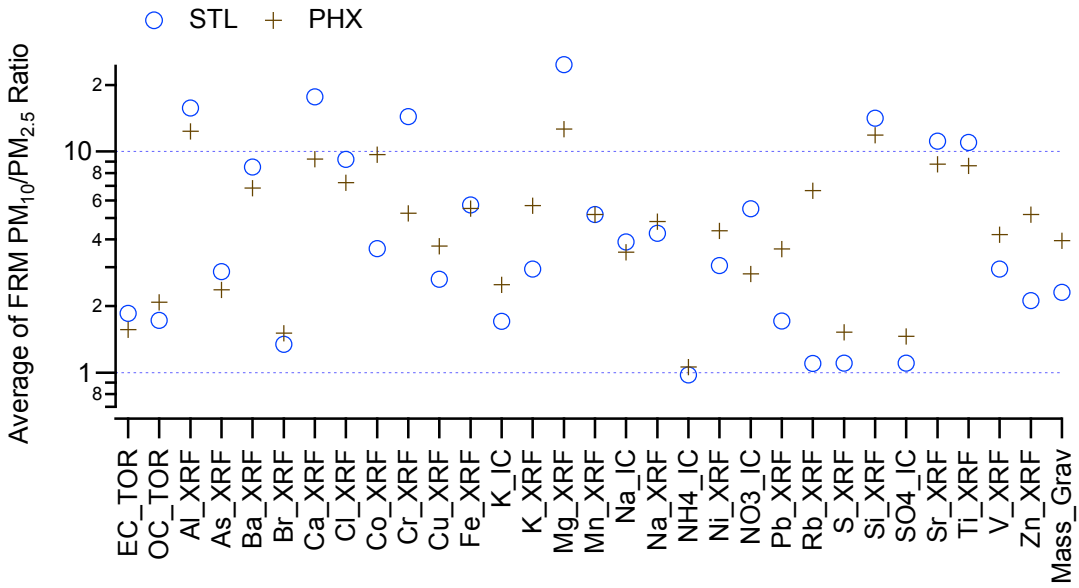

Figure 2-3. Average FRM $PM_{10}/PM_{2.5}$ ratio (log scale) by species for each site.

2.3 Collocated Precision of Dichot Measurements

A major component of the sampling plan was to periodically run the collocated dichots using the same filter type, making it possible to evaluate dichot measurement precision. **Figure 2-4** shows collocated dichot sampler comparisons for gravimetric mass and silicon including all data. As demonstrated later in this section, silicon collocated performance is representative of most crustal species. For these two parameters, the agreement appears good for both sites and for both particle sizes. Gravimetric mass data for PM_c at Phoenix does exhibit relatively more scatter at high concentrations. Measures of agreement for PM_c and PM_f at both sites are reported in **Tables 2-2 through 2-5** for gravimetric mass, elements used in the soil

equation, and OC. (In those tables, OC-TOR is organic carbon measured by thermal-optical reflectance.) The gravimetric mass data sets were conditioned to include only those samples with XRF elements also reported. Linear regressions of Dichot B concentrations on Dichot A concentrations were performed using reduced major axis regression, which assumes a constant measurement uncertainty for the two samplers. For most slopes, the 95% confidence intervals include unity, and for most intercepts, the 95% confidence intervals include zero.

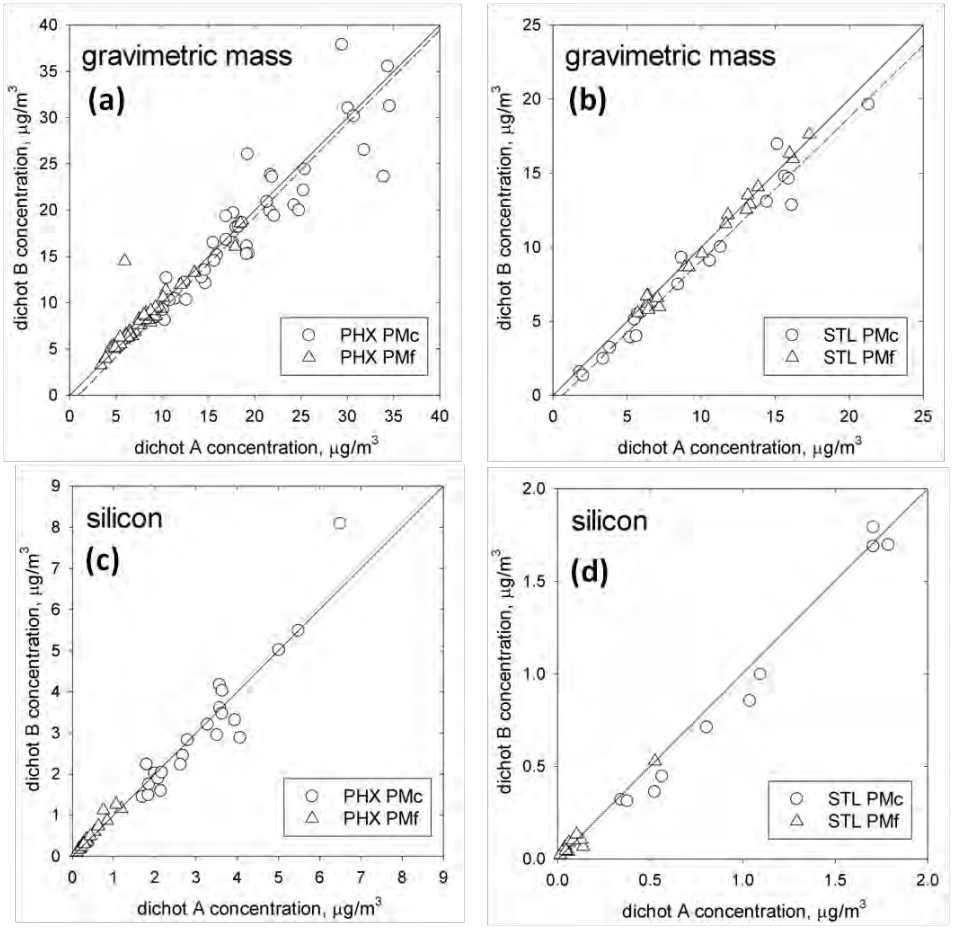

Figure 2-4. Collocated dichot versus dichot plots for (a) gravimetric mass at Phoenix; (b) gravimetric mass at St. Louis; (c) Si at Phoenix; (d) Si at St. Louis. The solid lines are 1:1 lines and the dashed lines in panels (a) and (b) are the reduced major axis regressions for the PM_c data; the regression coefficients are reported in Tables 2-2 through 2-5.

Table 2-2. Measures of agreement between the collocated dichot sampler data for PM_c measured at Phoenix. Slopes and intercepts are reported for reduced major axis regressions of Dichot B on Dichot A.

PHX PM_c (N=22)	Mean ($\mu g/m^3$)	Min, Max ($\mu g/m^3$)	Slope +/- 95% C.I.	Intercept +/- 95% C.I. ($\mu g/m^3$)	r^2	B/A Ratio: Mean (Median)	Collocated Precision ($\mu g/m^3$)
Grav. mass	18.87	8.09, 37.88	0.91 ± 0.13	2.2 ± 2.6	0.91	0.97 (0.95)	1.86 (10%)
Al	1.02	0.41, 2.57	1.19 ± 0.17	-0.22 ± 0.19	0.90	0.95 (0.94)	0.12 (12%)
Ca	1.19	0.44, 2.81	1.14 ± 0.17	-0.19 ± 0.22	0.90	0.96 (0.95)	0.15 (12%)
Fe	0.81	0.30, 1.78	1.04 ± 0.18	-0.06 ± 0.16	0.87	0.96 (0.97)	0.11 (13%)
Si	3.15	1.45, 8.09	1.22 ± 0.18	-0.77 ± 0.61	0.90	0.96 (0.95)	0.37 (12%)
Ti	0.061	0.024, 0.14	1.21 ± 0.21	-0.01 ± 0.01	0.86	0.97 (0.94)	0.01 (15%)
OC-TOR (N=14)	2.29	0.91, 4.01	1.04 ± 0.38	0.30 ± 0.84	0.67	1.23 (1.26)	0.43 (19%)

Table 2-3. Measures of agreement between the collocated dichot sampler data for PM_f measured at Phoenix. Slopes and intercepts are reported for reduced major axis regressions of Dichot B on Dichot A.

PHX PM_f (N=22)	Mean ($\mu g/m^3$)	Min, Max ($\mu g/m^3$)	Slope +/- 95% C.I.	Intercept +/- 95% C.I. ($\mu g/m^3$)	r^2	B/A Ratio: Mean (Median)	Collocated Precision ($\mu g/m^3$)
Grav. mass	8.10	3.24, 18.61	1.01 ± 0.21	-0.56 ± 1.94	0.8	1.09 (1.02)	1.35 (17%)
Al	0.14	0.03, 0.43	1.12 ± 0.11	-0.0005 ± 0.02	0.96	1.13 (1.07)	0.02 (15%)
Ca	0.17	0.04, 0.46	1.17 ± 0.15	-0.003 ± 0.03	0.92	1.14 (1.11)	0.03 (17%)
Fe	0.19	0.04, 0.53	1.01 ± 0.11	0.01 ± 0.02	0.95	1.08 (1.07)	0.02 (11%)
Si	0.43	0.10, 1.26	1.15 ± 0.12	-0.004 ± 0.06	0.95	1.13 (1.12)	0.07 (16%)
Ti	0.008	0.002, 0.025	1.33 ± 0.27	-0.0007 ± 0.002	0.81	1.26 (1.20)	0.002 (29%)
OC-TOR (N=14)	2.11	0.58, 3.75	0.91 ± 0.21	0.18 ± 0.49	0.87	1.05 (1.01)	0.25 (12%)

Table 2-4. Measures of agreement between the collocated dichot sampler data for PM_c measured at St. Louis. Slopes and intercepts are reported for reduced major axis regressions of Dichot B on Dichot A.

STL PM_c (N=11)	Mean ($\mu g/m^3$)	Min, Max ($\mu g/m^3$)	Slope +/- 95% C.I.	Intercept +/- 95% C.I. ($\mu g/m^3$)	r^2	B/A Ratio: Mean (Median)	Collocated Precision ($\mu g/m^3$)
Grav. mass	9.77	1.33, 21.31	1.07 ± 0.09	0.67 ± 0.95	0.99	0.84 (0.89)	1.08 (11%)
Al	0.27	0.01, 0.73	1.04 ± 0.11	-0.05 ± 0.04	0.98	0.81 (0.83)	0.03 (11%)
Ca	1.14	0.13, 3.64	0.98 ± 0.09	-0.08 ± 0.14	0.99	0.90 (0.92)	0.12 (10%)
Fe	0.29	0.08, 0.83	1.00 ± 0.02	-0.03 ± 0.03	0.99	0.88 (0.91)	0.03 (9%)
Si	0.83	0.10, 1.79	1.03 ± 0.10	-0.09 ± 0.10	0.98	0.90 (0.91)	0.07 (8%)
Ti	0.012	0.000, 0.031	1.05 ± 0.17	-0.002 ± 0.003	0.95	0.86 (0.87)	0.002 (13%)
OC-TOR (N=14)	1.71	0.49, 4.53	0.74 ± 0.38	0.25 ± 0.80	0.40	0.93 (1.00)	0.59 (34%)

Table 2-5. Measures of agreement between the collocated dichot sampler data for PM_f measured at St. Louis. Slopes and intercepts are reported for reduced major axis regressions of Dichot B on Dichot A.

STL PM_f (N=11)	Mean ($\mu g/m^3$)	Min, Max ($\mu g/m^3$)	Slope +/- 95% C.I.	Intercept +/- 95% C.I. ($\mu g/m^3$)	r^2	B/A Ratio: Mean (Median)	Collocated Precision ($\mu g/m^3$)
Grav. mass	11.21	6.33, 17.64	0.99 ± 0.09	0.12 ± 1.04	0.99	1.00 (1.02)	0.27 (2%)
Al	0.05	0.01, 0.27	1.04 ± 0.09	-0.002 ± 0.008	0.99	1.04 (1.03)	0.01 (13%)
Ca	0.09	0.01, 0.20	1.17 ± 0.35	0.001 ± 0.03	0.85	1.23 (1.15)	0.02 (20%)
Fe	0.08	0.03, 0.19	1.10 ± 0.23	-0.0001 ± 0.02	0.93	1.11 (1.04)	0.01 (15%)
Si	0.11	0.01, 0.53	0.99 ± 0.10	0.01 ± 0.02	0.98	1.18 (1.15)	0.01 (12%)
Ti	0.003	0.000, 0.019	1.10 ± 0.36	0.001 ± 0.002	0.81	1.72 (1.15)	0.002 (55%)
OC-TOR (N=14)	2.59	0.82, 5.30	1.07 ± 0.20	-0.51 ± 0.60	0.92	0.87 (0.90)	0.33 (13%)

For PM_c at Phoenix (Table 2-2) the mean ratio of 0.97 for gravimetric mass demonstrates that there is little mass bias between the samplers. Mean ratios for the crustal species are consistently in the range 0.95–0.97, which shows that, on average, Dichot B concentrations are a few percent lower than Dichot A concentrations for these species. In contrast, the mean ratio is 1.23 for OC, which shows that, on average, Dichot B concentrations are 23% higher than Dichot A concentrations. Collocated precision, defined as the root mean square (RMS) of the Dichot A-to-Dichot B concentration differences divided by the square root of 2, is in the range 12% to 19% for the PM_c components, with the highest value observed for OC. For PM_f at Phoenix (Table 2-3) the mean ratio of 1.09 for gravimetric mass demonstrates some bias, with Dichot B reading higher than Dichot A. This pattern is observed for all of the major crustal species with mean ratios ranging from 1.08 (Fe) to 1.26 (Ti). Similar to PM_c, the PM_f collocated precision estimates are in the range of 10% to 20% for each of the reported species.

Collocated precision for the St. Louis data was, with a few exceptions, similar to the Phoenix data. Precision was poorer in St. Louis for PM_c OC-TOR and PM_f titanium, and better in St. Louis for PM_f gravimetric mass.

Measurement error for the collocated dichot data collected at Phoenix was further examined by calculating the concentration differences between samplers (expressed as the natural logarithm of the concentration ratio) for all species. **Figure 2-5** shows scatterplots for the concentration differences between dichot samplers for the elements used in the soil equation, XRF sulfur, and gravimetric mass. For PM_c (Figure 2-5a), all of these species combinations show strong correlation. Interpreting the concentration difference between dichot samplers to be measurement error, these strong correlations mean that these species share the same dominant source of measurement error (Hyslop and White, 2011), and this measurement error leads to the small but consistent deviation in the mean ratios from unity for these species shown in Table 2-2. One possible source of such measurement error could be functional differences between the dichots in performance of the PM_{10} size-selective inlets.

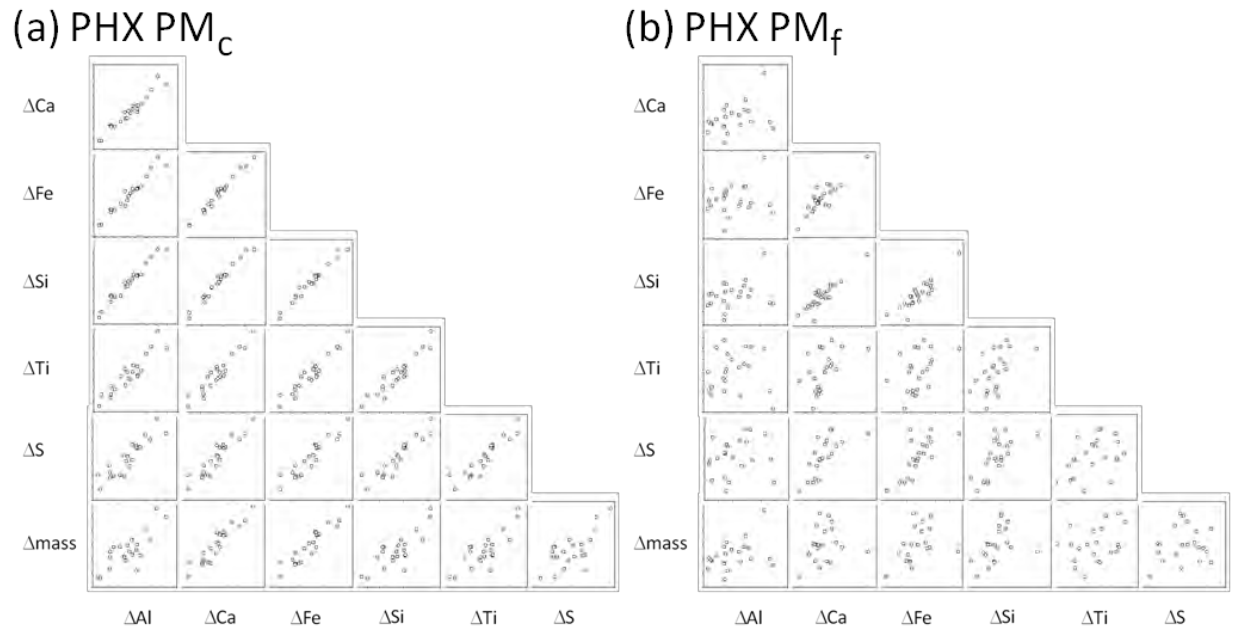

Figure 2-5. Scatterplot matrices of the observed differences, $\Delta x = \ln(C_{x,B} / C_{x,A})$, in the collocated concentrations at Phoenix: (a) PM_c and (b) PM_f.

For comparison, Figure 2-5b shows scatterplots for the observed concentration differences for PM_f from the collocated dichots at Phoenix. Ca, Fe, Si, and to some extent sulfur (S) show strong correlation. Correlations for Al and Ti with the other species are weaker; this weaker correlation might arise from the relatively greater contribution of analytical errors to the overall measurement errors for these species, which are at relatively low concentrations in the PM_f size range. Another potential source of measurement error is differences in the cutpoint curves between virtual impactors in the two dichots. This error could explain the Dichot B-to-Dichot A ratios for gravimetric mass and crustal species being less than one for PM_c and greater than one for PM_f (Tables 2-2 and 2-3). In this case, for a given species, the concentration differences between dichots should be anti-correlated for the PM_c and PM_f size ranges.

Figure 2-6 shows the observed differences for the major soil species. In each case, the correlation is very weak, and thus, if there are differences in virtual impactor performance between the two dichot samplers, the effect on concentration is masked by other measurement errors.

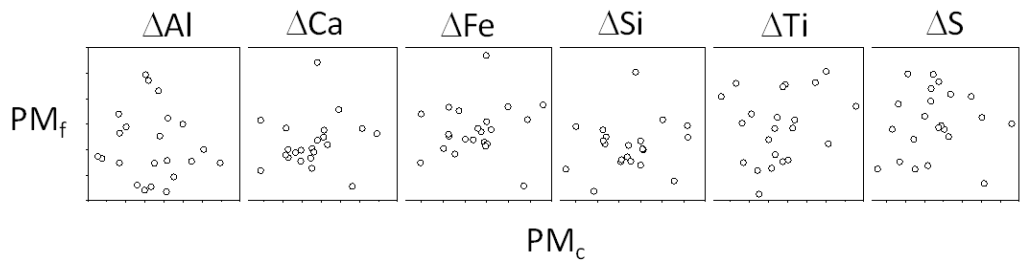

Figure 2-6. Scatterplot vector of the observed differences, $\Delta x = \ln(C_{x,B} / C_{x,A})$, across the fine and coarse PM size fractions in the collocated concentrations at Phoenix.

The average and median concentration ratios between collocated dichots by species, site, and size (fine or coarse) are summarized in Appendix B. **Figure 2-7** shows the average Dichot B-to-Dichot A ratio by species for both sites and size fraction, using only data above the MDL. For most species, the average ratio is near unity. One noteworthy exception is ammonium, which has low abundance in PM_c and has high uncertainty from the correction for fine particle intrusion into the dichot minor flow channel.

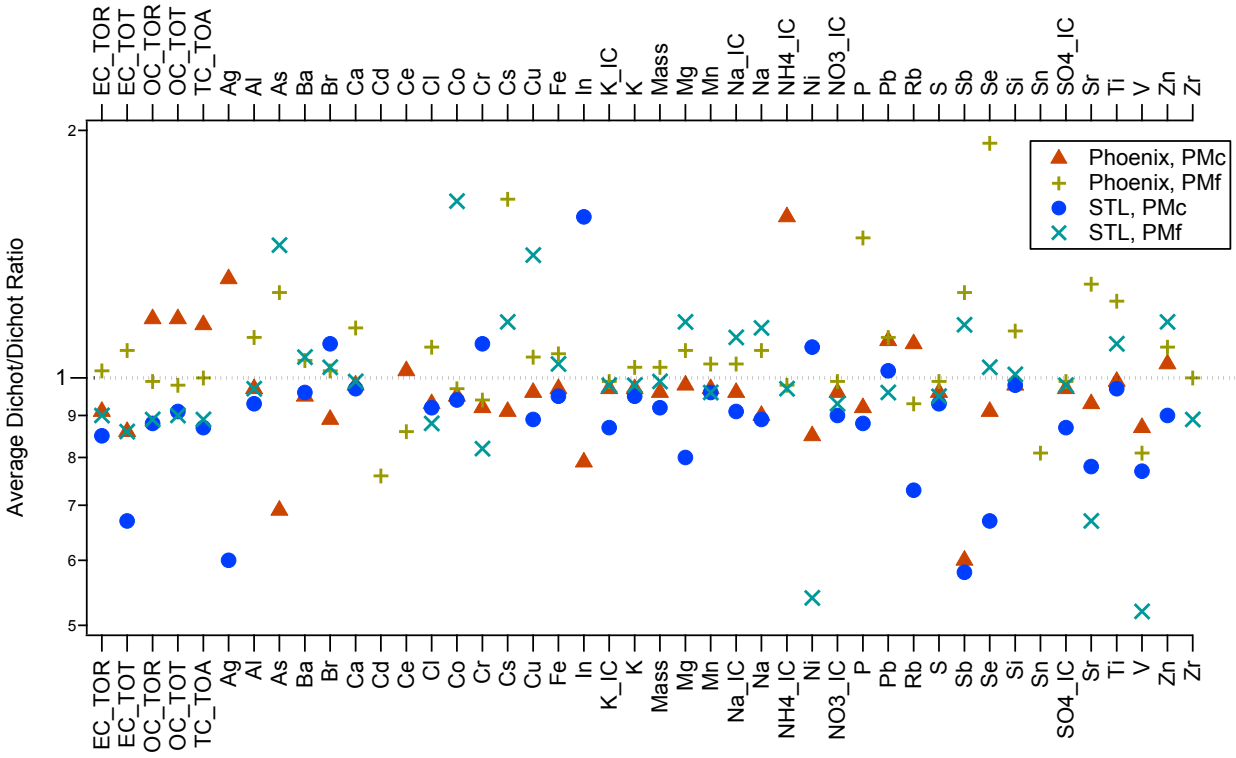

Figure 2-7. Average ratio of collocated dichot measurements (log scale) by site, species, and size, using only data above the MDL for both measurements.

3. Analysis of Elements

Species that were typically above the MDL in the $PM_{2.5}$ CSN were generally above the MDL in PM_c (Section 3.1), including the crustal species, OC and EC, sulfate, nitrate, and metals such as barium (Ba), chlorine (Cl), copper (Cu), potassium (K), manganese (Mn), sodium (Na), and zinc (Zn).

Unlike $PM_{2.5}$, ammonium was above the MDL only 60% of the time in St. Louis and 50% of the time in Phoenix, reflective of the low ammonium concentrations in PM_c. Agreement of individual species' PM_c concentrations between dichot and FRM measurements (Section 3.2) were generally similar to those seen for gravimetric mass (Section 2.1).

At St. Louis, dichot and FRM measurements compared fairly well for both fine and coarse fractions. At Phoenix, there was a consistent bias for PM_c, with FRM concentrations higher than dichot concentrations for most species, especially the crustal elements. Given that crustal oxides make up the majority of the PM_c mass, and that FRM $PM_{10-2.5}$ measurements of these species were consistently higher than dichot PM_c measurements, the sensitivity of these species' measurements to the assumptions in the XRF method was examined (Section 3.3).

Attenuation factors are negligible for $PM_{2.5}$ measurements; however, attenuation factors must be applied for PM_c measurements. The attenuation factors used in this study for PM_c were further investigated for a subset of samples. Results from ICP-MS analysis were compared to XRF results for a subset of samples (Section 3.4), which further indicated that the coarse particle concentrations measured by blank-corrected ICP-MS were greater than those measured by XRF. This pattern does suggest that the XRF attenuation corrections for these constituents are too large, although more is needed to verify these preliminary findings.

Lastly, Section 3.5 shows that there was little daily variation in the crustal composition, though the composition was somewhat different at the two monitoring sites.

3.1 Concentrations by Site and Size Fraction

Similar to CSN measurements, many species that were analyzed were often below detection. Twenty species were above the MDL more than 80% of the time at both sites. Appendix A summarizes average concentration and MDL, fraction of samples above MDL and 3×MDL, and the average uncertainty by species, site, and size (fine or coarse) for species analyzed from the Teflon and quartz filters. Elements were analyzed by XRF, and ions were analyzed by IC. Potassium and sodium were analyzed by both methods. **Figure 3-1** shows the fraction of samples above the MDL for dichot PM_c. Species were detected at similar rates at both sites, with a few exceptions: the detection rates for cobalt (Co), chromium (Cr), rubidium (Rb), and strontium (Sr) were higher at Phoenix. This is consistent with the higher PM_c crustal concentrations in Phoenix compared to St. Louis, but might also reflect differences in species abundance in the crustal material at these sites.

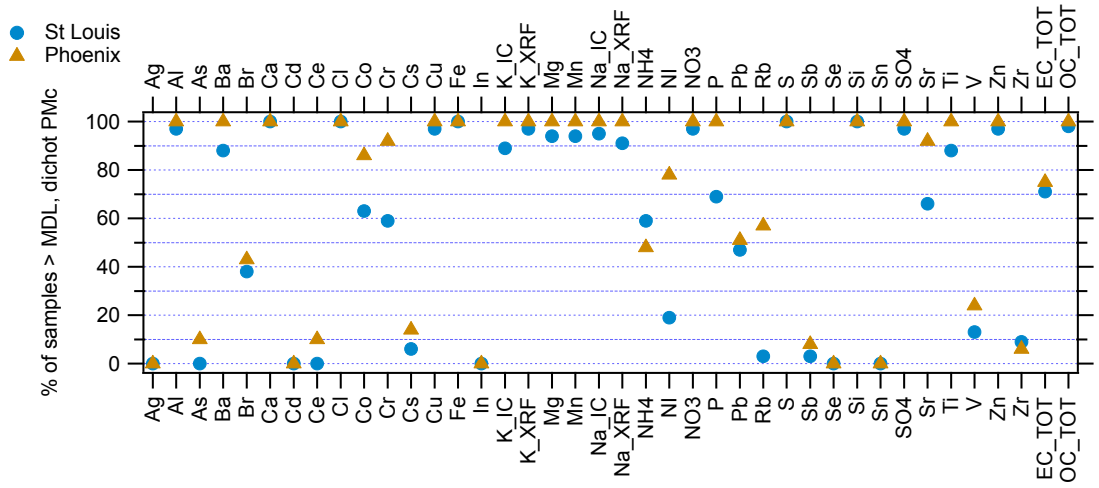

Figure 3-1. Percentage of samples above detection limit for dichot PM_c by site.

3.2 Concentrations of Elements: Comparison of Dichot and FRM

Trends in elements between dichot and FRM measurements were generally similar to those seen for gravimetric mass (Section 2.1). **Tables 3-1 through 3-4** summarize, and **Figure 3-2** shows, comparisons of dichot to FRM concentrations for four species (Ca, Fe, S, and Zn). The gravimetric mass data sets used for the tables were conditioned to include only those samples with XRF elements also reported. Sulfur is predominantly found in the fine fraction, zinc is present at relatively low concentrations, and calcium and iron are crustal components present at relatively high concentrations. At St. Louis, dichot and FRM measurements compared fairly well for both fine and coarse fractions. At Phoenix, there was a consistent bias for coarse PM with FRM concentrations higher than dichot concentrations. In particular, crustal elements (Al, Ca, Fe, Si) all had a similar bias, and in general, the bias was evident in all species that were above detection more than 75% of the time. Caution must be used when interpreting the collocated precision values reported in Tables 3-1 through 3-4 because in cases with large bias, the precision estimates are driven by the bias and not by random measurement error. Appendix C summarizes dichot-to-FRM ratios of average and median concentration by species, site, and size (fine or coarse) for species analyzed from the Teflon and quartz filters.

Table 3-1. Measures of agreement between the collocated FRM and dichot data for PM_c measured at Phoenix. Slopes and intercepts are reported for reduced major axis regressions of dichot on FRM.

PHX PM_c (N=35)	FRM Mean ($\mu g/m^3$)	FRM Min, Max ($\mu g/m^3$)	Slope +/- 95% C.I.	Intercept +/- 95% C.I. ($\mu g/m^3$)	r^2	D/F Ratio: Mean (Median)	Collocated Precision ($\mu g/m^3$)
Grav. mass	22.7	9.6, 54.9	0.64 ± 0.10	3.6 ± 2.5	0.80	0.83 (0.85)	5.1 (25%)
S	0.12	0.04, 0.28	1.11 ± 0.27	0.00 ± 0.04	0.53	1.17 (1.08)	0.03 (24%)
Zn	0.06	0.01, 0.57	0.46 ± 0.04	0.01 ± 0.00	0.94	0.83 (0.77)	0.04 (82%)
Ca	1.43	0.53, 4.06	0.65 ± 0.13	0.22 ± 0.22	0.68	0.86 (0.87)	0.40 (31%)
Fe	0.99	0.35, 2.34	0.71 ± 0.12	0.10 ± 0.13	0.79	0.85 (0.85)	0.23 (26%)
Si	4.23	1.59, 11.26	0.65 ± 0.14	0.65 ± 0.65	0.64	0.85 (0.87)	1.10 (29%)

Table 3-2. Measures of agreement between the collocated FRM and dichot data for PM_f measured at Phoenix. Slopes and intercepts are reported for reduced major axis regressions of dichot on FRM.

PHX PM_f (N=35)	FRM Mean ($\mu g/m^3$)	FRM Min, Max ($\mu g/m^3$)	Slope +/- 95% C.I.	Intercept +/- 95% C.I. ($\mu g/m^3$)	r^2	D/F Ratio: Mean (Median)	Collocated Precision ($\mu g/m^3$)
Grav. mass	8.4	3.5, 19.6	0.98 ± 0.08	-0.5 ± 0.77	0.94	0.92 (0.93)	0.8 (10%)
S	0.31	0.09, 1.02	1.03 ± 0.04	-0.01 ± 0.01	0.99	0.99 (1.01)	0.01 (3%)
Zn	0.015	0.003, 0.047	1.00 + 0.10	0.000 + 0.002	0.91	1.00 (0.95)	0.002 (14%)
Ca	0.18	0.04, 0.63	0.85 ± 0.10	0.00 ± 0.02	0.88	0.88 (0.87)	0.04 (24%)
Fe	0.24	0.04, 0.67	0.92 ± 0.12	-0.01 ± 0.03	0.86	0.89 (0.90)	0.05 (22%)
Si	0.42	0.10, 1.74	0.91 ± 0.10	-0.01 ± 0.05	0.90	0.91 (0.89)	0.08 (20%)

Table 3-3. Measures of agreement between the collocated FRM and dichot data for PM_c measured at St. Louis. Slopes and intercepts are reported for reduced major axis regressions of dichot on FRM.

STL PM_c (N=18)	FRM Mean ($\mu g/m^3$)	FRM Min, Max ($\mu g/m^3$)	Slope +/- 95% C.I.	Intercept +/- 95% C.I. ($\mu g/m^3$)	r^2	D/F Ratio: Mean (Median)	Collocated Precision ($\mu g/m^3$)
Grav. mass	12.3	3.1, 24	0.99 ± 0.08	-0.9 ± 1.1	0.98	0.90 (0.93)	1.0 (8%)
S	0.10	-0.13, 0.24	0.42 ± 0.19	0.07 ± 0.03	0.28	-0.75 (0.84)	0.06 (57%)
Zn	0.025	0.004, 0.136	0.96 ± 0.08	-0.001 ± 0.003	0.98	1.01 (0.99)	0.004 (17%)
Ca	1.51	0.15, 3.92	0.95 ± 0.08	0.02 ± 0.15	0.97	0.97 (0.98)	0.13 (9%)
Fe	0.39	0.1, 0.98	0.84 ± 0.08	0.03 ± 0.04	0.97	0.94 (0.9)	0.05 (13%)
Si	1.14	0.18, 2.75	0.88 ± 0.08	0.07 ± 0.12	0.97	0.96 (0.96)	0.12 (11%)

Table 3-4. Measures of agreement between the collocated FRM and dichot data for PM_f measured at St. Louis. Slopes and intercepts are reported for reduced major axis regressions of dichot on FRM.

STL PM_f (N=18)	FRM Mean ($\mu g/m^3$)	FRM Min, Max ($\mu g/m^3$)	Slope +/- 95% C.I.	Intercept +/- 95% C.I. ($\mu g/m^3$)	r^2	D/F Ratio: Mean (Median)	Collocated Precision ($\mu g/m^3$)
Grav. mass	12.0	6.3, 18.1	1.01 ± 0.09	0.0 ± 1.1	0.97	1.01 (1)	0.4 (3%)
S	0.88	0.44, 1.36	0.99 + 0.11	0.00 + 0.10	0.95	1.00 (1.01)	0.03 (3%)
Zn	0.019	0.003, 0.067	0.98 + 0.13	0.000 + 0.003	0.930	1.00 (0.95)	0.003 (16%)
Ca	0.09	0.02, 0.20	1.13 + 0.21	-0.01 + 0.02	0.87	1.08 (1.00)	0.02 (22%)
Fe	0.09	0.02, 0.24	1.07 + 0.13	0.00 + 0.01	0.95	1.05 (1.00)	0.01 (11%)
Si	0.11	0.02, 0.54	0.96 + 0.08	0.00 + 0.01	0.98	1.04 (0.98)	0.01 (9%)

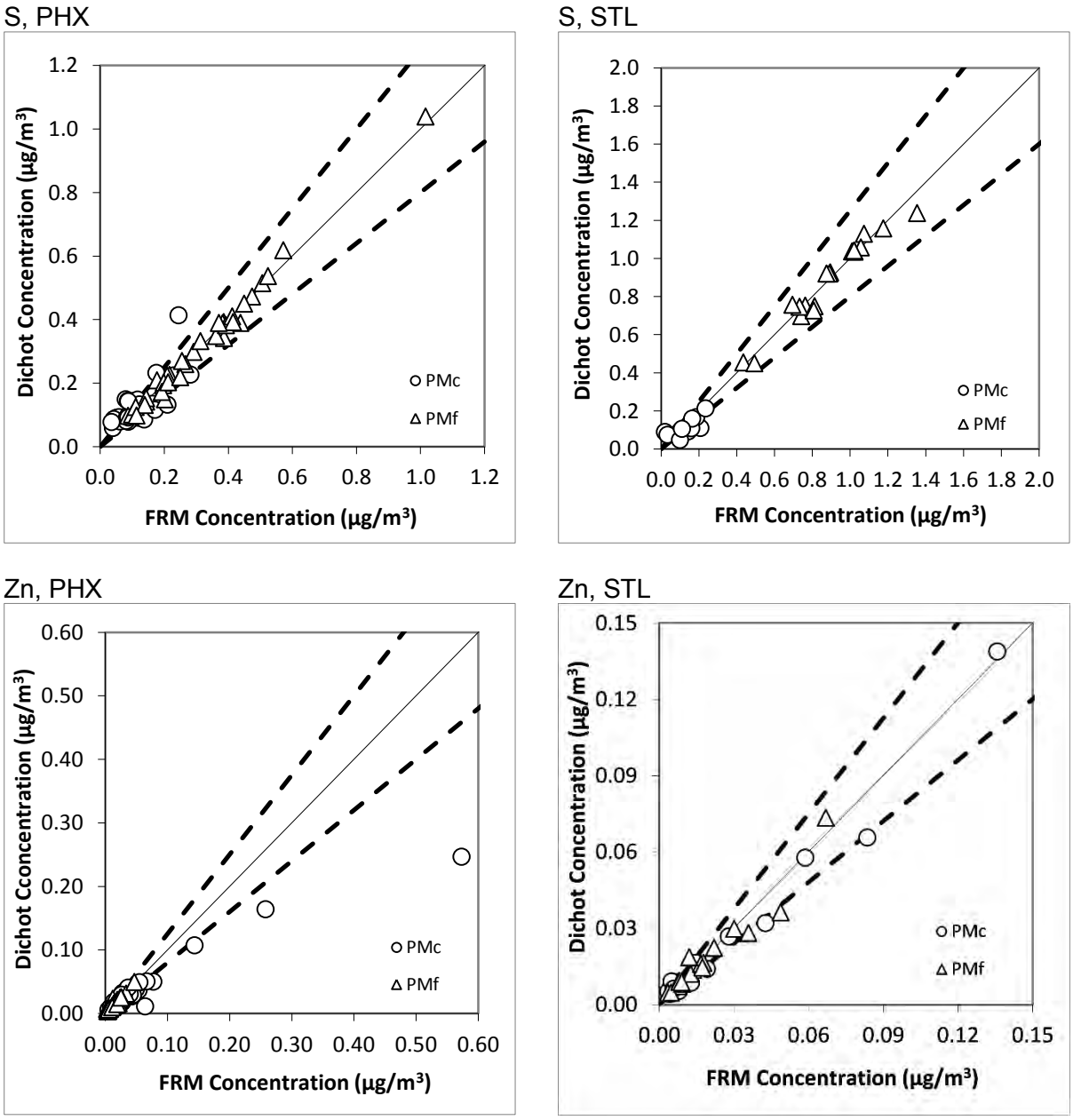

Figure 3-2. Scatter plots of PM_f and PM_c concentrations from dichot (y-axis) and FRM (x-axis) at Phoenix (left column) and St. Louis (right column) for S, Zn, Ca, and Fe. Solid lines are the 1:1 lines and dashed lines indicate the +/-20% difference between measurements. *(Figure continued on next page.)*

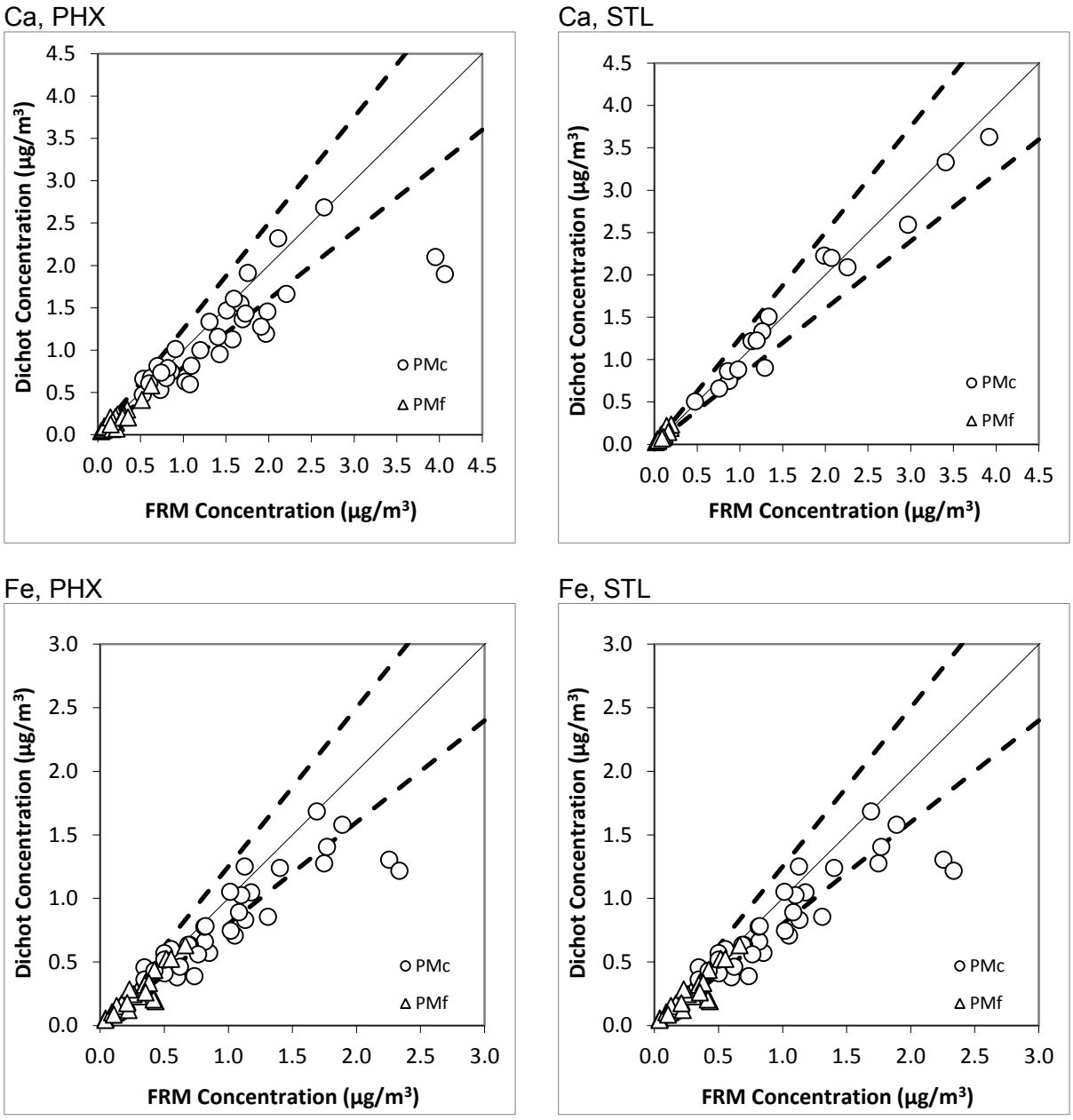

Figure 3-2 *(continued)*. Scatter plots of PM_f and PM_c concentrations from dichot (y-axis) and FRM (x-axis) at Phoenix (left column) and St. Louis (right column) for S, Zn, Ca, and Fe. Solid lines are the 1:1 lines and dashed lines indicate the ± 20% difference between measurements.

3.3 Attenuation of X-Ray Intensity for Light Elements

Measurement error can arise from both sampling errors and analytical errors. A potentially significant source of analytical error for PM_c elements is X-ray attenuation during XRF analysis (self-attenuation). This error is not captured in the collocated dichot comparisons and is only indirectly captured in the dichot-to-FRM comparisons through the dependence of the attenuation effect on the size distribution of collected particles.

RTI applied attenuation factors (A_i), calculated using proprietary software, to estimate attenuation-corrected mass loadings (m_i) from the XRF instrument-reported mass loadings ($m_{no\ corr,i}$):

$$m_i = \frac{m_{no\,corr,i}}{A_i} \qquad \textbf{(Eq. 3-1)}$$

Attenuation factors are in the range $A_i \leq 1$, and they vary with both element and PM size range (PM_f, PM_c, PM_{10}, and $PM_{2.5}$). For $A_i = 1$, there is no attenuation correction, while for $A_i < 1$, the attenuation-corrected mass loading is higher than the instrument-reported mass loading. These adjustments are made to the "raw" mass loadings on the filter reported by the XRF. RTI provided A_i for a subset of PM_{10} FRM samples and dichot major flow channel (PM_f filter) and minor flow channel (PM_c filter) samples. $PM_{2.5}$ FRM attenuation factors are identical to the dichot PM_f attenuation factors. For $PM_{2.5}$ FRM, PM_{10} FRM, and dichot PM_f samples, the attenuation factor linearly propagates through the calculation of ambient concentrations. For dichot PM_c, however, the dichot minor flow attenuation factors do not linearly propagate through the calculation of ambient calculations because the dichot minor flow channel mass loadings are corrected for fine particle intrusion.

Attenuation factors are specific to each sample (Gutknecht et al., 2010) and are automatically generated and applied by the signal processing software. RTI provided the uncorrected mass loadings for a subset of samples and back-calculated the sample-specific attenuation factors. The results are summarized in **Table 3-5**. **Figure 3-3** demonstrates that samples selected for the dichot minor flow channel were well distributed over the observed range of gravimetric mass loadings. Attenuation factors were unity for all elements with atomic numbers (Z) greater than 20. For each element and sample type, the standard deviation of the sample-specific attenuation factors was relatively small, so the arithmetic mean attenuation factor is deemed representative of all samples. **Figure 3-4** shows the mean attenuation factors stratified by element and sample type.

Because of the physics of self-attenuation, coarse particles are affected more than finer particles. Since PM_{10} includes both PM_c and PM_f, the attenuation factors for PM_{10} should be intermediate between those of PM_c and $PM_{2.5}$. Thus, for any element, attenuation factors occur in the order $APM_c < APM_{10} < (APM_{2.5} = APM_f)$. When comparing attenuation results for PM_c with the dichot vs. the FRM (i.e., PM_{10}-$PM_{2.5}$ vs. PM_c [dichot]), the intrusion of PM_f into the PM_c deposit must be taken into account.

Table 3-5. Average attenuation factors (A) back-calculated by RTI for a subset of samples.

Element	Z	Dichot Major Flow Channel (PM_f), *N*=13		Dichot Minor Flow Channel (PM_c), *N*=6		PM_{10} FRM, *N*=9	
		N > MDL	*A*	*N* > MDL	*A*	*N* > MDL	*A*
Na	11	12	0.96 ± 0.02	6	0.44 ± 0.00	8	0.51 ± 0.00
Mg	12	11	0.97 ± 0.01	6	0.46 ± 0.00	7	0.54 ± 0.00
Al	13	12	0.98 ± 0.01	6	0.51 ± 0.00	7	0.58 ± 0.00
Si	14	12	0.99 ± 0.01	6	0.57 ± 0.00	8	0.61 ± 0.00
P (phosphorus)	15	3	0.99 ± 0.00	5	0.70 ± 0.00	7	0.84 ± 0.00
S	16	12	0.99 ± 0.00	6	0.85 ± 0.00	8	0.96 ± 0.01
Cl	17	12	0.99 ± 0.00	6	0.79 ± 0.00	7	0.85 ± 0.00
K	19	13	1.00 ± 0.00	6	0.87 ± 0.00	8	0.90 ± 0.00
Ca	20	12	1.00 ± 0.00	6	0.86 ± 0.00	8	0.88 ± 0.00
--	>20	12	1.00 ± 0.00	6	1.00 ± 0.00	7	1.00 ± 0.00

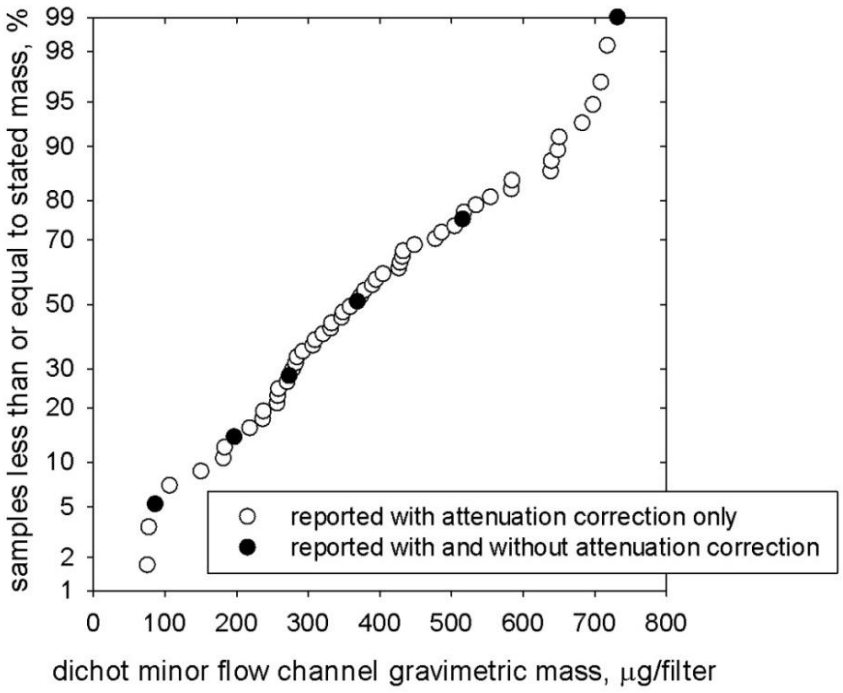

Figure 3-3. Cumulative distribution of gravimetric mass concentrations for all dichot sampler minor flow channel (PM_c) samples that were analyzed by XRF (open circles) and the six samples with mass loadings reported by RTI both with and without attenuation correction (closed circles). The sample shown at the 99th percentile was the sample with the highest mass loading.

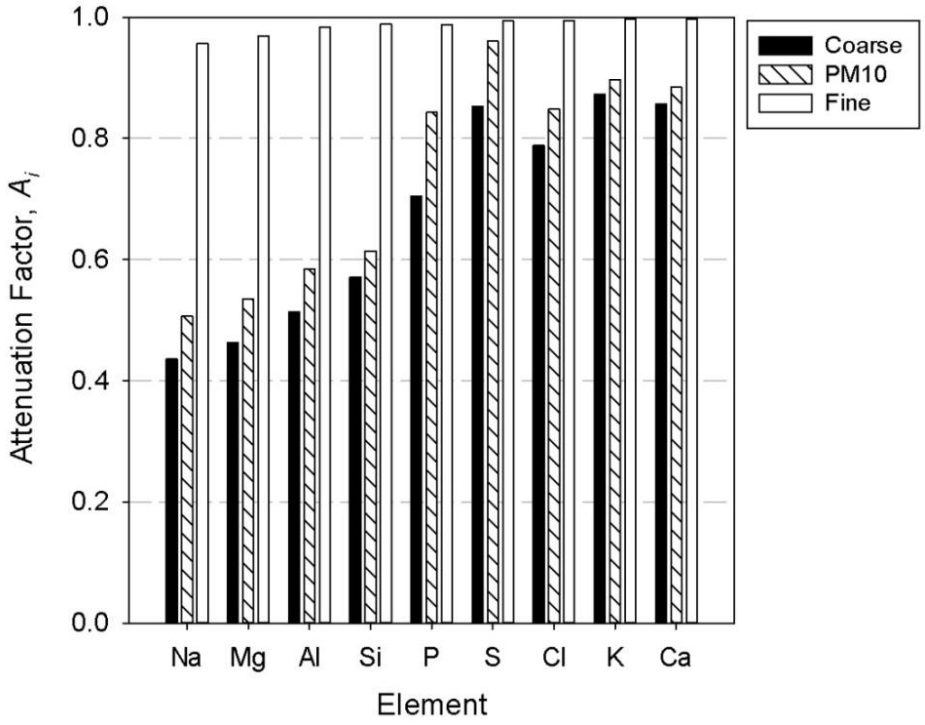

Figure 3-4. Attenuation factors for dichot minor flow channel samples (Coarse), PM_{10} FRM samples (PM_{10}), and dichot major flow channel samples (Fine).

In addition to the elemental concentrations reported for elements with $Z \leq 20$, because Al, Si, and Ca are typically included in the crustal material estimation and mass closure calculations, the corrections for self-attenuation affect the total PM concentration assigned to crustal material. For example, throughout this study, crustal PM (also called "resuspended soil oxides") has been estimated using the standard formula applied to IMPROVE network data, which includes terms for Al, Ca, Fe, Si, and Ti (see Section 6). Assuming the mean attenuation factors reported in Table 3-5 are applicable to all samples, **Figure 3-5** shows the impact of the applied attenuation factors on the crustal PM_c mass concentration estimates. Because the attenuation factors are unity for Fe and Ti, attenuation corrections affect only Al, Si, and Ca. Attenuation-corrected crustal PM_c mass concentrations are approximately 50% greater than the uncorrected mass concentrations. Corrections for self-attenuation have been applied throughout this study; in the absence of these corrections, the estimated crustal PM_c mass concentrations would be considerably lower.

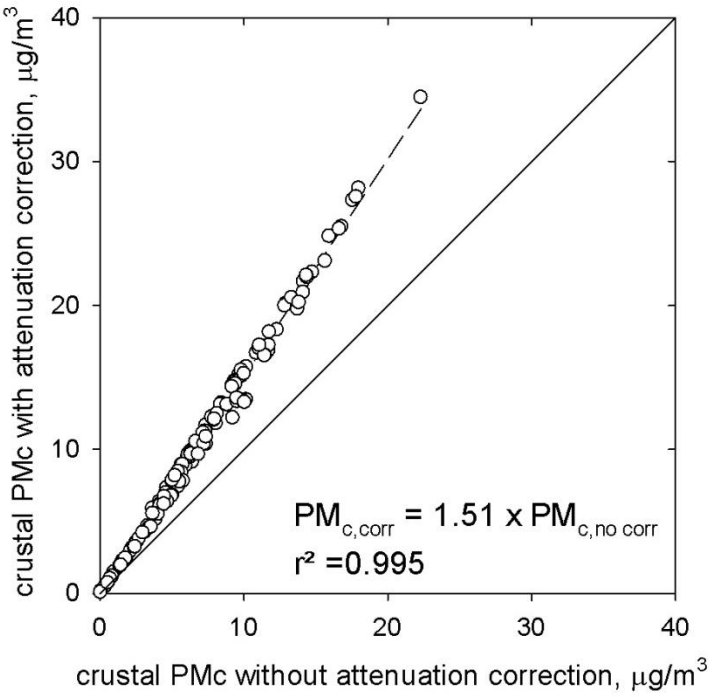

Figure 3-5. Estimated crustal PM_c mass concentrations with (*y*-axis) and without (*x*-axis) corrections for self-attenuation applied to the dichot sampler data.

3.4 XRF versus ICP-MS Measurements and Implications

To assess the adequacy of the attenuation factors being applied to the RTI XRF results, filters from 18 sampling events (10 from Phoenix, 8 from St. Louis) were selected for elemental analysis at RTI using both XRF and ICP-MS. ICP-MS was chosen as an independent "referee" method because of its sensitivity and immunity to the attenuation effect that is seen in XRF. The 10 sets of filters from Phoenix exhibited a broader range of crustal species concentrations than those from St. Louis. Samples were analyzed by XRF and then digested for analysis by ICP-MS using a microwave-assisted, mixed acid extraction method[2] to get the more difficult metals into solution (e.g., Al, Si, Mg, Fe, and Cr).

Figure 3-6 shows the dichot PM_c data for Al with A = 0.51 for XRF and no adjustments to the ICP-MS data. The oblique solid line represents 1:1 agreement between *x* and *y*. The sample within the square was an outlier for many elements and has been excluded from the remainder of the analysis. Al concentrations by ICP-MS are biased high, and a reduced major axis (RMA) regression[3] of ICP-MS concentration on XRF concentration has intercept

[2] Microwave-assisted digestion was performed on the filters using 2.5 mL nitric acid, 2.5 mL hydrochloric acid, and 0.5 mL hydrofluoric acid. (This digestion matrix is more aggressive than the 8% HCl/3% HNO_3 matrix recommended for analysis of $PM_{2.5}$ samples on Teflon filters (RTI, 2010).) A two-step digestion protocol was conducted using a CEM MARS5 unit, with the first step a 15-minute ramp to 100°C at 400W, followed by a 20-minute ramp to 200°C at 1600W. The pressure limit was 800 psi for both steps. Deionized water was used to bring the contents to a final volume of 50 mL. Analysis was conducted using a Thermo X-Series II ICP-MS with a collision cell and cell gas 10% hydrogen and 90% helium.

[3] Reduced major axis regression is an orthogonal regression method. Smith (2009) discusses the use of ordinary least squares and reduced major axis regressions.

0.88 ± 0.27 µg/m^3, which is statistically greater than zero at the 95% confidence level. This intercept value implies background contamination for the ICP-MS measurement (as described below). The slope of 0.75 ± 0.16 is less than unity and implies that the attenuation factor applied to the XRF data is too small (i.e., the data are overcorrected).

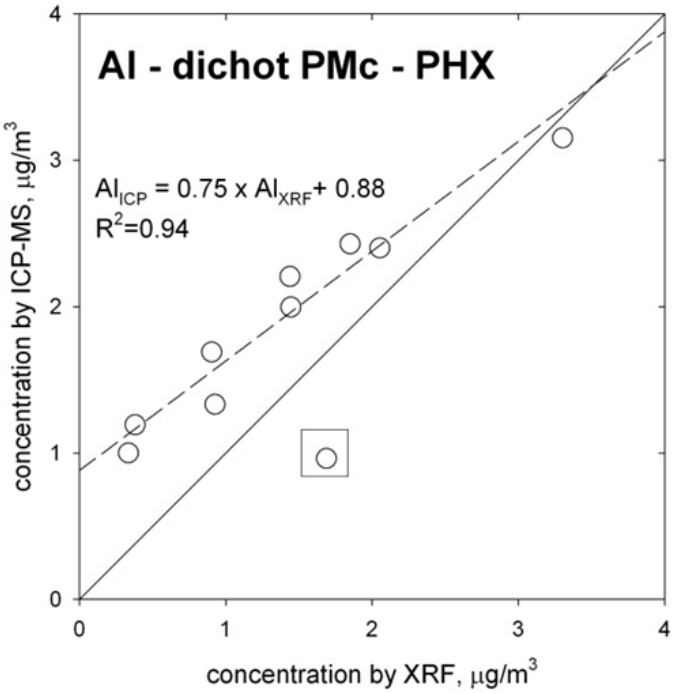

Figure 3-6. PHX dichot PM_c aluminum concentrations by XRF (A = 0.51) and ICP-MS.

Four field blanks (whole 47 mm Teflon filters), extracted and analyzed by ICP-MS along with the ambient samples, revealed high background levels for several elements, including Al. The mean and median Al field blank effective concentrations (assuming 24 m^3 air volume sampled) were equal to 1.4 and 1.2 µg/m^3, respectively. These concentration values are consistent with the intercept in Figure 3-6 (indeed, are modestly higher than the intercept of 0.88 ± 0.27 µg/m^3) and suggested the presence of significant filter contamination for certain elements. Given that high blank levels were observed for ICP-MS but not XRF, our hypothesis was that certain elements are present in the filter outside the XRF beam zone, with the likely sources being the adhesive that attaches the support ring to the membrane filter, or the ink used to stamp the filter ID number onto the support ring.

RTI subsequently analyzed by ICP-MS seven clean filters with the support ring first removed from the membrane; these components (membrane versus support ring) were separately digested and analyzed. **Table 3-6** shows the effective concentration values for the membrane, support ring, and also the four field blanks. The support ring has elevated concentrations for several elements, including Al. Another possible confounder when comparing ICP-MS to XRF data is the recovery of elements from the sample during the digestion step that precedes analysis by ICP-MS.

Table 3-6. ICP-MS analysis of laboratory blanks with the membrane separated from the support ring (with adhesive) and of field blanks. For each cell, the top row is the median and the bottom row is the mean and standard deviation. Values are concentrations reported in μg/m^3 for an effective air volume sampled of 24 m^3 (16.7 LPM for 24 hours).

Element	Laboratory Blanks (N = 7)		Field Blanks (N = 4)
	Membrane	Support Ring	
Na	0.003 0.003 ± 0.001	0.294 0.271 ± 0.041	0.418 0.493 ± 0.159
Mg	0.003 0.003 ± 0.001	0.428 0.419 ± 0.026	0.378 0.379 ± 0.116
Al	0.004 0.004 ± 0.004	1.152 1.088 ± 0.111	1.163 1.406 ± 0.525
Si	-0.018 0.004 ± 0.081	1.271 1.414 ± 0.590	1.660 2.647 ± 2.176
P	-0.002 -0.004 ± 0.006	0.251 0.242 ± 0.018	0.246 0.253 ± 0.018
S	-0.011 -0.011 ± 0.005	0.030 0.032 ± 0.004	0.091 0.140 ± 0.134
K	0.004 0.006 ± 0.005	0.009 0.009 ± 0.002	0.028 0.127 ± 0.214
Ca	-0.021 -0.017 ± 0.009	0.229 0.210 ± 0.040	0.334 0.711 ± 0.812
Fe	0.003 0.009 ± 0.016	0.007 0.011 ± 0.008	0.049 0.246 ± 0.422
Ti	-0.001 0.000 ± 0.001	0.013 0.016 ± 0.008	0.012 0.012 ± 0.002
Zn	-0.001 -0.001 ± 0.001	0.027 0.034 ± 0.024	0.025 0.026 ± 0.022

Analysis of a Standard Reference Material (SRM) is commonly used to characterize recoveries. RTI analyzed five samples (each nominally 10 mg) of NIST SRM 1648a, which is an urban particulate matter reference material. One sample had anomalous recoveries for several elements and was excluded from the data analysis. **Table 3-7** summarizes the results. Recoveries were about 90% for several elements of interest to this study, such as Al and Ca.

Table 3-7. Recoveries for urban particle matter NIST standard reference material for the sample digestion protocol and ICP-MS analysis used in this study. S.E. is the standard error of the mean.

Element	SRM 1648a Recovery (%) (N = 4)[a]	
	Median	Mean ± S.E.
Na	90	89 ± 1
Mg	91	90 ± 2
Al	94	91 ± 4
S	88	89 ± 1
K	91	90 ± 2
Ca	89	89 ± 2
Ti	69	71 ± 5
V (vanadium)	79	96 ± 27
Cr	73	72 ± 5
Mn	81	82 ± 3
Fe	91	92 ± 1
Co	81	81 ± 2
Ni (nickel)	103	100 ± 4
Cu	83	83 ± 2
Zn	119	113 ± 8
As (arsenic)	103	102 ± 2
Se (selenium)	123	116 ± 8
Sr	96	95 ± 2
Ag (silver)	110	108 ± 9
Cd (cadmium)	111	107 ± 5
Sb (antimony)	95	91 ± 7
Pb (lead)	86	86 ± 2

[a] Excludes one run that exhibited low recoveries for Al, Mg, K, Zn, and Se, and high recoveries for V and As.

In light of these results, the following approach was taken to evaluate the XRF attenuation factors. For a given element analyzed by both XRF and ICP-MS:

1. For the dichot minor flow channel filters (i.e., PM_c filters), use the XRF attenuation factors A_i reported in Table 3-5 and Equation 3-1 to back-calculate the XRF mass loadings without correction for self-attenuation, $m_{no\ corr,i}$.
2. Estimate a revised attenuation factor A_i' and use Equation 3-1 to calculate revised mass loadings m_i'. Calculate XRF PM_c elemental concentrations, PM_c', using the revised mass loadings for the PM_c filter data. Attenuation factors for the dichot minor flow channel filters (i.e., PM_f filters) are close to unity (Table 3-5) and were not revised. Thus, no

adjustments were made to the PM_f concentrations that are used to correct the PM_c concentrations for fine particle intrusion into the dichot PM_c filter channel.

3. Blank-correct the ICP-MS mass loadings data using the laboratory blanks results (i.e., the mass loadings data underlying Table 3-6). Mean loadings from the support ring and membrane were summed and subtracted from the dichot PM_c and PM_f filter mass loadings.
4. Calculate ICP-MS PM_c elemental concentrations using the blank-corrected dichot PM_c and PM_f filter mass loadings.
5. Calculate the square difference between the PM_c concentration values for blank-corrected ICP-MS data and XRF data with revised attenuation factors (PM_c').
6. Calculate the sum of squared differences (SOSD) over the nine samples and iterate on the revised attenuation factor A_i' to determine the best-fit A_i' that minimizes the SOSD.
7. Repeat the above steps, adding to Step 5 an adjustment for the ICP-MS recoveries using the mean recoveries data reported in Table 3-7.

Figure 3-7 shows the PM_c aluminum concentrations after blank-correcting the ICP-MS data using the mean laboratory blank value in Table 3-6 (support ring plus membrane) and using no adjustment for XRF attenuation (A = 1, left panel) and the best-fit XRF attenuation factor (A = 0.73, right panel). For Al, the best-fit attenuation factor was 0.73, assuming 100% recovery for the digestion and ICP-MS analysis. This attenuation factor is 43% higher than the value of 0.51 used by RTI (Table 3-5) and would decrease the RTI-reported PM_c aluminum concentrations by about 30%. If the Al recovery of 91% (Table 3-7) is included in the analysis, the best-fit attenuation factor is 0.63 and decreases the RTI-reported PM_c aluminum concentrations by about 20%.

Table 3-8 shows the best-fit attenuation factors for the light elements. Best-fit attenuation factors (assuming 100% recovery for the ICP-MS analysis) are in good agreement with the RTI-reported values for Na and S, about 5% higher for Ca, and 20% to 45% higher for (in increasing order) K, P, Si, and Al. The best-fit attenuation factor for K is greater than unity; this suggests that another source of error is present; such as poor digestion recovery or calibration bias for XRF or ICP-MS. Silicon has a very low coefficient of linear correlation (r^2 = 0.07) and high RMS error (RMSE; 78%), which makes the results for silicon suspect. The best-fit attenuation factor for Mg is about 20% lower than the RTI-reported value. When recoveries for ICP-MS analysis are included, the best-fit attenuation factors are as much as 20% lower than the factors that are estimated assuming 100% recovery, but are still higher than the RTI-reported factors for Al, K, and Ca (recovery data are not available for Si and P).

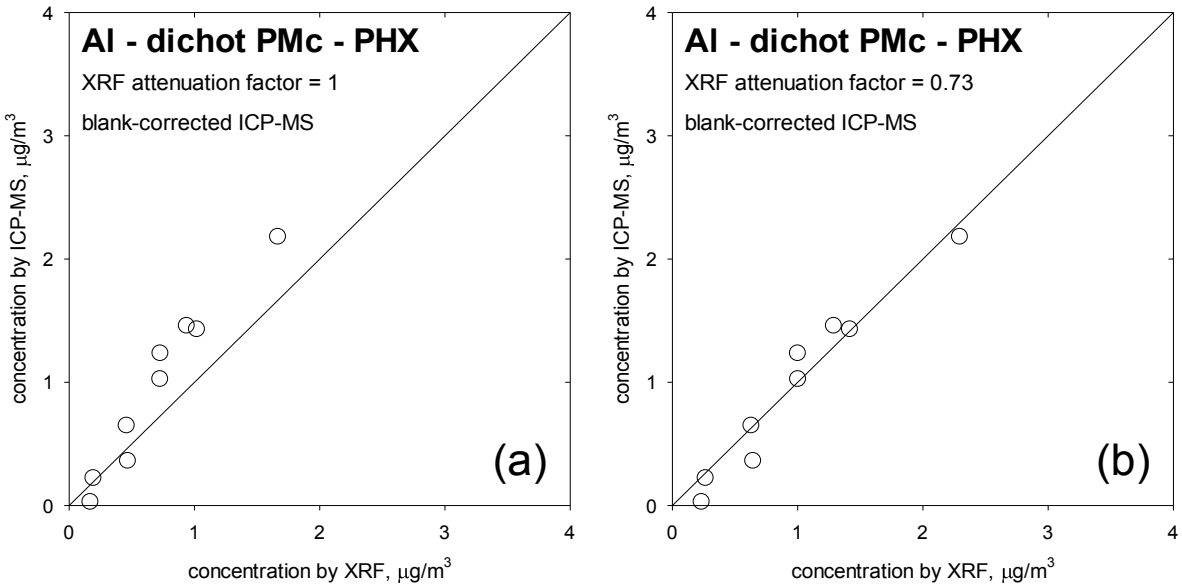

Figure 3-7. PHX dichot PM_c aluminum concentrations by ICP-MS with blank correction (mean laboratory blank of 1.092 µg/m^3 from Table 3-6) and assuming 100% recovery, and by XRF with (a) XRF attenuation factor of unity; and (b) best-fit attenuation factor to reconcile the XRF and ICP-MS data.

Table 3-8. Attenuation factors for dichot PM_c aluminum at PHX. Values in parenthesis for the best-fit attenuation factor with 100% recovery are the ranges for SOSD at 110% of the minimum. RMSE is divided by the mean concentration. Elements in **bold** appear in the equation used to estimate crustal PM.

Element	*Z*	Dichot PM_c Filter Attenuation Factor			Metrics for best-fit *A* with 100% recovery	
		A (RTI)	*A* (best-fit, 100% recovery)	*A* (best-fit, recovery adj.)	r^2	*RMSE* (%)
Na	11	0.44	0.44 (0.40-0.47)	0.37	0.81	34
Mg	12	0.46	0.39 (0.36-0.41)	0.31	0.88	24
Al	13	**0.51**	**0.73** (0.70-0.75)	0.63	0.95	16
Si	14	**0.57**	**0.78** (0.63-1.01)	--	0.07	78
P	15	0.70	0.90 (0.81-1.00)	--	0.79	48
S	16	0.85	0.87 (0.85-0.90)	0.87	0.96	16
Cl	17	0.79	NR	NR	NR	NR
K	19	0.87	1.06 (1.04-1.08)	0.96	0.98	9
Ca	20	**0.86**	**0.91** (0.87-0.95)	0.91	0.95	16

NR = analyte not resolved by ICP-MS
-- = no recovery data

The response surface for the minimization (SOSD versus A) was examined by calculating the attenuation factors for 110% of the minimum SOSD. The attenuation factor ranges, shown in Table 3-8 in parenthesis after the best-fit *A* assuming 100% recovery, have relatively narrow bounds except for P and Si. Attenuation factors were also calculated by excluding each data point one at a time ("leave one out" analysis) and minimizing the SOSD. In this case, the range of attenuation factors for Al was 0.70 to 0.75.

These preliminary results suggest that the RTI-reported dichot PM_c filter attenuation factors for some crustal elements (e.g., Al, Ca, and possibly Si) are perhaps too low and thus the attenuation-corrected concentrations overestimate the true concentrations. The software used by RTI to apply attenuation factors should be examined to tabulate the assumptions being made about particle size distribution and particle composition. These assumptions could be adjusted within reasonable ranges to assess whether a better fit between XRF and ICP-MS can be achieved. The comparison between XRF and ICP-MS should be repeated for a larger data set, with samples collected at sites that have high crustal loadings, and ideally including coarse PM from different sources, such as desert dust and agricultural dust. XRF should be performed on each filter, and then the membrane should be separated from the support ring prior to digesting the particle-laden membrane for ICP-MS analysis. This approach will dramatically decrease the blank levels and thus reduce the uncertainty introduced by the blank correction. Samples suitable for particle size analysis, e.g., by electron microscopy, should be collected in parallel so the assumptions used to develop the attenuation factors can be evaluated.

3.5 Variation in Crustal Composition

The defining feature of the PM_c elemental data is the high concentrations of species associated with crustal material. Since crustal species are the dominant component of PM_c mass, the variation of crustal composition between sites and over the course of the study was examined. Seasonal variation of crustal composition could be expected if there was influence of dust from long-range transport (e.g., Asian dust event) rather than locally generated dust, and if the mix of regional and local dust varied across seasons. **Figure 3-8** shows a simple visualization of the crustal composition, comparing the fraction of Si, Fe, and Ca to the sum of these elements. At both sites, there is little temporal variability in the ratio of these species. However, Si accounts for nearly twice the fraction of crustal mass measured at Phoenix compared to St. Louis, the latter having more mass from Ca. This finding is consistent with likely different soil composition at the two sites, with St. Louis having karst topography, which could lead to higher abundance of calcium in the crustal PM profile.

(a) Phoenix

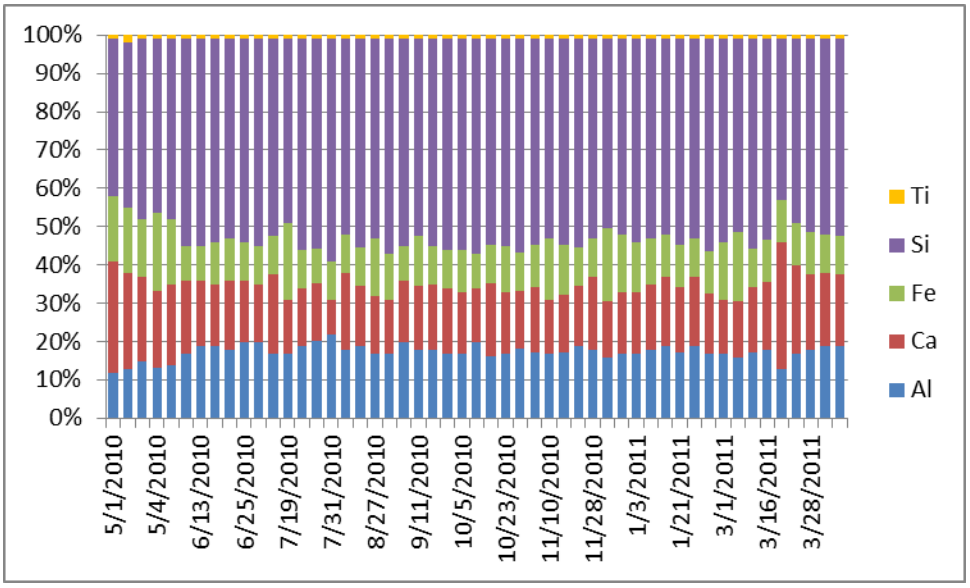

(b) St. Louis

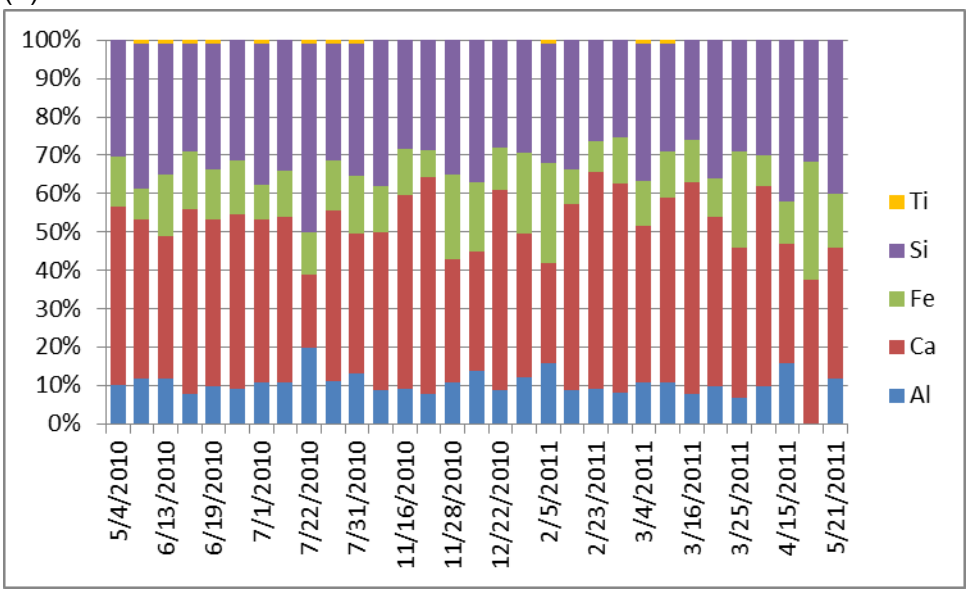

Figure 3-8. Simple visualization of major crustal elements: fraction of the sum of Ti, Si, Fe, Ca, and Al by element for primary dichot PM_c at (a) Phoenix (N = 51) and (b) St. Louis (N = 31).

4. Analysis of Carbon

After crustal species, carbon was the second largest contributor to PM_c mass, on average about 15% (see Section 2). Unlike crustal species, there is only marginal agreement between dichot PM_c and FRM $PM_{10-2.5}$ carbon measurements; most points were beyond a ±20% difference (Section 4.1), though without the bias towards the FRM that was seen with crustal species and gravimetric mass.

Analysis of OC and EC by thermal fraction indicate that the composition of OC and EC is different between Phoenix and St. Louis, though there is little difference at each site between the fine and coarse OC and EC composition by thermal fraction (Section 4.2).

Carbonate was measured for a subset of samples (Section 4.3). PM_f carbonate was below the detection limit for all samples analyzed. In contrast, PM_c carbonate was on average 6% of PM_c gravimetric mass at Phoenix and 12% of PM_c gravimetric mass at St. Louis. Carbonate carbon was on average 9% of PM_c total carbon (TC) at Phoenix and 14% of PM_c TC at St. Louis. Thus, at these two sites, carbonate significantly contributes to gravimetric mass and total carbon.

Unlike fine PM, OC mass loadings on backup filters for the dichot minor flow (used to calculate PM_c concentrations) are statistically indistinguishable from the trip and field blanks (Section 4.4). This finding, together with other analyses presented in this section, lead to the conclusion that there is very little volatile OC in the coarse PM size range, and thus a low capacity for negative artifacts. Since coarse OC may comprise biological material, 54 samples for biological analysis were collected between February and May 2011 (see Section 4.5). Concentrations of biomarkers (proteins, (1,3)-β-D-glucans, and endotoxin) were relatively low compared to the OC, with a median PM_c glucan concentration of about 0.2 ng/m^3, protein concentrations of about 0.08 µg/m^3 in both Phoenix and St. Louis, and endotoxin concentrations of 0.017 EU/m^3 at St. Louis; endotoxin values at Phoenix were well outside typical variability and were suspect.

4.1 Total Carbon Comparisons Between Dichot and FRM Samplers

Figure 4-1 shows a comparison of total carbon (TC; sum of OC and EC) as measured in each size fraction by dichot and FRM. Most of the measurements for $PM_{2.5}$ at both sites are within 20% (as indicated by dashed lines on the plot), and are well correlated (r^2 varying from 0.91 to 0.96). PM_{10} measurements similarly have a high correlation (greater than 0.90), and most measurements are within 20%. However, the dichot PM_c and FRM $PM_{10-2.5}$ measurements have lower correlations than either $PM_{2.5}$ or PM_{10} measurements, with more points beyond ±20% difference. At each site, each of the dichots yields different correlation statistics when compared with the FRM measurements (i.e., correlation of dichot to FRM varies between 0.64 and 0.84 at St. Louis and between 0.67 and 0.84 at Phoenix, depending on which dichot is compared to the FRM). However, the striking feature is that PM_c total carbon does not exhibit the dichot-to-FRM bias that is prevalent for PM_c gravimetric mass and the crustal species (Figure 2-1 and Tables 3-1 and 3-3).

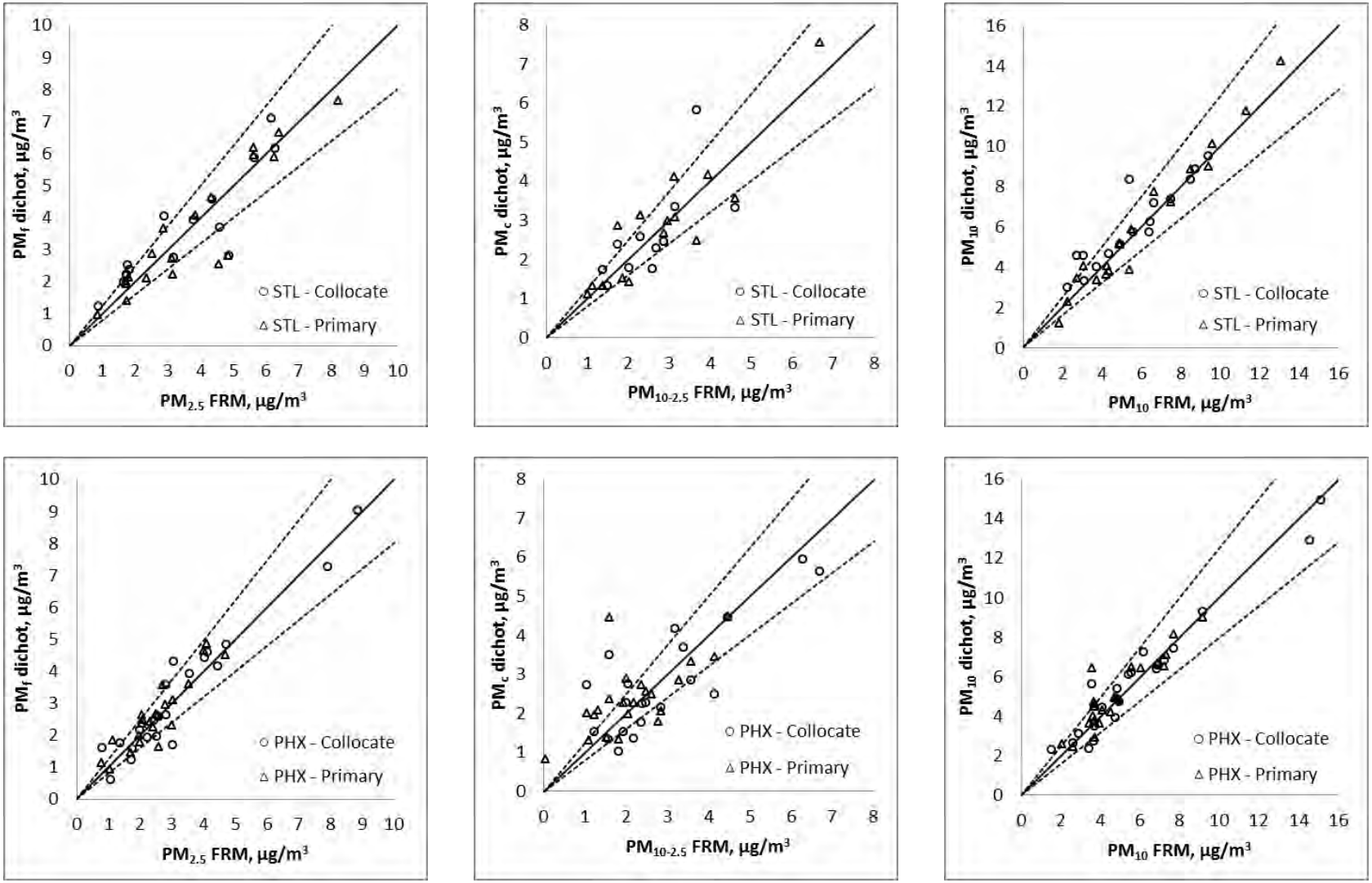

Figure 4-1. Dichot versus FRM total carbon concentrations for St. Louis (top row) and Phoenix (bottom row) for $PM_{2.5}$ (left), $PM_{10\text{-}2.5}$ (center), and PM_{10} (right). Triangles are data from the primary dichot sampler and circles are data from the collocated dichot sampler. Diagonal lines are 1:1 (solid) and ±20% of 1:1 (dashed).

4.2 Thermal Fraction Analysis (OC/EC Split)

In Section 3.6, the variation in PM_c crustal composition between sites was examined. In this section, the variation in carbon fractions across sites and size fractions is examined. **Figure 4-2** shows the carbonaceous PM average concentration values by site, size fraction, and carbon subfraction from the dichotomous samples. These data have not been adjusted for carbon artifacts. The average coarse PM total carbon concentration (height of the stacked bar) is nearly equal to the fine concentration in Phoenix and is less than the fine concentration in St. Louis. For both fine and coarse PM, the EC and OC concentrations are higher in St. Louis than in Phoenix.

Figure 4-3 shows the relative distribution of the organic carbon subfractions. For each size range, the distributions at Phoenix and St. Louis are quite similar. The fine PM has relatively higher OC1 and OC2 concentrations, whereas the coarse PM has relatively higher OC3 and OC4 concentrations. This suggests differences in the composition of organic carbon between the fine and coarse fractions at both sites.

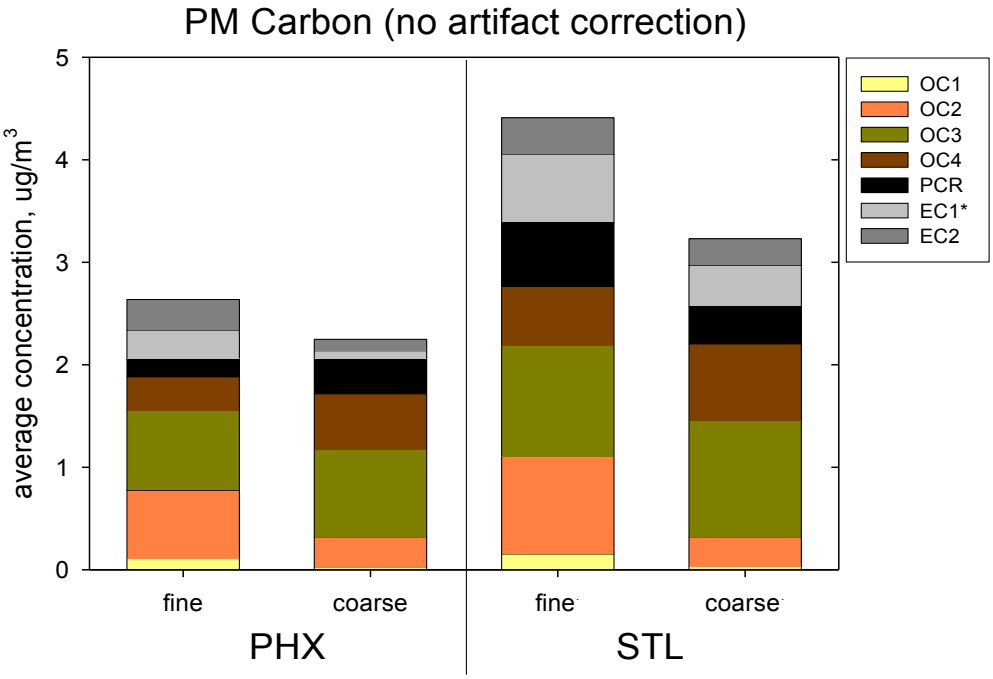

Figure 4-2. Carbonaceous PM average concentration values at Phoenix (N = 30) and St. Louis (N = 22). No artifact correction has been applied to these data. Concentration values are stratified by the IMPROVE protocol carbon subfractions, with PCR = pyrolytic carbon by the reflectance method and EC1* = EC1 – PCR. The average EC3 concentration was zero for all cases and is not shown.

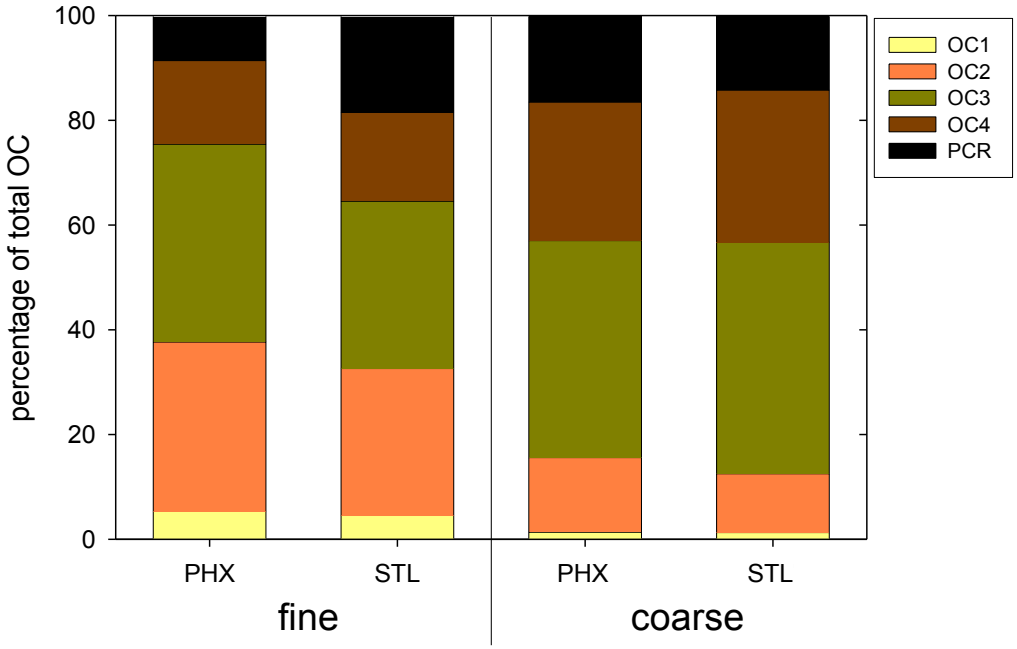

Figure 4-3. Distribution of organic carbon average concentration values at Phoenix (N = 30) and St. Louis (N = 22). No artifact correction has been applied to these data. Concentration values are stratified by the IMPROVE protocol carbon subfractions, with PCR = pyrolytic carbon by the reflectance method.

4.3 Carbonate Concentrations

Carbon can be present in ambient particulate matter as carbonate (CO_3^2). Assuming that carbonate decomposes at temperatures greater than 800°C, carbonate should not confound measurement of EC and OC used during TOA temperature protocols with maximum temperatures below 800°C (Chow and Watson, 2002). The maximum temperature for the IMPROVE_A protocol is 800°C. Carbonate in geological samples is most commonly present as calcium carbonate; its presence will bias low the estimate of crustal-derived PM using conventional soil estimation equations, which assume that calcium is present as calcium oxide (CaO).

The Desert Research Institute (DRI) used a TOA protocol with sample acidification to analyze selected quartz fiber filter samples for carbonate. Initially, dichot filters from 15 sampling events (six from Phoenix and nine from St. Louis) were selected, which reflected a range of Si/Ca ratios, based on the hypothesis that differences in Si/Ca ratio may be indicative of differences in PM_c composition, and thus the amount of calcium carbonate ($CaCO_3$) in a given sample. For PM_f, only one sample exceeded the reported carbonate uncertainty value of 0.17 µgC/m^3—a Phoenix sample with PM_f carbonate concentration of 0.18 µg C/m^3.[4, 5] In

[4] Carbonate concentrations are reported as carbonate carbon, i.e., µgC/m^3.

[5] The 3σ MDL reported by DRI, based on a standard set of laboratory blanks, is 0.93 µgC/m^3, which corresponds to 0.51 µgC/m^3 for PMf and 0.46 µgC/m^3 for PM_c. The error structure has the form $Unc_i = \sqrt{(CV \times C_i)^2 + (MDL/3)^2}$, where Unc_i is the uncertainty for sample i, CV is the coefficient of variance from replicate analyses, and C_i is the sample concentration. Thus, at low concentrations, the uncertainty is MDL/3.

contrast, for this relatively small set of samples, the dichot PM_c carbonate was on average 0.43 µg C/m^3 for Phoenix and 0.36 µg C/m^3 for St. Louis. Dichot PM_c carbonate corrections for fine particle intrusion into the minor flow channel were at most 5%, so no additional dichot PM_f filter samples were analyzed.[6]

Subsequently, 12 collocated quartz filters sampling events were selected (six from each site) with carbonate analysis on both dichot PM_c filters; PM_{10} and $PM_{2.5}$ FRM filters were analyzed for six of these samples. Dichot PM_c filters from an additional 42 mass balance protocol sampling events were analyzed (31 from Phoenix and 11 from St. Louis).

Figure 4-4a shows the PM_c carbonate data for collocated dichot samples. The collocated precision was statistically indistinguishable between the sites, with a pooled collocated precision of 0.053 µg C/m^3 (22% relative precision). This precision is much better than the laboratory-reported uncertainty of 0.15 µg C/m^3 for low carbonate concentrations, and suggests that the reported MDL of 0.46 µg C/m^3 is conservative. **Figure 4-4b** compares the PM_c carbonate from the dichots (mean of the collocated values) to FRM by difference (i.e., $PM_{10-2.5}$) for the six samples for which collocated dichot and FRM filters were analyzed for carbonate. The precision of 0.072 µg C/m^3 (23% relative precision) is only slightly degraded compared to the collocated dichots. The ratio of means is 1.00, which demonstrates no bias between the dichot and FRM carbonate measurements, similar to results for total carbon; this result is in sharp contrast to gravimetric mass and species measurements from the Teflon filters, which showed higher loadings for FRM $PM_{10-2.5}$ than for dichot PM_c.

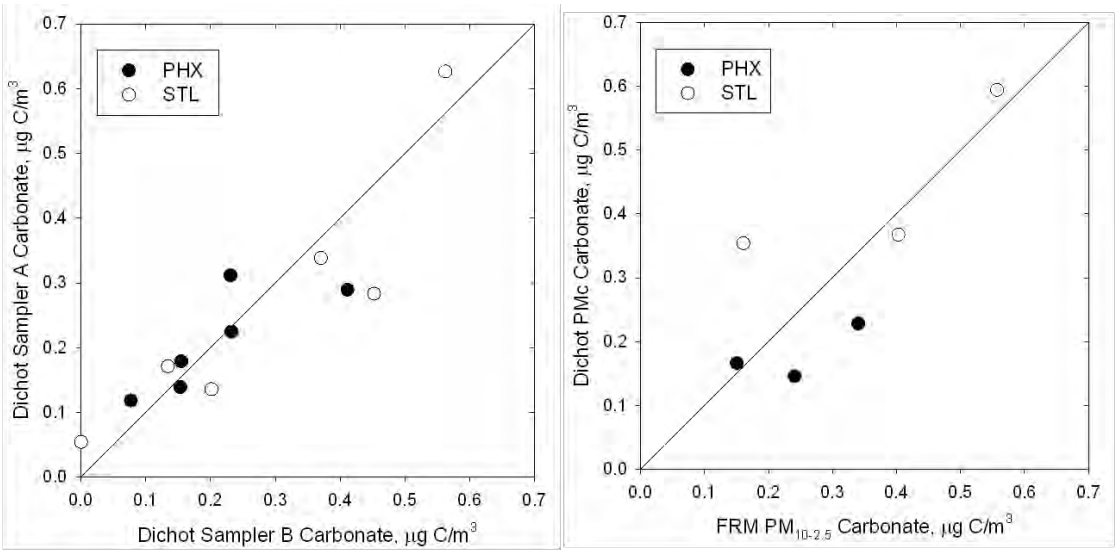

Figure 4-4. PM_c carbonate from (a) collocated dichots and (b) mean collocated dichot versus FRM-by-difference.

[6] For the remainder of this section, dichot PM_c carbonate data do not include a correction for fine particle carbonate.

PM_c carbonate from the mass balance protocol sampling events was compared to PM_c mass, carbon (TC, EC-TOR, and OC-TOR), major crustal species (Al, Ca, Fe, Si) and S. Correlation coefficients (*r*) were statistically significant at the 95% confidence level (CL) for all comparisons except EC in Phoenix and OC and S in St. Louis. However, at both sites, the carbonate was most highly correlated with PM_c Ca (r = 0.85 for Phoenix, r = 0.97 for St. Louis); in Phoenix, none of the other comparisons exceeded r = 0.7.

Figure 4-5 shows the relationship between PM_c carbonate and PM_c calcium on a molar basis; data shown in Figure 4-5 include 37 samples from Phoenix and 20 samples from St. Louis. Carbonate can on average explain two-thirds of the PM_c calcium, and there are virtually no samples with a carbonate-to-calcium molar ratio greater than one. For the subset of these sampling events with FRM $PM_{10-2.5}$ data available, PM_c carbonate can explain 67% of the $PM_{10-2.5}$ Ca in St. Louis (N = 12), but only 52% of the $PM_{10-2.5}$ calcium in Phoenix (N = 24). With the majority of calcium in $CaCO_3$ rather than CaO form, using the typical equation for calculating crustal mass (see Section 6) likely underestimates the contribution from crustal material. However, this result should be qualified by the differences in particle losses between the dichot Teflon and quartz filters used to measure calcium and carbonate, respectively, since a larger correction of fine particle intrusion is used for calcium than for carbonate.

The grand mean PM_c carbonate concentrations were 0.23 µg C/m^3 for Phoenix (N = 43) and 0.27 µg C/m^3 for St. Louis (N = 26). The molecular weight of carbonate is five times as great as the molecular weight of carbon. For those sampling events with PM_c mass available, the carbonate mass was, on average, 6% of the PM_c gravimetric mass in Phoenix (range 0% to 20%, N = 37) and 12% of the PM_c gravimetric mass in St. Louis (range 0% to 21%, N = 20).

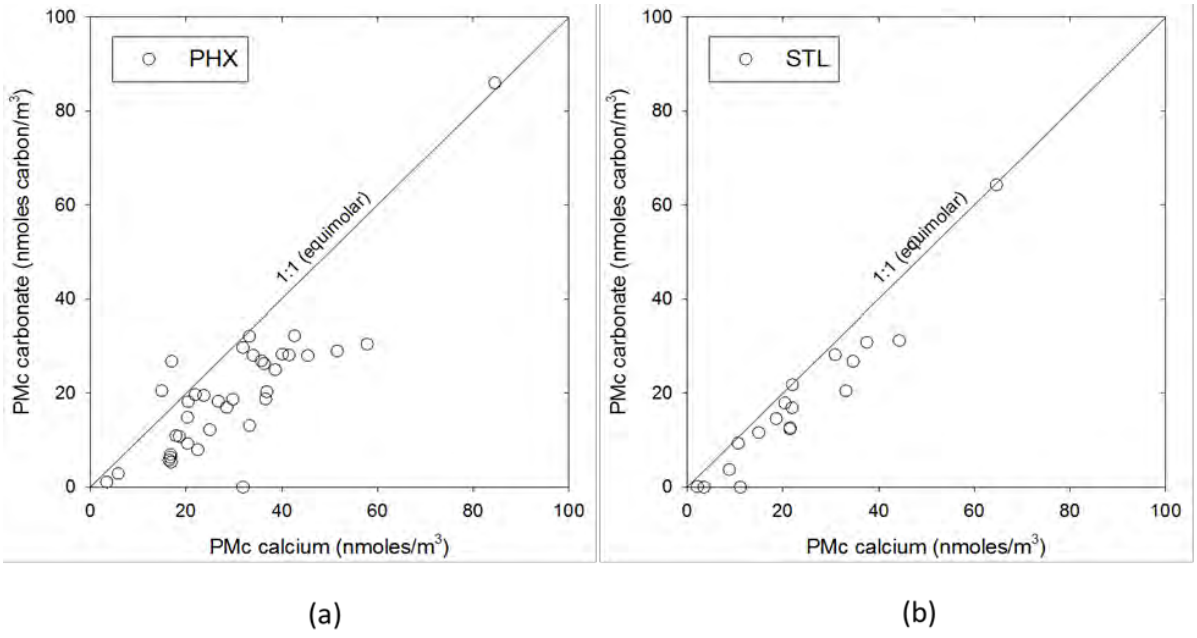

Figure 4-5. Relationship between dichot PM_c carbonate and dichot PM_c calcium expressed as molar concentrations in (a) Phoenix and (b) St. Louis.

Dichot PM_c carbonate mass was on average 5% of the FRM $PM_{10-2.5}$ mass in Phoenix (N = 24) and 11% of the FRM $PM_{10-2.5}$ mass in St. Louis (N = 12).

These results demonstrate that carbonate can be a major contributor to PM_c mass. For these data, PM_f carbonate was negligible, and measurement of carbonate on the dichot minor flow channel filter is adequate to characterize PM_c carbonate; i.e., no correction for fine particle intrusion appears necessary. While pure calcium carbonate decomposes at temperatures above 800°C, analysis conditions and matrix effects with other PM constituents might cause the carbonate carbon to decompose at lower temperatures (Chow and Watson, 2002). Thus, given the relatively large ratio of PM_c carbon present as carbonate to PM_c carbon present as EC and OC (averages of 9% in Phoenix and 14% in St. Louis), more work is needed to evaluate whether carbonate evolves during TOA by the IMPROVE_A protocol and thereby biases high the EC, OC, or both.

4.4 Carbon Artifacts

Filter-based sampling to quantify organic carbon in ambient particulate matter is prone to measurement artifacts. Positive artifacts can arise from the adsorption of vapor onto the sample (including the quartz filter), while negative artifacts can arise from the volatilization of collected particulate matter. The two major $PM_{2.5}$ monitoring networks deployed in the United States take different approaches to addressing these artifacts.

In the past, IMPROVE network OC data were adjusted on the assumption that the OC measured on backup quartz filters at a subset of sites is representative of the positive artifact at all sites in the network. Adjustments were derived and applied on a monthly basis. Although field blanks, trip blanks, and backup quartz filter blanks are collected by the CSN, the OC data currently reported for the CSN network are not adjusted for artifacts; the trip blanks, field blanks, and backup filter data are available to the user through EPA's AQS data base. A workgroup of EPA and IMPROVE technical experts was convened to explore OC artifact corrections in both the CSN and IMPROVE monitoring networks. The initial recommendation based on a series of exploratory analyses is to use monthly network-wide quartz filter field blanks for adjustment. Field blank filters are collected at all CSN sites and housed in the sampler for the entire duration of the sampling event. The field blanks are less variable over time and space, decrease the additive artifact, and do not over-correct by including the multiplicative factor. At the finalization of this report, the IMPROVE network has begun implementing these recommendations and the CSN plans to begin January 2015.

This section summarizes an analysis of carbon artifacts from this study. All samples collected for carbon analysis used a Q/Q filter sandwich. A subset of samples was analyzed for chemical speciation with carbon analysis performed at the DRI using the IMPROVE_A thermal-optical analysis protocol. This analysis focuses on organic carbon measured by optical reflectance (OC-TOR).

4.4.1 OC Trip Blanks and Field Blanks

OC loadings on trip blanks and field blanks provide a context for characterizing and interpreting OC on the front and backup filters. The blanks data were examined and the key results are summarized in this section, with additional details provided in Appendix D. Seven sets of trip blanks were analyzed by OC-TOR. Each set included two to four filters per site. The May 2010 data were excluded from the analysis because of data quality issues (discussed in Appendix D); after this date, there was evidence that the trip blanks data could be pooled across all samples and sites. The pooled trip blanks data have mean and median OC mass loadings of 5.4 $\pm$ 5.7 and 4.2 µg/filter, respectively (N = 44). These mass loadings are the same as the estimated IMPROVE_A analysis MDL for OC of 5.3 µg/filter.[7]

The same statistical analyses were performed for the seven sets of field blanks that were collected at the same times as the trip blanks. Each set included four to twelve filters per site, with the maximum case being front and back filters in the $PM_{2.5}$ FRM, PM_{10} FRM, and both channels of both dichot samplers. While in principle the sampler type and filter position (front versus back) could be treated as additional factors, their effects were deemed inconsequential, and samples pooled across these factors were treated as pseudo-replicates. As described in Appendix D, the site had a statistically insignificant effect, whereas the date had a statistically significant effect on OC mass loadings, even after removing the May 2010 data. The pooled field blanks data have mean and median OC mass loadings of 6.6 $\pm$ 5.5 and 5.2 µg/filter, respectively (N = 130).

Our interpretation of the blanks data concludes that (1) in May, which was a one-month intensive to shake down the field operations prior to the start of routine sampling in June, there were anomalously high trip blank and field blank mass loadings; and (2) for subsequent months, the trips blanks mass loadings were statistically indistinguishable, while the field blanks mass loadings decreased as the study progressed. The temporal behavior confounds the use of the 95th percentile OC mass loading as a robust estimate of the lower quantifiable limit (LQL) but it can be used as a conservative estimate. Excluding the May 2010 samples, the 95th percentile trip blank and field blanks mass loadings are each 19 µg/filter. The May 2010 measurements are not included in the results presented in the remainder of this section.

4.4.2 OC Mass Loadings on the Backup Filters

Backup filter OC mass loadings can arise from contamination and vapor adsorption during sampling. Adsorption can be from "native" vapor (semivolatile OC entering the sampler in the vapor phase) or semivolatile OC volatilized (desorbed) from particles on the front filter as a result of the filter face velocity and pressure drop across the filter during sampling. $PM_{2.5}$ and PM_{10} backup filters are exposed to the same flow rate (16.7 LPM) with incrementally more particulate matter OC on the PM_{10} front filter than on the $PM_{2.5}$ front filter. **Figure 4-6** shows the OC mass loading on the back filter for these two samplers. For both Phoenix and St. Louis, the data are scattered about the 1:1 line. The median $PM_{2.5}/PM_{10}$ OC ratios for the backup filters are

[7] Carbon analysis MDL values for this study were estimated by assuming the same MDL as the CSN network when expressed as µg/cm^2 filter area. Reported CSN network MDL values are 1.5 µg/filter for OC and 0.42 µg/filter for EC and were scaled using filter diameters of 25 mm for the CSN network and 47 mm for this study.

nearly equal to unity (1.02 and 1.10 for Phoenix and St. Louis, respectively). Nearly all OC mass loadings are greater than the 95th percentile trip blank, and several OC mass loadings are greater than the 95th percentile field blank. Based on these lines of evidence, there is no compelling evidence for coarse particle volatilization. In particular, the $PM_{2.5}$ and PM_{10} FRM backup filters have nearly identical OC mass loading, which means that coarse particle volatilization from the PM_{10} front filter is likely negligible.

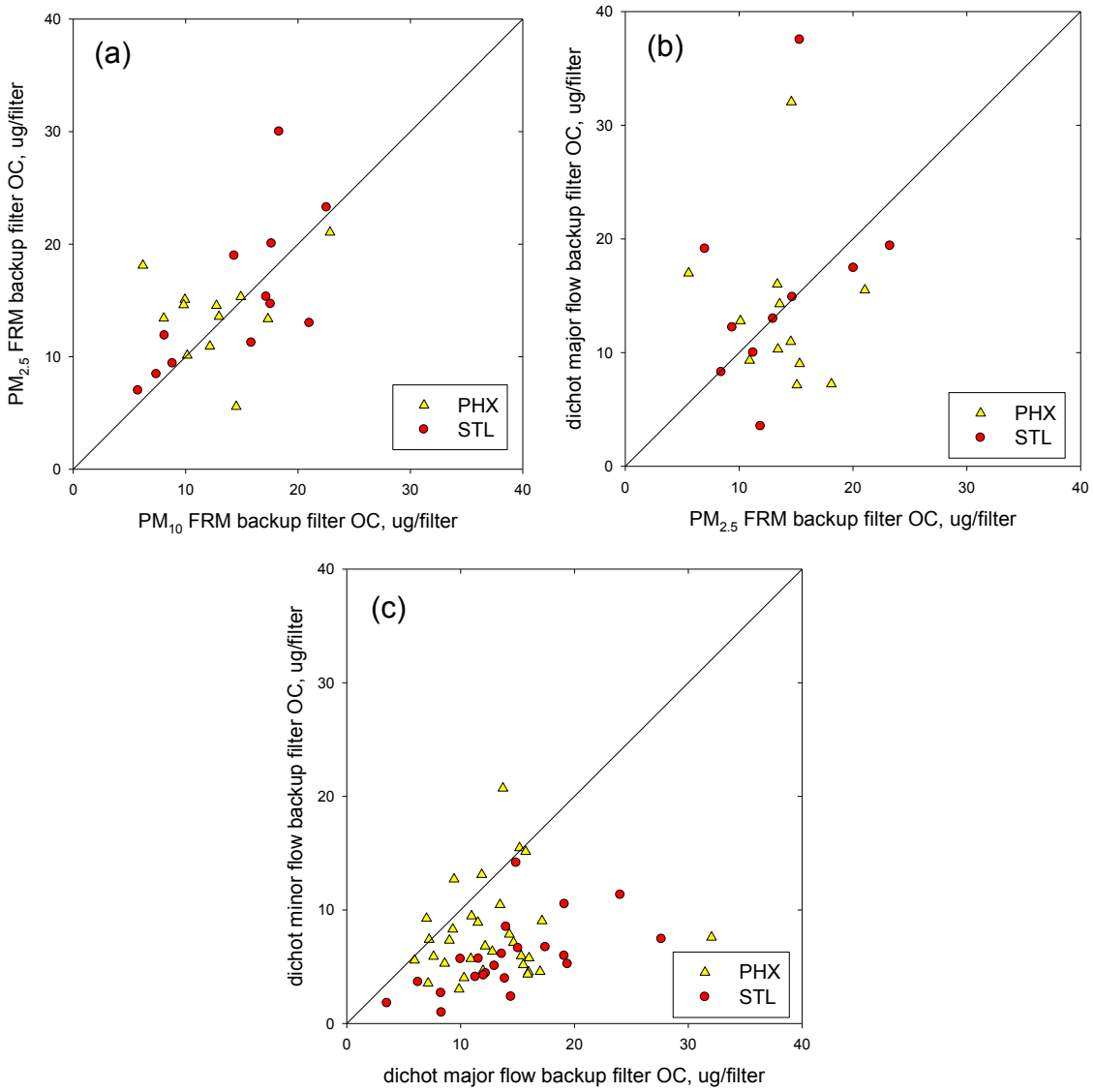

Figure 4-6. OC mass loadings on backup filters: (a) $PM_{2.5}$ FRM versus PM_{10} FRM; (b) dichot major flow versus $PM_{2.5}$ FRM; and (c) dichot minor flow versus dichot major flow. Data from May 2010 are excluded.

Filters in the dichot major flow channel are exposed to 90% of the flow rate and 90% of the fine particles sampled by the $PM_{2.5}$ FRM. Figure 4-6b shows the OC mass loading on the backup filters for these two samplers. Data are widely scattered, with median dichot/$PM_{2.5}$ OC ratios of 0.81 for Phoenix and 0.99 for St. Louis. There appears to be, on average, modestly

less OC mass on the dichot major flow channel backup filters compared to the $PM_{2.5}$ FRM backup filters. This pattern could arise from less adsorption of native vapor at the lower flow rate of the dichot major flow channel (the flow rate is 10% lower than the $PM_{2.5}$ FRM flow rate), or less volatilization of fine PM from the dichot front filter compared to the $PM_{2.5}$ FRM front filter (the dichot major flow channel collects only 90% of the fine PM entering the sampler), or both. More data are needed to determine whether the suggested patterns are real.

Figure 4-6c shows the OC mass loadings on backup filters for the dichot minor flow (used to measure coarse PM) against the dichot major flow (used to measure fine PM). There is virtually always more OC on the backup filter for the major flow compared to the minor flow. The excess at St. Louis is greater than the excess at Phoenix, with median major/minor OC ratios of 1.8 for Phoenix and 2.6 for St. Louis. Again, it is not clear whether the trend occurs from higher adsorption of native vapor at the nine-fold higher flow rate for the major flow, or from particle volatilization from the fine particles which are distributed 90% to the major flow and 10% to the minor flow, or both.

4.4.3 Comparison of OC Blanks, Front Filters, and Backup Filters

Enhanced OC on the major flow backup filter compared to the minor flow backup filter is consistent with measurements conducted at each site using a dichotomous TEOM with FDMS modules (Section 7). For mid-to-late summer through mid-winter, the TEOM data exhibited FDMS volatile component concentrations for the major flow that were 3.3 times (Phoenix) to 4.3 times (St. Louis) higher than measured for the minor flows. For both sites, the major-to-minor flow TEOM-derived volatile OC enhancement is approximately 1.7 times greater than major-to-minor flow OC enhancement on the dichot sampler backup filters. The FDMS volatility component is an upper bound on the semivolatile losses from the integrated sampler filter, and this analysis suggests that fine PM on the integrated sampler front filter could be volatilizing with at least a portion of the evolved OC adsorbing onto the backup filter. For the data collected over the mid-to-late summer through mid-winter period, there was relatively little nitrate, so the semivolatile fine PM is assumed to be dominated by OC.

Figure 4-7 shows box-whisker plots for OC mass loadings on trip and field blanks, the dichot major and minor flow backup filters, and dichot major and minor flow front filters. The minor flow backup filter mass loadings are statistically indistinguishable from the trip and field blanks loadings (95% confidence level), and the backup filter loading is more than 7% of the corresponding front filter loading for 25% of the samples. Major flow backup filter mass loadings are statistically higher than the trip and field blanks loadings (95% confidence level), and the backup filter loading is more than 17% of the corresponding front filter loading for 25% of the samples. These trends reaffirm that, at least for these two sites, backup filter measurements have more OC in fine PM, but might not bring added value to characterizing OC in coarse PM.

Figure 4-8 shows the OC mass loadings relationships for the paired front and back filters of the major and minor flows. Solid and dashed horizontal lines are the 95th percentile trip blanks and field blanks OC mass loadings, respectively. As previously discussed, the field blanks mass loadings decreased as the study progressed, and the 95th percentile value was not a good representation of the LQL. Thus, the trip blanks 95th percentile mass loading was used as an LQL proxy. Figure 4-8a shows that most of the major flow backup filter OC mass loadings

are above the trip blanks-based LQL. Front and backup filter mass loadings are weakly correlated (0.29). In contrast, a recent analysis of the URG-3000N sampler data for Missouri $PM_{2.5}$ CSN sites shows a stronger positive correlation between the front and backup filter mass loadings (not shown). OC mass loadings on the front and backup filter might positively correlate if semivolatile OC vapor concentrations increase with increasing front filter OC particulate matter loading, or if more particulate matter OC volatilization occurs at increasing front filter OC particulate matter loading, or both. Front and back filter mass loadings for the minor flow are uncorrelated (-0.07), consistent with the backup filter mass loadings being indistinguishable from the trip and field blanks.

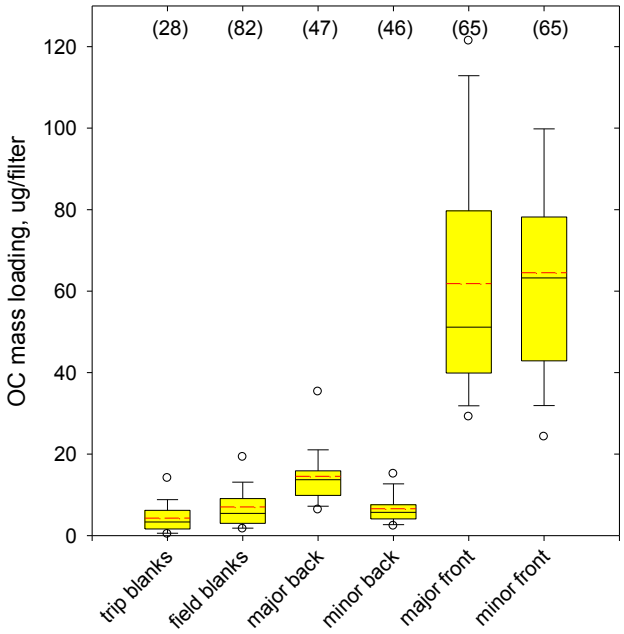

Figure 4-7. OC mass loading distributions (µg/filter) for the dichotomous samples. The interior solid blank line is the median and the interior dashed red line is the arithmetic mean. Whiskers are 10th/90th percentiles, and closed circles are 5th/95th percentiles. Values in parentheses above each box are the number of samples in the respective distribution. Data from May 2010 are excluded. Mass loadings were averaged for days with collocated carbon sampling.

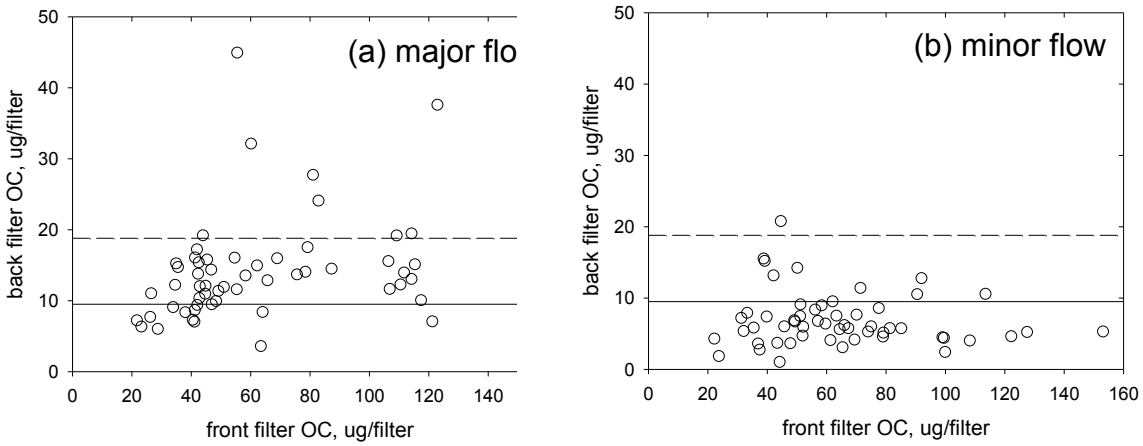

Figure 4-8. Dichotomous sampler OC mass loadings (µg/filter) for paired front and back filters: (a) major flow and (b) minor flow. The horizontal lines are the 95th percentile trip blanks (solid) and field blanks (dashed).

As shown in **Table 4-1**, mean OC mass loadings on the dichot minor flow backup filters are very similar to the mean field blank mass loadings. In contrast, mean OC mass loadings on the dichot major flow backup filters are higher than the site-specific mean field blanks by 1.7 times for Phoenix and 2.5 times for St. Louis.

Table 4-1. Mean mass loadings on the field blanks and dichot backup filters. Mass loadings are in µg/filter.

Mean Mass Loading Item	Phoenix	St. Louis
Field blanks	8.1	6.0
Dichot minor flow backup filters	7.8	5.7
Dichot major flow backup filters	13.6	15.1

Figure 4-9 shows OC concentration scatter plots for collocated dichot samplers at each site, excluding the May 2010 data. Collocated precision with no artifact correction is 0.44 µg/m^3 (14% of the average OC) for dichot $PM_{2.5}$ and 0.61 µg/m^3 (23% of the average OC) for dichot PM_c. Future work could include examining the sensitivity of collocated precision to different forms of the artifact correction. Backup filters are collected with every example, so it would be possible to evaluate whether the collocated precision improves or degrades when using sample-specific artifact corrections versus a single-valued correction derived from an ensemble of backup filters or field blanks. In principle, it would be possible to examine whether the collocated precision can be explained by the variation in the field blanks, but this is confounded by the apparent changes in field blank OC mass loadings as the study has progressed. For dichot PM_c, there are additional considerations. The minor flow collocated precision could be calculated and compared to the PM_c collocated precision to determine the influence from applying the correction for fine particle intrusion. However, as demonstrated in Figure 4-9b, analysis of the dichot PM_c collocated OC data is confounded by an apparent bias between the samplers; such bias was also observed for crustal species.

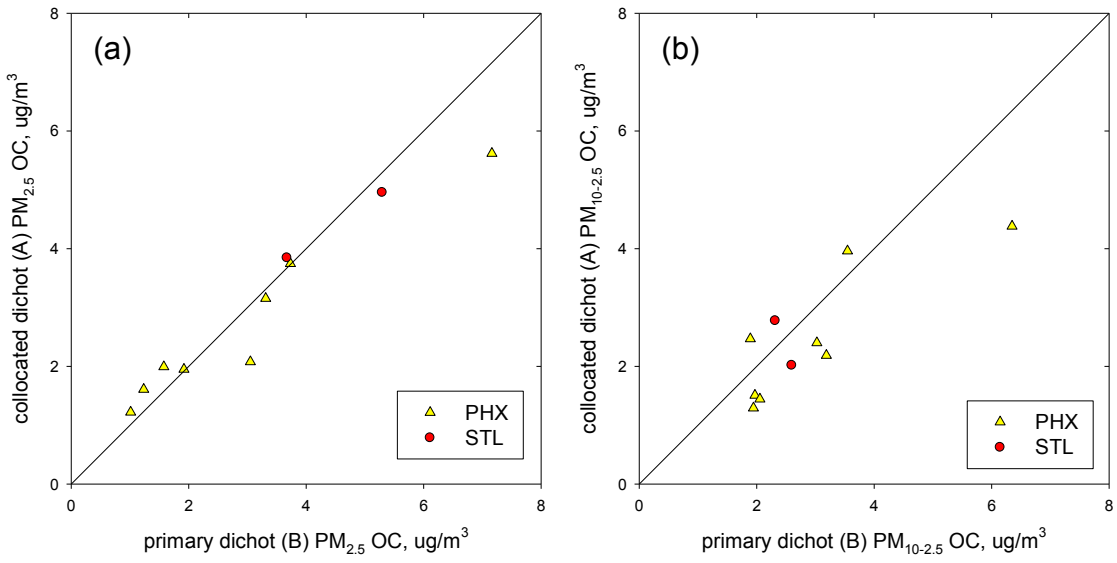

Figure 4-9. OC concentrations for collocated dichot samplers: (a) $PM_{2.5}$ and (b) PM_c. Data from May 2010 are excluded.

4.4.4 Summary of Carbon Artifacts

Based on TOA analysis of samples, the following conclusions are drawn. First, as described in Appendix D, OC mass loadings for the field blanks decreased as the study progressed, and the most recent mass loadings were comparable to the trip blanks. Second, OC mass loadings on backup filters for the dichot minor flow are statistically indistinguishable from the trip and field blanks. This finding, together with other analyses presented in this section, lead to the conclusion that there is very little volatile OC in the coarse PM size range, and thus a low capacity for negative artifacts. In contrast, fine PM exhibits enhanced OC mass loadings on the backup filters. The study design cannot distinguish whether these higher loadings are from adsorption of native vapors or adsorption of OC that volatilized PM on the front filter.

4.5 Biological Data

In addition to the routine one-in-three day sampling, additional dichot samples were collected between routine sampling days and analyzed for biomarkers. The data set includes 22 sampling events in Phoenix and 19 sampling events in St. Louis over the period from February to May 2011. Four field blanks and two trip blanks were also taken. RTI analyzed Teflon filters from the dichot minor flow channel (i.e., coarse particles with no correction for fine particle intrusion) for gravimetric mass, (1,3)-β-D-glucans, endotoxins, and proteins. RTI used water to extract the samples prior to using the assays specific to each biomarker.

- The (1-3)-β-D-glucans are found in the cell walls of many types of fungi. While this constituent is not unique to fungi, it is commonly used as a proxy to evaluate spatiotemporal patterns in fungal concentrations. The (1-3)-β-D-glucans were measured using Glucatell®, a commercially available assay.

- Endotoxin was measured by the sample reaction with Pyrochrome®, a commercially available Limulus Amebocyte Lysate (LAL) assay.
- Protein, an indirect marker of total biological load, was measured using the Molecular Probes® NanoOrange® Protein Quantitation Kit. Seven of these sampling events included the collection of collocated samples (four at Phoenix, three at St. Louis). For these seven sample pairs, the collocated precision was 9% for dichot minor flow channel mass concentration (PM_c not corrected for fine particle intrusion).

RTI analyzed samples in two batches, with the field blanks and trip blanks data corresponding to each batch (**Table 4-2**) used to blank-correct the data. Blank values were converted to concentration units using the target air volume sampled of 24 m^3. Field blanks and trip blanks were statistically indistinguishable at the 95% confidence level. Samples with negative biomarker concentration after blank correction were deemed to be below the operational detection limit. **Table 4-3** summarizes the glucan and endotoxin data by batch and also pooled across the two batches. **Figure 4-10** shows the concentration distributions for these data. Protein was excluded from these summaries for reasons described below.

Table 4-2. Biomarker field and trip blank data summary. Each batch included two field blanks and one trip blank. Field blanks and trip blanks were statistically indistinguishable at the 95% confidence level. Concentration units were calculated using a total air volume sampled of 24 m^3. ND = not detected.

Analysis Batch (Sample Dates)	Mean ± 1σ		
	Glucans, ng/m³	*Endotoxin, EU/m³*	*Protein, µg/m³*
Batch 1 (2/3/11 to 3/18/11)	0.0056 ± 0.0003	ND	0.14 ± 0.02
Batch 2 (3/23/11 to 5/20/11)	0.0071 ± 0.0019	ND	0.07 ± 0.05
Pooled	0.0063 ± 0.0015	ND	0.10 ± 0.05

Table 4-3. Biomarker data summary for blank-corrected data. Values are the geometric mean (GM), with the geometric standard deviation (GSD) in parentheses.

Analysis Batch	Phoenix			St. Louis		
	N	*Glucans,* ng/m³	*Endotoxin,* EU/m³	*N*	*Glucans,* ng/m³	*Endotoxin,* EU/m³
Batch 1 (2/3/11 to 3/18/11)	10	0.18 (1.3)	2.8 (2.1)	10	0.17 (1.5)	0.04 (2.6)[a]
Batch 2 (3/23/11 to 5/20/11)	12	0.16 (2.5)	0.30 (2.3)	9	0.21 (1.8)	0.13 (2.8)
Pooled	22	0.17 (2.0)	0.81 (4.0)	19	0.19 (1.6)	0.07 (3.1)[a]

[a] Endotoxin was not detected in one sample at STL. A concentration value of 0.01 EU/m^3 was imputed, which corresponds to one-half of the lowest observed concentration.

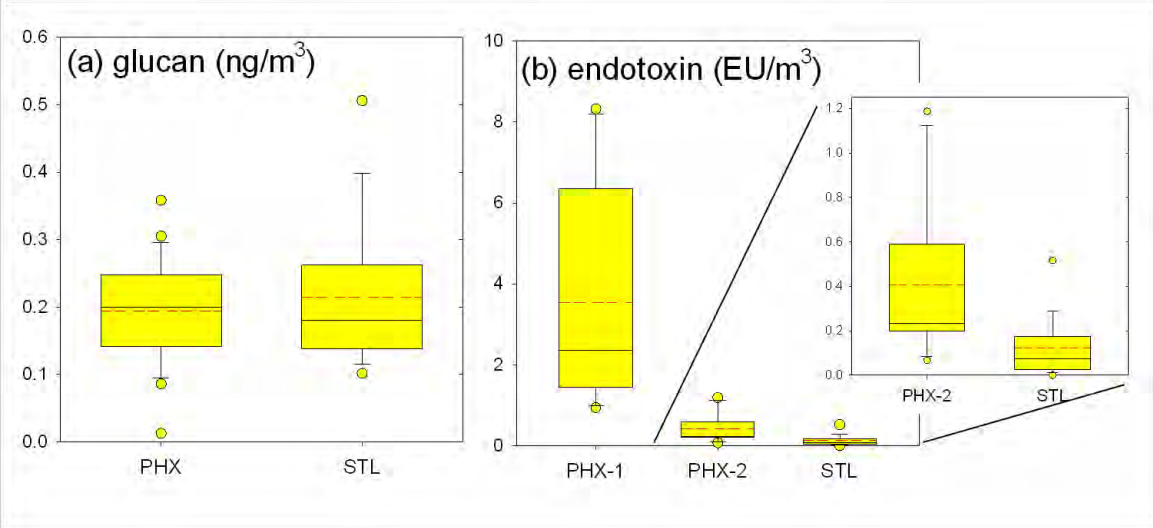

Figure 4-10. Box-whisker plots by site of (a) glucan (ng/m^3) and (b) endotoxin (EU/m^3). Endotoxin data at Phoenix are stratified by analysis batches (PHX-1, February 3 to March 18, 2011; and PHX-2, March 23 to May 20, 2011).

For protein, the collocated precision on blank-corrected data was 0.07 µg/m^3 (70%) for the four sample pairs that had both samples above the operational detection limit. The protein data have high uncertainty because the blanks correction is relatively large. Only six samples (two in Phoenix, four in St. Louis) had raw protein loadings more than three times the pooled blank level, and at both sites only about 40% of the raw protein loadings were more than two times the pooled blank level. Geometric means and standard deviations cannot be reliably computed because the results will be very sensitive to the method used to impute values that are negative (i.e., smaller than the blank correction). The median blank-corrected protein concentrations are 0.18 µg/m^3 for Phoenix and 0.07 µg/m^3 for St. Louis; these concentrations are close to the blank values (Table 4-2). Given that the protein concentration values are subject to large uncertainties, further interpretation of these data is not warranted.

Glucans had good detectability, with concentration values for all but one sample at least ten times higher than the blank correction. Collocated precision on glucan blank-corrected data was 0.04 ng/m^3 (19%). Geometric mean glucan mass concentrations were 0.17 ng/m^3 at Phoenix and 0.19 ng/m^3 at St. Louis.

Endotoxin was not detected in the blanks samples. Collocated precision for endotoxin was 0.51 EU/m^3 (99%), including all seven sample pairs, and 0.19 EU/m^3 (48%) when excluding the March 2, 2011, sample at Phoenix. The geometric mean endotoxin level was ten times higher for Phoenix than for St. Louis, and also exhibited more variability for Phoenix. Samples were analyzed in two batches, with batch-specific geometric mean endotoxin values for Phoenix of 2.8 EU/m^3 for the first batch (February to mid-March) and 0.3 EU/m^3 for the second batch (late March to May). While the between-batch variability in endotoxin was large, monthly median PM_{10} endotoxin concentrations for Fresno, California, reported by Tager et al. (2010) exhibited similar range and variability. Thus, while the Phoenix endotoxin levels exhibit a large step-change precisely coinciding with the batches, it is not clear whether this change is real or from measurement error. While there is not clear evidence that the data are invalid, caution should be used when interpreting results for Phoenix endotoxin concentrations.

5. Analysis of Ions

This section describes analyses focused on concentrations of ions. Coarse-mode ion concentrations, including nitrate and sulfate, were very low at both sites throughout the monitoring period, and much lower than fine-mode concentrations (Section 2 and Section 5.3). Coarse-mode nitrate appears to be non-volatile compared to fine-mode nitrate, since the majority of the coarse-mode nitrate was retained on the Teflon filter (Section 5.1). Ammonium predictions based on anion concentrations were much higher than observed, indicating the coarse-mode nitrate is predominantly paired with cations other than ammonium (Section 5.4), though there was no consistent correlation of PM_c nitrate with other ions (Appendix E). Concentrations of both fine- and coarse-mode nitrate were similar with and without a denuder to remove nitric acid in the sampling stream (Section 5.5). Coarse-mode XRF sulfur predominantly consisted of sulfate, and coarse-mode XRF sodium predominantly consisted of sodium ion, so the ion measurements are largely redundant. In contrast, most of the potassium was nonionic (Section 5.6). Given these findings, laboratory analysis of PM_c ions as part of a routine monitoring network does not appear to justify the necessary costs, except in environments, such as coastal areas, where coarse-mode nitrate is expected to be significant.

5.1 Approaches to Measuring Ions

Ambient $PM_{2.5}$ ions are routinely measured in both the CSN and IMPROVE networks. In both cases, there is a devoted sample collection channel to ions, with a nylon filter and an upstream acid gas denuder to minimize positive artifacts from the uptake of such gases by the nylon filter. The filter samples are extracted in water and analyzed by IC. The ion measurements serve three purposes:

1. They are the only measurement of nitrate (both networks) and ammonium (CSN only), which can be significant contributors to ambient $PM_{2.5}$ burdens.
2. Together with the element concentration measurements from the Teflon filter, they allow for a quality check on the sampling and laboratory analyses.
3. The fraction of a given element that is present in ionic form can provide insights into the relevant sources.

In contrast to the CSN and IMPROVE networks, which feature a dedicated sampling channel for ion measurements using a nylon filter, to reduce the total number of samplers needed for this study, ions were measured using a nylon-behind-Teflon filter sandwich. Ion analysis was performed on both the Teflon and nylon filters with the ions from nonvolatile salts (e.g., ammonium sulfate) to be found only on the Teflon filters, and the ions from semivolatile salts (e.g., ammonium nitrate) to be found on both the Teflon and nylon filters. The nylon filter is used specifically to measure nitrate and ammonium from the volatilization of ammonium nitrate from the Teflon filter, although other ions might be present in the nylon filter from chemistry that takes places on the Teflon filter that displaces ions. In cases where semivolatile forms of nitrate are low, the nylon filter sampling and analysis might be unwarranted. The Teflon and nylon filters are in series in the same sampling channel, so although the ion and elemental measurements (e.g., XRF sulfur and IC sulfate) do not provide a quality check on the sampling, they do provide a quality check on the laboratory analyses.

5.2 Nitrate Concentrations on Teflon and Backup Nylon Filter

As described in Section 2, PM_c nitrate concentrations were generally low. Some forms of nitrate can be lost or volatilized off of Teflon filters, so backup nylon filters were used to quantify the amount of nitrate volatilized off of the Teflon filter. **Table 5-1** summarizes average concentrations at each site, size fraction of nitrate by filter, and the average fraction of nitrate on the Teflon filter. Most of the nitrate is retained on the PM_c Teflon filter (71% to 77% on average) while half or less of the nitrate is retained on the PM_f Teflon filter (40% to 53%). This is consistent with coarse-mode nitrate consisting of salts that are less volatile than fine-mode nitrate, which is predominantly ammonium nitrate.

If only Teflon filters are used in routine sampling, with no backup nylon filters, then fine-mode nitrate would be severely under-measured (Ashbaugh and Eldred, 2004), though the majority of the coarse-mode nitrate will be captured. Nitrate is a small fraction of coarse mass in these two locations, so the effect of not having backup nylon filter measurements on coarse mass balance would be negligible at these and similar sites. Thus, the decision on whether to use nylon backup filters and analyze them by IC will be dictated by the extent to which the PM_c speciation sampling network will also be used for $PM_{2.5}$ speciation.

Table 5-1. Summary of nitrate concentrations via dichot on Teflon, nylon, and total (Teflon + nylon), plus fraction of total nitrate on Teflon filter.

Site	Size Fraction	Avg. Nylon NO_3 ($\mu g/m^3$)	Avg. Teflon NO_3 ($\mu g/m^3$)	Avg. Total NO_3 ($\mu g/m^3$)	Avg. % of NO_3 on Teflon
PHX	PM_c	0.13	0.42	0.54	77
PHX	PM_f	0.44	0.50	0.94	53
STL	PM_c	0.13	0.43	0.56	71
STL	PM_f	0.54	1.01	1.54	39

5.3 Nitrate Partitioning Between Fine and Coarse Modes

Figure 5-1 shows the partitioning of PM_{10} nitrate between the fine and coarse fractions as measured by the dichotomous samplers (Figure 5-1a) and PM_f nitrate partitioning to the front Teflon filter compared to the Teflon/nylon filters (Figure 5-1b). This analysis assumes negligible loss of nitrate during XRF analysis; however, results from an EPA study on $PM_{2.5}$ speciation indicated that the vacuum applied during XRF can reduce the amount of nitrate on a Teflon filter by as much as 40% (U.S.EPA, 2001). If nitrate measurements need to be made using a dichot then the issue of nitrate loss from theTeflon filter due to XRF would need to be addressed. The data set includes all Dichot A nitrate data and Dichot B nitrate data for days on which no Dichot A nitrate data were collected. Figure 5-1(a) shows that some samples with PM_f nitrate below about 1 $\mu g/m^3$ have more PM_c nitrate than PM_f nitrate. However, PM_c nitrate is not elevated on days of high PM_f nitrate concentrations. Deviations below the 1:1 (diagonal) line in Figure 5-1(b) represent PM_f nitrate volatilization loss from the front filter that is captured by the back filter. At low nitrate concentrations, PM_f nitrate volatilization losses are generally lower in Phoenix

compared to St. Louis (this observation is not discernible in Figure 5-1b). This difference between the two sites might reflect a counter-ion other than ammonium for nitrate in many of the Phoenix PM_f samples, or the differential influences of environmental conditions on nitrate volatilization. For PM_f nitrate greater than about 2.5 µg/m^3, the mean Teflon filter nitrate loss is 0.7 ± 0.3 µg/m^3 (N = 12) at St. Louis, and 1.5 ± 1.3 µg/m^3 (N = 6) at Phoenix,[8] reflecting greater and more variable absolute loss of nitrate from the Teflon filter at Phoenix compared to St. Louis for high nitrate concentrations.

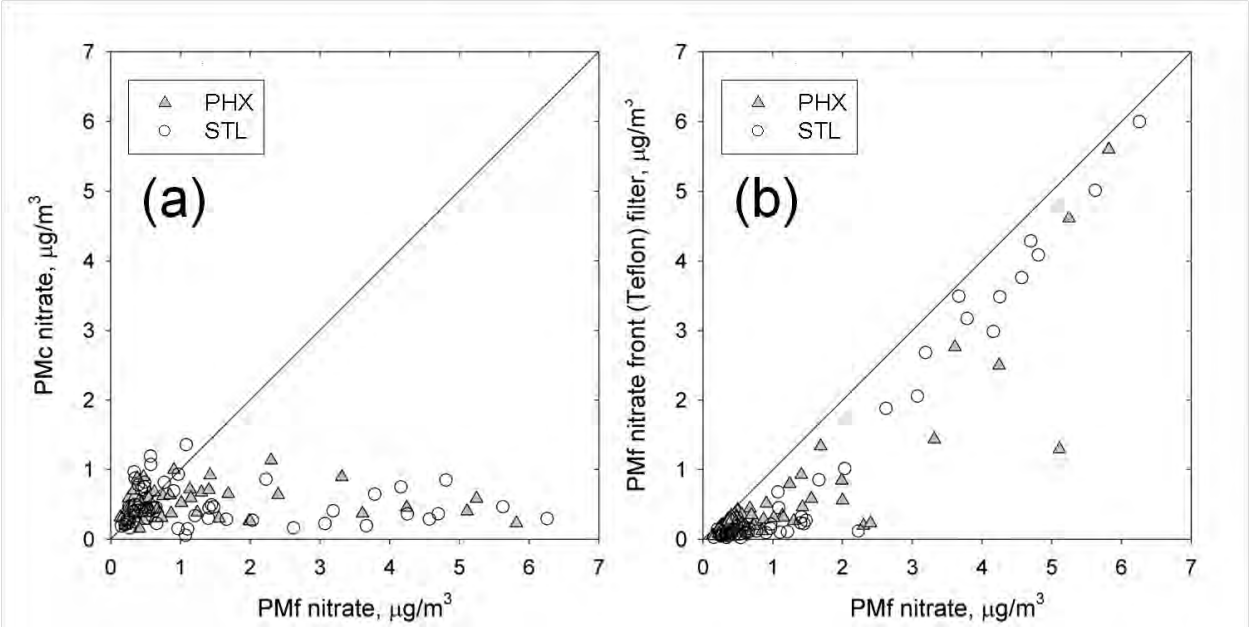

Figure 5-1. Scatter plots for dichotomous sampler nitrate showing (a) the partitioning of nitrate between the fine and coarse PM fractions and (b) total fine nitrate and the nitrate on the front (Teflon) filter. Phoenix is represented by gray triangles and St. Louis by open circles.

5.4 Ammonium Balance and Implications for Ammonium Measurements

To understand whether sulfate (SO_4) and nitrate (NO_3) are associated with ammonium (NH_4), or whether they are associated with other cations, such as sodium, it is useful to compare measured ammonium to the amount of ammonium expected based on sulfate and nitrate concentrations.

Figure 5-2 shows measured versus predicted ammonium for Teflon and backup nylon dichot and FRM filters at each site for fine and coarse aerosol. Full neutralization of sulfate and nitrate was assumed for predicted ammonium:

$$Predicted\ ammonium\ based\ on\ NH_4NO_3\ and\ (NH_4)_2SO_4 = 0.29(NO_3^-) + 0.38(SO_4^=)$$

[8] Excluding the Phoenix value at (5.1, 1.3) in Figure 5-1b, for PM_f nitrate greater than 2.5 µg/m^3, the mean Teflon filter nitrate loss is 1.1 ± 0.7 µg/m^3 (N = 5).

For PM_f on the Teflon filter, whether dichot or FRM, at both sites, the predicted and measured ammonium concentrations are highly correlated with quantitative agreement in St. Louis and overprediction of the measured ammonium in Phoenix. The latter overprediction may indicate that the sulfate aerosol is not fully neutralized by ammonium, and so ammonium is not the sole counter-ion for sulfate and nitrate. For PM_c on the Teflon filter, ammonium is grossly overpredicted, again indicating that the sulfate and/or nitrate are associated with non-ammonium cations. At both sites, the PM_c ammonium concentrations are low (only one value greater than 0.1 $\mu g/m^3$).

For PM_f on the nylon filter, predicted and measured ammonium are highly correlated; in this case, there is quantitative agreement at Phoenix and overprediction for St. Louis. The reason for this overprediction is not known. For PM_c on the nylon filter, ammonium is underpredicted for the FRM in St. Louis and overpredicted for all other samplers at both sites. At both sites, the PM_c ammonium concentrations are low.

The low PM_c ammonium concentrations at both sites on the Teflon and nylon filter indicate that PM_c ammonium measurements may not be warranted.

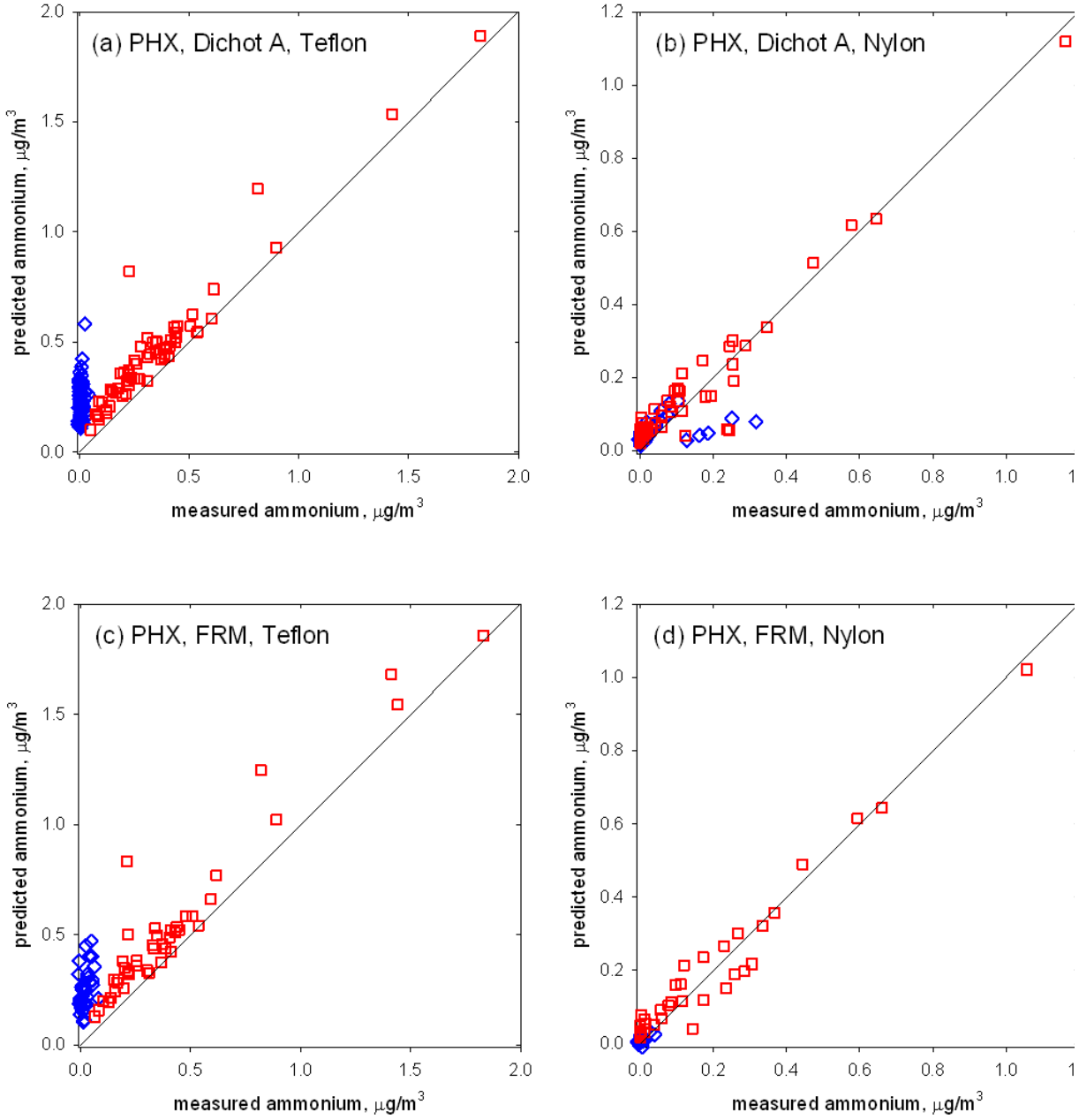

Figure 5-2. Measured ammonium versus predicted ammonium scatter plots at Phoenix (a–d) and St. Louis (e–h) on Teflon and nylon. Coarse particles are represented by blue diamonds and fine particles by red squares. Diagonal lines show the 1:1 relationship.
(Figure continued on next page.)

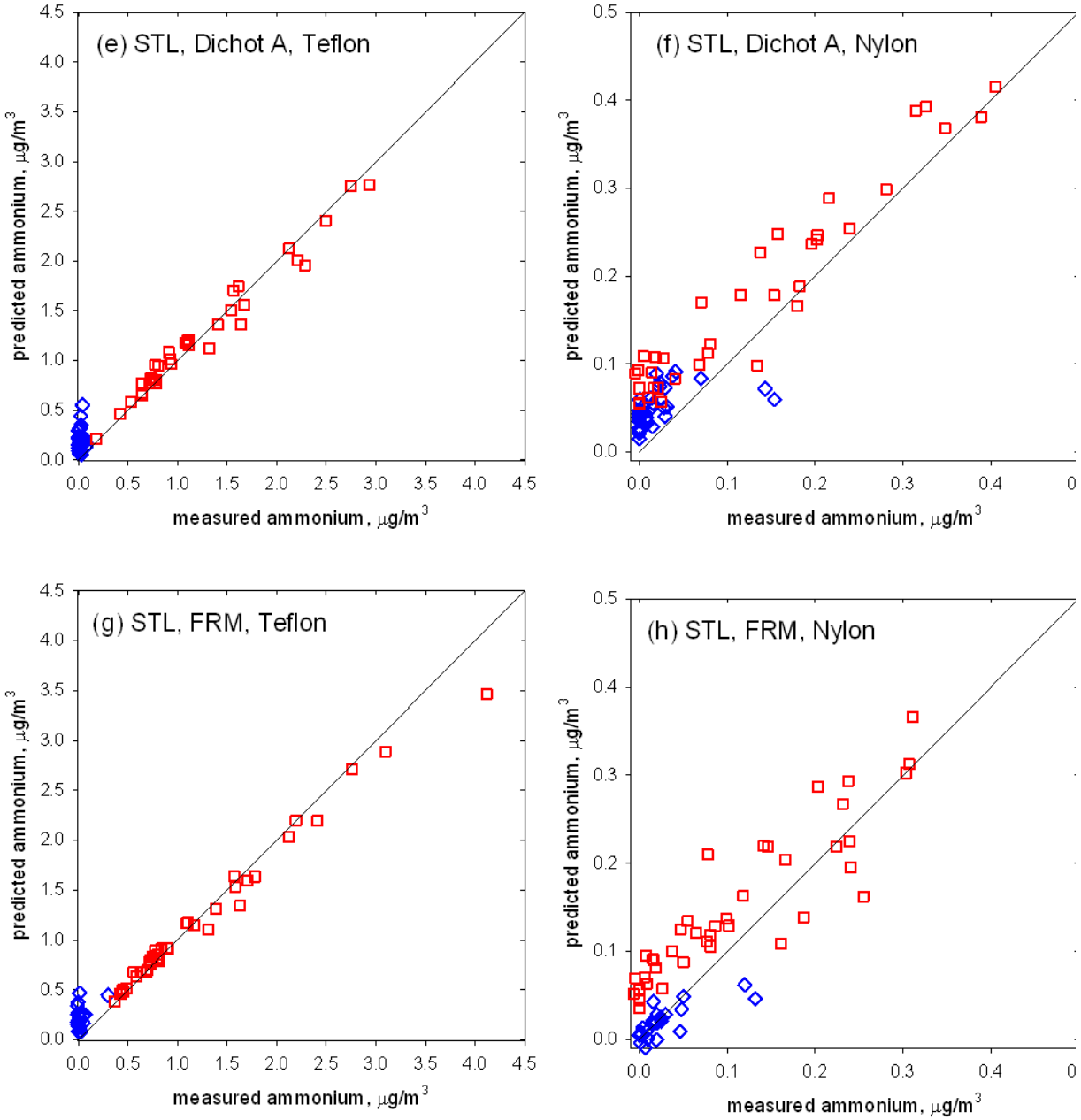

Figure 5-2 *(continued)*. Measured ammonium versus predicted ammonium scatter plots at Phoenix (a–d) and St. Louis (e–h) on Teflon and nylon. Coarse particles are represented by blue diamonds and fine particles by red squares. Diagonal lines show the 1:1 relationship.

5.5 Comparison of Concentrations With and Without Denuders

To test the influence of using a denuder on ammonium and nitrate concentrations, on a subset of days, one dichot was run with a denuder and the other dichot was run without a denuder. Multi-channel annular denuders coated with magnesium oxide were placed in the sampler down tubes. The collocated sampler data were used to examine whether nitric acid is adsorbing onto the Teflon filter and then being quantified as aerosol nitrate, since a denuder strips out gaseous nitric acid. As shown in **Figure 5-3**, concentrations for both fine and coarse mode ammonium and nitrate were essentially no different whether or not a denuder was used. For comparison, sulfate and crustal species also showed no difference between measurements with and without a denuder, as expected. Thus for dichot measurements at locations similar to Phoenix and St. Louis, a denuder is likely not needed. If some other sites are deemed to warrant denuders based on a denuder/no denuder comparison study, the good quantitative agreement for PM_c crustal species demonstrates that the denuder used in this study can be used with negligible particle losses.

(a) ammonium

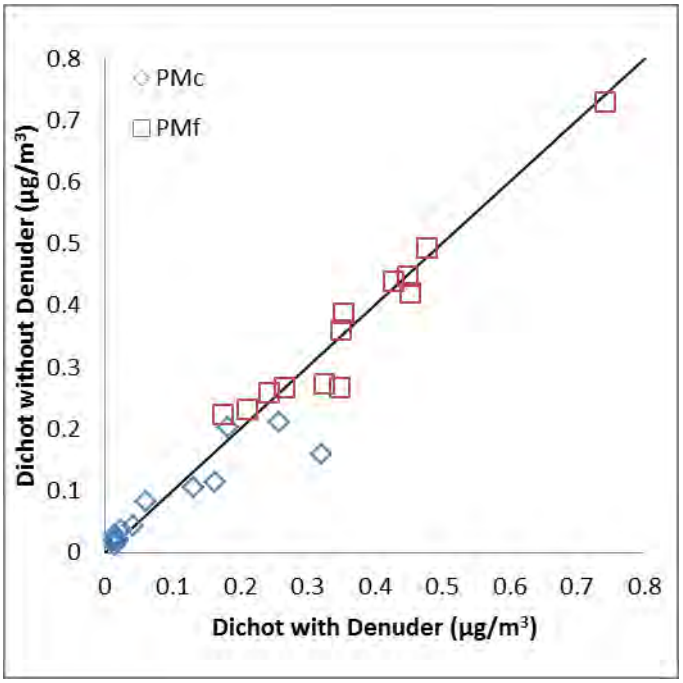

(b) nitrate

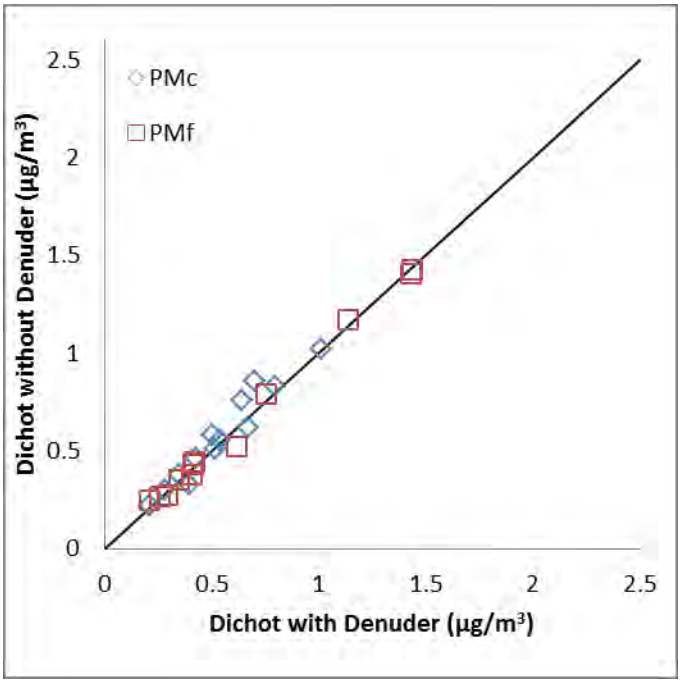

(c) sulfate

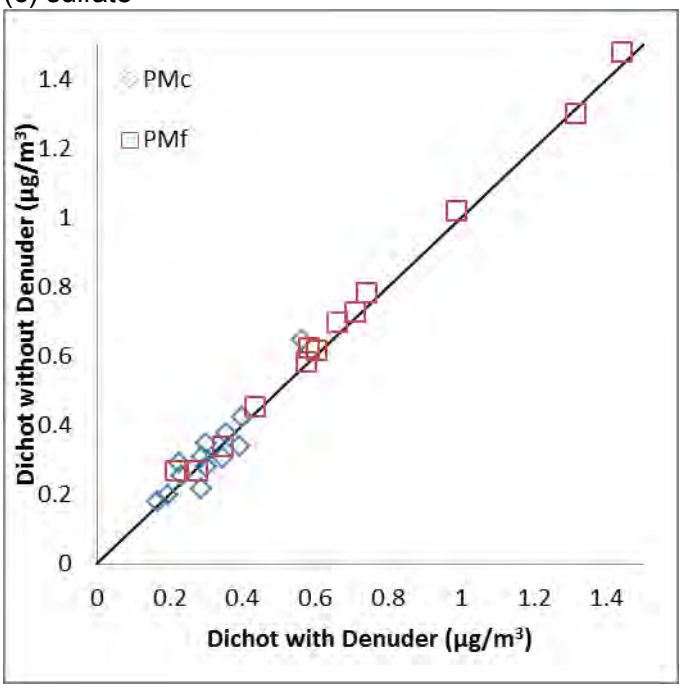

(d) crustal species (Ca+Fe+Si)

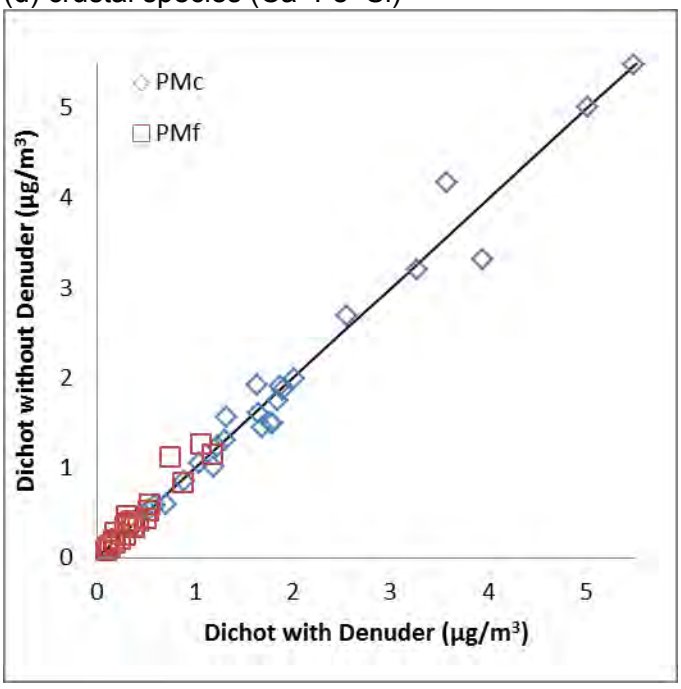

Figure 5-3. Collocated dichot (dichot with denuder versus dichot without denuder) scatter plots for (a) NH_4, (b) NO_3, (c) SO_4, and (d) Ca, Fe, and Si at Phoenix. Coarse particles are represented by blue diamonds and fine particles by red squares. Diagonal lines show the 1:1 relationship.

5.6 Comparison of Ion and Corresponding Element Concentrations

Figures 5-4 and 5-5 display the correlation between total elemental concentration (analyzed by XRF) and ion concentration (analyzed by IC) for certain elements measured on Teflon filters from Dichot A and B and the FRM samplers. If an ion is well-correlated with the corresponding element, then the element could feasibly be used to estimate ion concentrations without having to conduct IC analysis for ions. At both sites, PM_f potassium was primarily ionic, while PM_c potassium was primarily nonionic. Sodium was primarily ionic for both size fractions and both sites. Sulfate ion (reported as sulfur in the figures) accounted for most of the sulfur at both sites for both coarse and fine fractions. Thus, based on the data from these two sites, the added value from the measurement of ions is the ability to measure nitrate and to resolve PM_c potassium ion compared to elemental potassium. Given the limited added value, at least for sites with low PM_c nitrate concentrations, and the superior detection limits for XRF compared to IC for most of the reported ions, the added cost for ion analysis is not justified except possibly in cases with high PM_c nitrate.

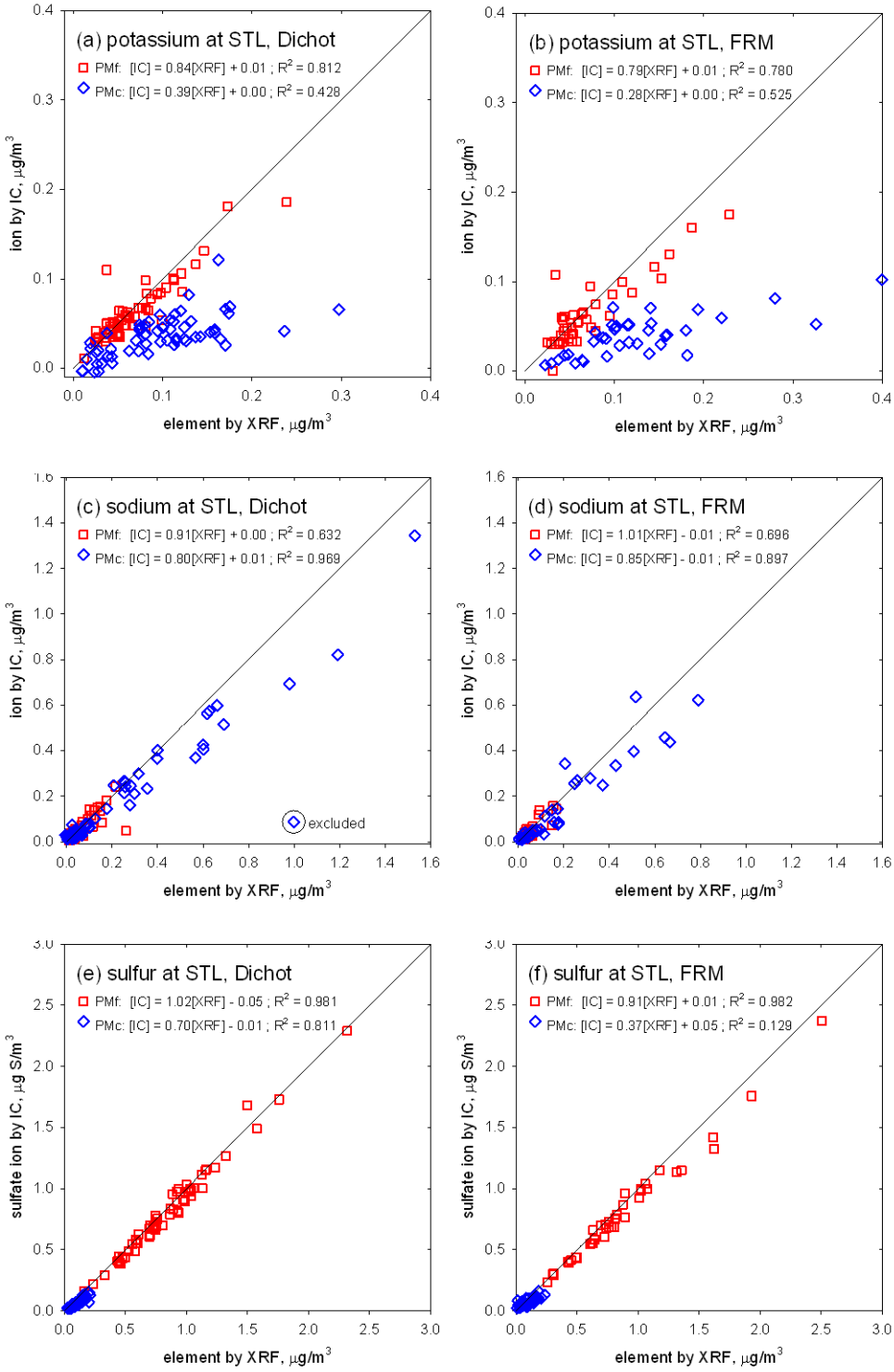

Figure 5-4. Comparison of ion and element concentrations (µg/m^3) at St. Louis for K and K+, Na and Na+, and S and SO_4^{2-} via dichot and FRM samplers for PM_c and PM_f.

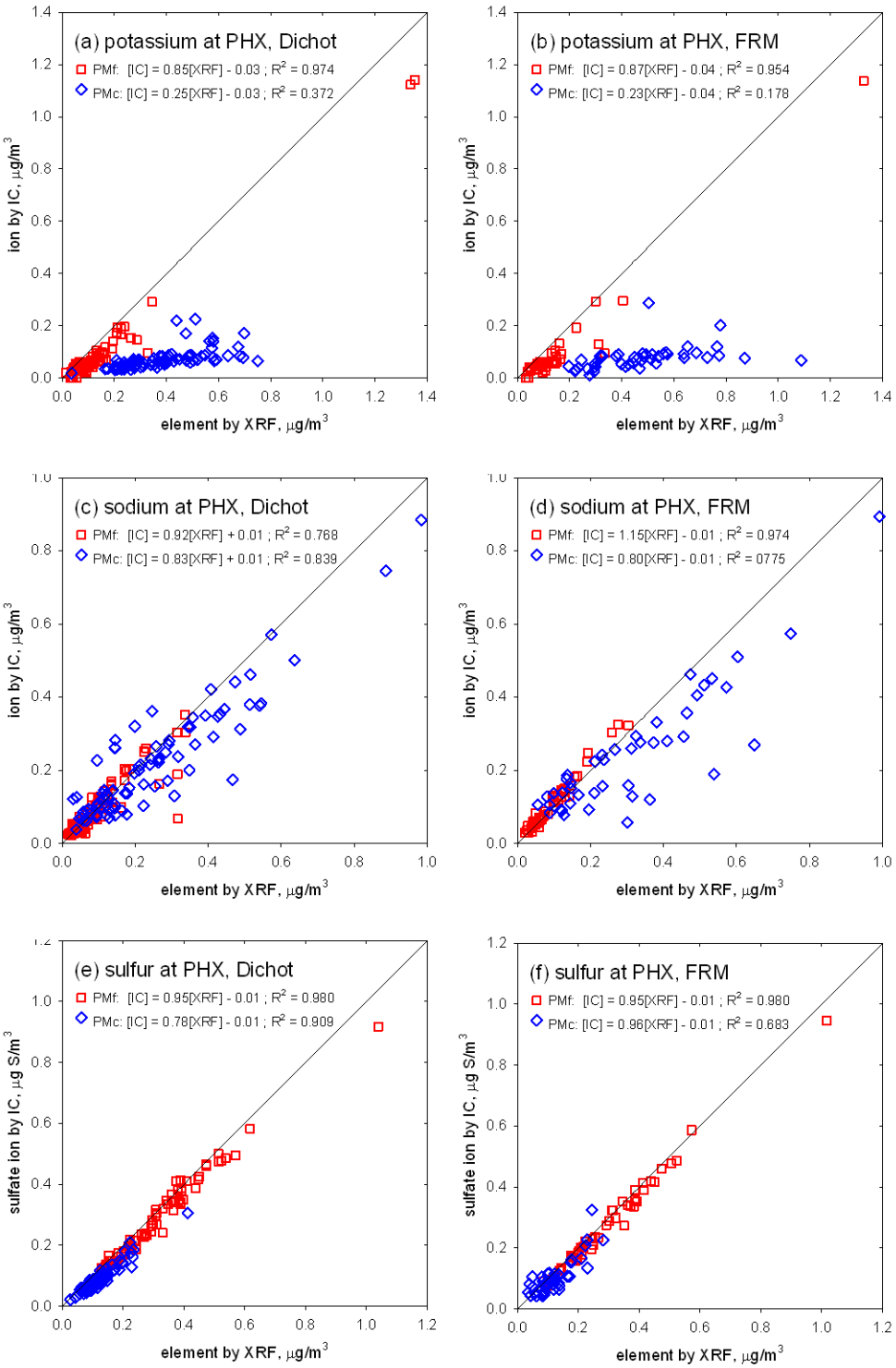

Figure 5-5. Comparison of ion and element concentrations (µg/m^3) at Phoenix for K and K+, Na and Na+, and S and SO_4^{2-} via dichot and FRM samplers for PM_c and PM_f.

6. Mass Balance

Mass balance closure reflects the ability to reconstruct the observed Teflon filter gravimetric mass from the chemical species data. It is an uncertain process because not all species are quantified (e.g., retained water), and some of the chemical species data are derived from parallel samples that have different measurement artifacts (e.g., carbon data from a quartz filter). The objective of this analysis is to account for the mass on the Teflon filter rather than to make a best estimate of the species concentrations in the atmosphere. Thus, the data were not corrected for nitrate volatilization measured as the nitrate taken up by the nylon backup filter. The approach also assumes that the fraction of fine-particle nitrate loss from the dichot major flow Teflon filter is the same as the fraction of fine-particle nitrate loss from the dichot minor flow Teflon filter.

The organic carbon data have not corrected for OC artifacts, and a sensitivity study showed that including an estimate of the artifact correction did not change the key findings. To account for other elements in the organic aerosol, OM was assumed to be OC multiplied by 1.6 (i.e., [OM] = [OC] $\times$ 1.6). An OC multiplier of 1.6 was chosen because it is the midpoint of the commonly used range of 1.4 to 1.8, but, as discussed in the next section, sensitivity studies were performed using various OC multipliers. Other species included in the reconstructed mass include sulfate ion, nitrate ion, major inorganic cations (ammonium [NH4+], sodium [Na+], and potassium [K+]), Cl (as measured by XRF on the Teflon filter), EC, soil oxides (estimated as 2.20[Al] + 2.49[Si] + 1.63[Ca] + 2.42[Fe] + 1.94[Ti]),[9] and other metals.[10] The species group "other metals" was included to initially generate a reconstructed mass estimate that would be conservatively high. It was deemed inconsequential to the mass balance reconstruction and, given that such metals are factored to some extent into the above soil equation, this species group could have been omitted from the mass reconstruction. As described in Section 3, RTI applied XRF attenuation factors to the low atomic number elements ($Z \leq 20$).

6.1 Results for Dichotomous Samplers

Figure 6-1 shows the species distributions and mass balance closure for each sample. Soil oxides dominate PM_c, while organic matter accounts for 10% to 20% of the PM_c mass. **Figure 6-2** compares the reconstructed mass and gravimetric mass for PM_f and PM_c with statistical metrics summarized in **Table 6-1**. Ordinary least squares (OLS) regression, which assumes there is no uncertainty in the x-axis values, was used for this analysis. This should be a robust approach because the uncertainty in gravimetric mass is much smaller than the uncertainty in the reconstructed mass.

[9] This soil-oxides estimate is the standard formula applied to IMPROVE network data (http://vista.cira.colostate.edu/improve/tools/aertypeeqs.htm).

[10] Other metals=(silver [Ag] + arsenic [As] + barium [Ba] + bromine [Br] + cadmium [Cd] + cerium [Ce] + cobalt [Co] + chromium [Cr] + cesium [Cs] + copper [Cu] + indium [In] + magnesium [Mg] + manganese [Mn] + nickel [Ni] + phosphorus [P] + lead [Pb] + rubidium [Rb] + antimony [Sb] + selenium [Se] + tin [Sn] + strontium [Sr] + vanadium [V] + zinc [Zn] + zirconium [Zr]).

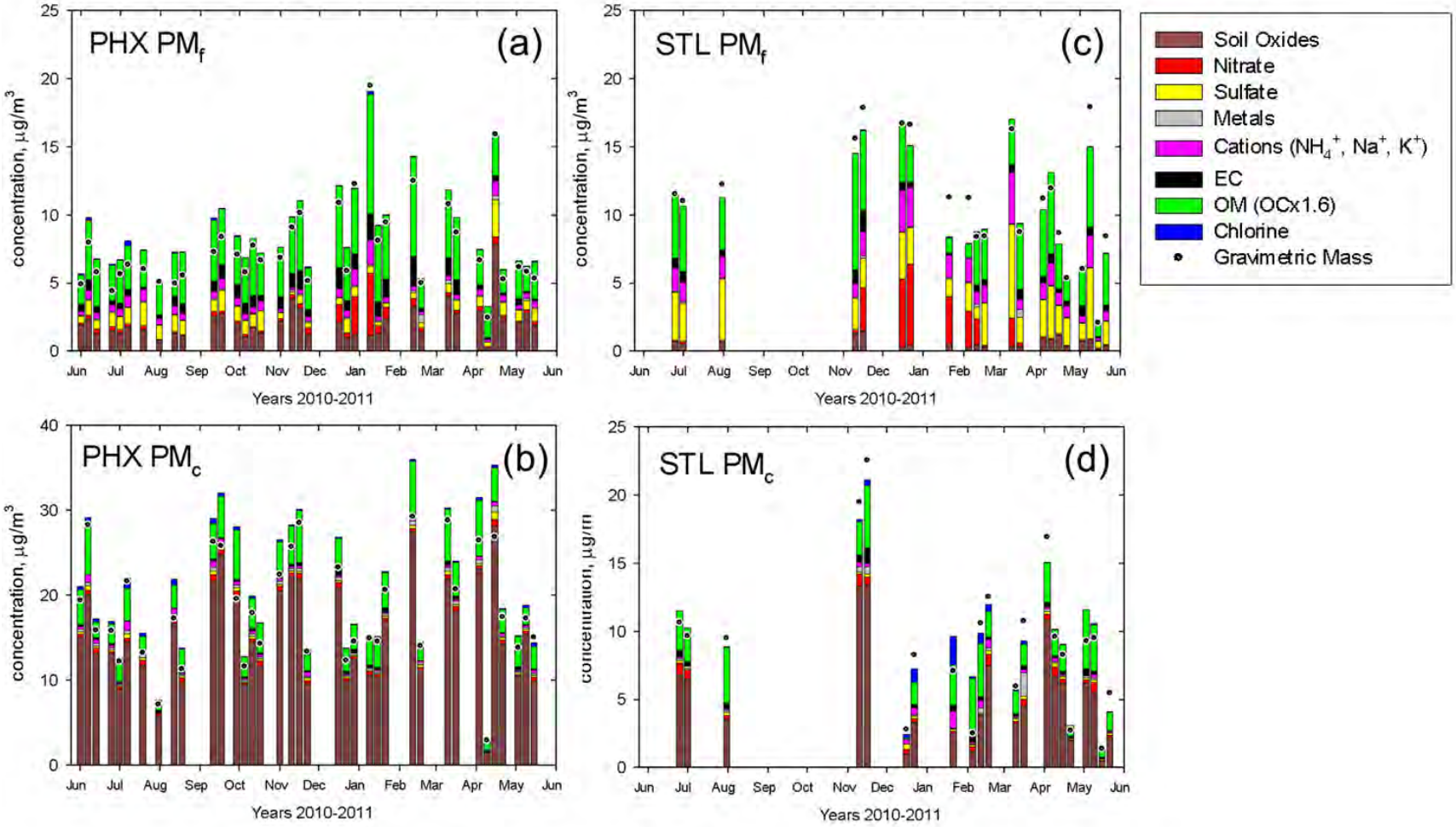

Figure 6-1. Mass balance closure between Teflon filter gravimetric mass and the chemical speciation data for dichot samples. All species were measured on the Teflon filter except EC and OC, which were measured on the quartz filter from a collocated dichot sampler. Organic matter was estimated using OM = 1.6 × OC, and the OC was not corrected for measurement artifacts.

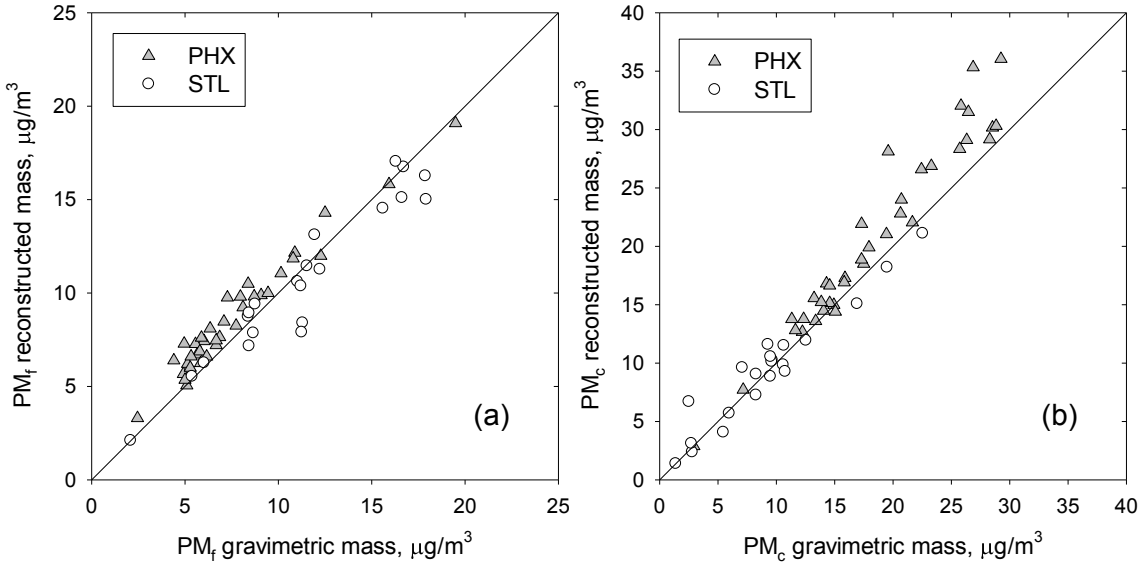

Figure 6-2. Reconstructed mass versus gravimetric mass for the dichotomous sampler Teflon filters: (a) PM_f and (b) PM_c for Phoenix and St. Louis. Organic matter was estimated using OM = 1.6 × OC, and the OC data were not corrected for measurement artifacts.

Table 6-1. Measures of agreement between reconstructed and gravimetric mass for Phoenix and St. Louis, using OM = 1.6 × OC and no correction for OC artifacts.

Site and Size	*N*	OLS Regression, µg/m³ [a]	r^2	Ratio of Means[b]
PHX PM_f	37	[recon] = 0.92 [grav] + 1.6	0.96	1.14
PHX PM_c	37	[recon] = 1.18 [grav] – 1.0	0.94	1.13
STL PM_f	21	[recon] = 0.90 [grav] + 0.5	0.92	0.94
STL PM_c	21	[recon] = 0.87 [grav] + 1.3	0.92	1.01

[a] OLS regression of reconstructed mass on gravimetric mass.

[b] The PM_c ratio of means is 1.09 for PHX PM_c and 0.96 for STL PM_c when applying a multiplier of 0.82 to the OM to correct for the presumed carbon losses from the Teflon filter. This multiplier is the dichot-to-FRM mean ratio for gravimetric mass (Table 2-1). The PM_c ratios of means further decrease to 1.07 and 0.93, respectively, when also neglecting K+ and other metals, assuming these species are present as crustal material and are included in the standard formula for soil oxides.

Several factors that may influence the quality of mass balance closure include, but are not limited to, the assumed OM/OC ratio, OC measurement artifact corrections, the assumed oxide forms of the crustal elements, and XRF attenuation factors applied to light elements. As detailed in Section 3.5, the latter is particularly relevant for PM_c. In this section, the attenuation factors developed and applied by RTI were used for all data. An alternative form for the soil oxides equation that excludes Al and increases the Si multiplier from 2.49 to 3.48 (Simon et al., 2011) yields soil oxides contributions that are, on average, 5% higher for PM_c.

For Phoenix data using OM/OC = 1.6 and no OC artifact correction, the reconstructed mass consistently overestimates the gravimetric mass for both PM_f and PM_c, with an average difference of approximately 13% for both size ranges (9% for PM_c after applying a correction for loss of carbonaceous matter from the Teflon filter as described in a footnote to Table 2-1). The OM/OC ratio that best closes mass balance (i.e., the minimum difference between reconstructed and gravimetric mass, which are shown as root-mean-square (RMS) residuals in **Figure 6-3**) is 1.2 to 1.3 for PM_f. This ratio is consistent with the value of 1.25 reported by Simon et al. (2011) for Phoenix IMPROVE $PM_{2.5}$ data. The best-fit OM/OC ratio for PM_c is 0.6 (off the scale range in Figure 6-3) with the same ratio obtained when applying a multiplier of 0.82 to the carbon data to account for losses from the Teflon filter. The PM_c ratio of 0.6 is implausibly low (OM/OC must be greater than or equal to unity), and in this case there must be other factors driving the observed bias.

For St. Louis data using OM/OC = 1.6 and no OC artifact correction, the reconstructed mass underestimates the gravimetric mass by 6% for PM_f, and the agreement is within 1% for PM_c. The OM/OC ratio that yields the best agreement for PM_f is 1.8; this ratio is consistent with the value of 1.81 reported by Bae et al. (2006) for $PM_{2.5}$ data collected at the East St. Louis site. For PM_c, shown as the open circles in Figure 6-3b, the best-fit OM/OC ratio is 1.4 to 1.6 with a ratio of 1.8 obtained when applying a multiplier of 0.82 to the carbon data (to account for losses from the Teflon filter). However, the RMS residual varies by only 0.3 $\mu g/m^3$ over the range of OM/OC ratios between one and two. This flat response surface means the best-estimate OM/OC ratio of 1.4 to 1.6 for St. Louis PM_c is highly uncertain.

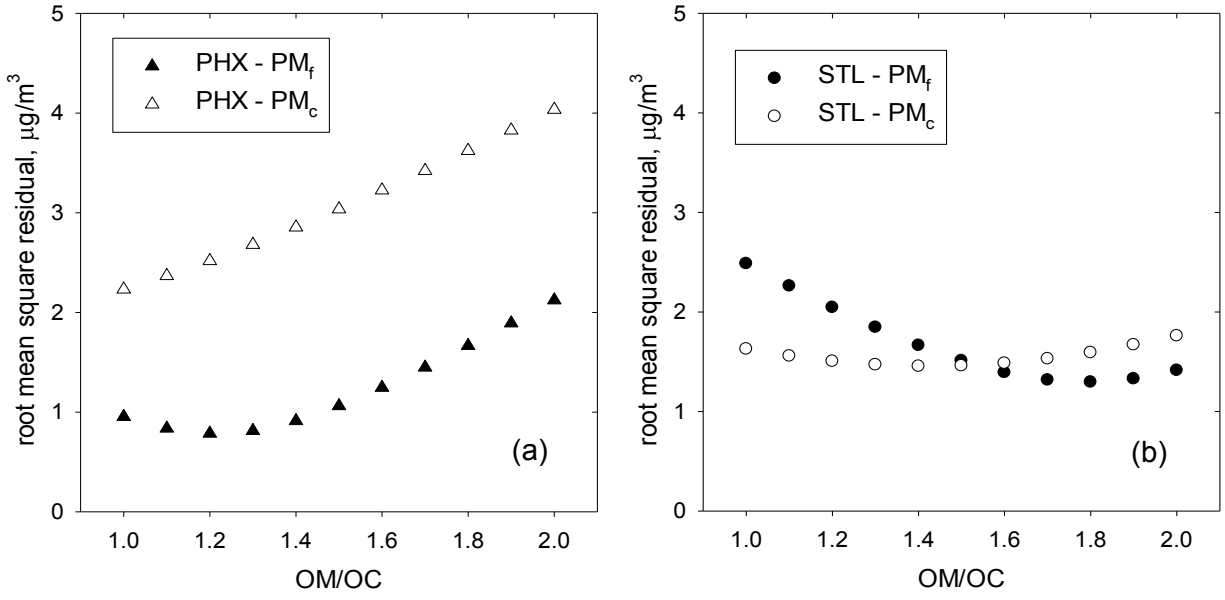

Figure 6-3. RMS residuals between reconstructed mass and gravimetric mass as a function of the assumed OM/OC ratio: (a) Phoenix and (b) St. Louis.

The sensitivity of mass balance closure to OC artifact correction was examined by assuming a negligible negative artifact and assuming the grand mean field blank mass loading. (Appendix D is a representative measure of the positive artifact for both the dichot major and minor flow channel samples). Artifact-corrected OC ambient mass concentrations for PM_f and PM_c were calculated after subtracting the filter- and trip-blank pooled mean OC loading of 6.6 µg/filter from the major and minor flow channels. The best-fit OM/OC ratios were 1.4 for PM_f at Phoenix and 2.1 for St. Louis. For PM_c, the best-fit OM/OC ratios were 0.5 at Phoenix and 1.6 at St. Louis. Once again, the ratio for PM_c at Phoenix is implausible and the response surface for the RMS residual at St. Louis is very flat, which means the ratio is highly uncertain.

6.2 Mass Balance Implications

Mass balance closure for PM_c can be influenced by several factors, including but not limited to OC artifact correction, the assumed OM/OC ratio, the assumed soil oxides composition, and XRF attenuation factors used for light elements. If all else is equal, a correction applied for a negative OC artifact decreases the reconstructed mass and requires a higher OM/OC ratio to achieve closure compared with the case of no artifact correction.

For PM_c at St. Louis, plausible OM/OC ratios were estimated when including and excluding a correction for positive artifacts. However, the estimated OM/OC ratios are highly uncertain.

For PM_c at Phoenix, implausible OM/OC ratios were estimated for no OC artifact correction and also for when a correction was applied for positive artifacts using field blanks data. In both cases, the reconstructed mass is greater than the gravimetric mass for OM/OC ratios larger than approximately 0.5. This finding demonstrates that the reconstructed mass is being systematically overestimated, with possible explanations being bias in the XRF attenuation factors applied to Al, Si, and Ca; or bias in the multipliers used to account for the oxide forms of the crustal elements; or both. Mass balance closure alone cannot be used to obtain meaningful best-fit attenuation factors and oxides multipliers. Furthermore, the best-fit values depend on assumed OC artifact correction and OM/OC ratio.

7. Comparison of FDMS TEOM and Filter Coarse PM Measurements

In addition to the dichot and FRM measurements, each site also had a Thermo 1405-DF dichotomous TEOM with FDMS®. The Thermo 1405-DF dichotomous sampler with FDMS is an approved FEM for $PM_{2.5}$. The 1405-DF measures fine ($PM_{2.5}$) and coarse ($PM_{10\text{-}2.5}$) particulate matter mass concentrations at six-minute time resolution. Its deployment in this study provides insights into the climatology of coarse PM by placing the 24-hour integrated chemical speciation samples in a broader context with daily, high-time resolved, coverage of PM mass, and also by providing the ability to examine diurnal behavior.

The dichot TEOM includes a 16.7 LPM standard PM_{10} inlet followed by a virtual impactor that splits the sample stream into major (15.0 LPM) and minor (1.67 LPM) flows. A portion of the major flow stream and the entire minor flow stream pass through Nafion dryers; subsequently, the entrained particles are deposited onto TEOM filters for mass determination.

The major flow includes only fine particles, whereas the minor flow includes all of the coarse particles and 10% of the fine particles; therefore, $PM_{2.5}$ mass concentrations are calculated directly from the major flow, and $PM_{10\text{-}2.5}$ mass concentrations are calculated by correcting the minor flow for fine-particle intrusion. In both cases, the size-segregated mass is further partitioned into volatile (reference) and nonvolatile (base) components by the dual-channel FDMS (Meyer et al., 2002). This partitioning is operationally defined by the measurement method. $PM_{2.5}$ FDMS volatility component concentrations are the same as the major flow volatility component concentrations. *It is often not appreciated that the instrument reports FDMS volatility component (base and reference) concentrations for the minor flow rather than for $PM_{10\text{-}2.5}$*. The base and reference flows contain 10% of the fine particles; therefore, the user must apply Equation 7-1 to calculate the $PM_{10\text{-}2.5}$ volatile and nonvolatile mass concentrations from the instrument-reported data.

$$PM_{10-2.5}(k) = PM_{\text{minor}}(k) - \frac{Q_{\text{minor}}}{Q_{\text{total}}} PM_{\text{major}}(k) \qquad \textbf{(Eq. 7-1)}$$

where *PM* is the mass concentration, *Q* is the volumetric flow rate, and *k* is the FDMS volatility component, i.e., volatile (reference) or nonvolatile (base).

Previous work has linked the volatile component of fine PM, as measured by the FDMS TEOM, to semivolatile particulate matter, including ammonium nitrate and semivolatile organic compounds (Grover et al., 2005; Faveza et al., 2007). The project team's immediate objective, as described below, was to use the dichot TEOM data to examine the temporal behavior of the volatile and nonvolatile components of both fine and coarse PM at the two contrasting sites.

Dichot TEOMs were deployed at the Phoenix and St. Louis sites, with data reporting starting in July 2010 and September 2010, respectively. Data were collected on six-minute cycles and converted to hourly averages. Raw (unvalidated) hourly fine and coarse PM mass concentrations were automatically uploaded to AirNow-Tech (www.airnowtech.org). Data for mass and FDMS volatility components were periodically provided by the Maricopa County Air

Quality Department (for Phoenix) and the Air Quality Laboratory at Washington University (for St. Louis) to the data analysis team for further validation and interpretation.

The data were censored to remove records with unstable base and reference readings (e.g., large fluctuations within the hour). In the case of Phoenix, this resulted in the removal of 18 days (about 10% of the total data set), including the six days for which the highest concentrations were reported. The removal of these data does not significantly affect the analyses presented in this report, which focuses on central tendencies of the data sets.

Non-volatile/volatile data at Phoenix after February 2011 were unstable and showed unusually high noise, and so are not included in analyses here; data at St. Louis after replacement of a Nafion dryer in mid-March exhibited noise as well, and are not included here.

7.1 Results

Figure 7-1 compares daily-average dichot TEOM total and nonvolatile mass concentrations to 24-hour integrated gravimetric mass concentrations using the sequential dichot sampler (St. Louis) and paired $PM_{2.5}$ and PM_{10} FRM samplers (Phoenix) with Teflon filters. The Phoenix dichot TEOM data are compared to the paired FRM samplers, rather than the dichot sampler, because the latter suffered from significant particle losses at Phoenix. For $PM_{2.5}$ at St. Louis (Figure 7-1a), the filter-based gravimetric mass concentrations are bounded by the TEOM-measured total and nonvolatile mass concentrations. This pattern is consistent with the Teflon filter retaining only a portion of the volatile ambient particulate matter due to partial loss of species such as ammonium nitrate and semivolatile organic matter. For $PM_{10\text{-}2.5}$ at St. Louis (Figure 7-1b), there is also very good agreement between the dichot TEOM and Teflon filter data, especially at low concentrations. The volatile component of $PM_{10\text{-}2.5}$ is relatively small. For $PM_{2.5}$ (Figure 7-1c), there is good agreement at low concentrations, with the Teflon filter mass closely tracking the dichot TEOM nonvolatile mass. The FRM filter sampler retains virtually none of the volatile mass, with the nonvolatile mass in nearly quantitative agreement with the Teflon filter gravimetric mass data. At high concentrations, the dichot TEOM $PM_{2.5}$ mass is biased high compared to the FRM $PM_{2.5}$ mass. This bias is also observed at all concentrations for the $PM_{10\text{-}2.5}$ data (Figure 7-1d). For all samples, the Phoenix $PM_{10\text{-}2.5}$ is essentially nonvolatile.

The minor flow volatile mass was typically 1 $\mu g/m^3$ or smaller. $PM_{10\text{-}2.5}$ volatile mass calculated using Equation 7-1 was about 50% of the minor flow volatile mass and the propagation of uncertainties through Equation 7-1 suggests that the $PM_{10\text{-}2.5}$ volatile mass concentration for such cases is highly uncertain. PM chemical composition data are available for many of these days, but the dichot TEOM $PM_{10\text{-}2.5}$ volatile component mass concentrations are too small and too uncertain to support meaningful comparisons to the speciation data. The remainder of this report focuses on time series analysis of the data collected to date. The project team's primary interest is the $PM_{10\text{-}2.5}$ trends, but $PM_{2.5}$ trends are also shown for comparison.

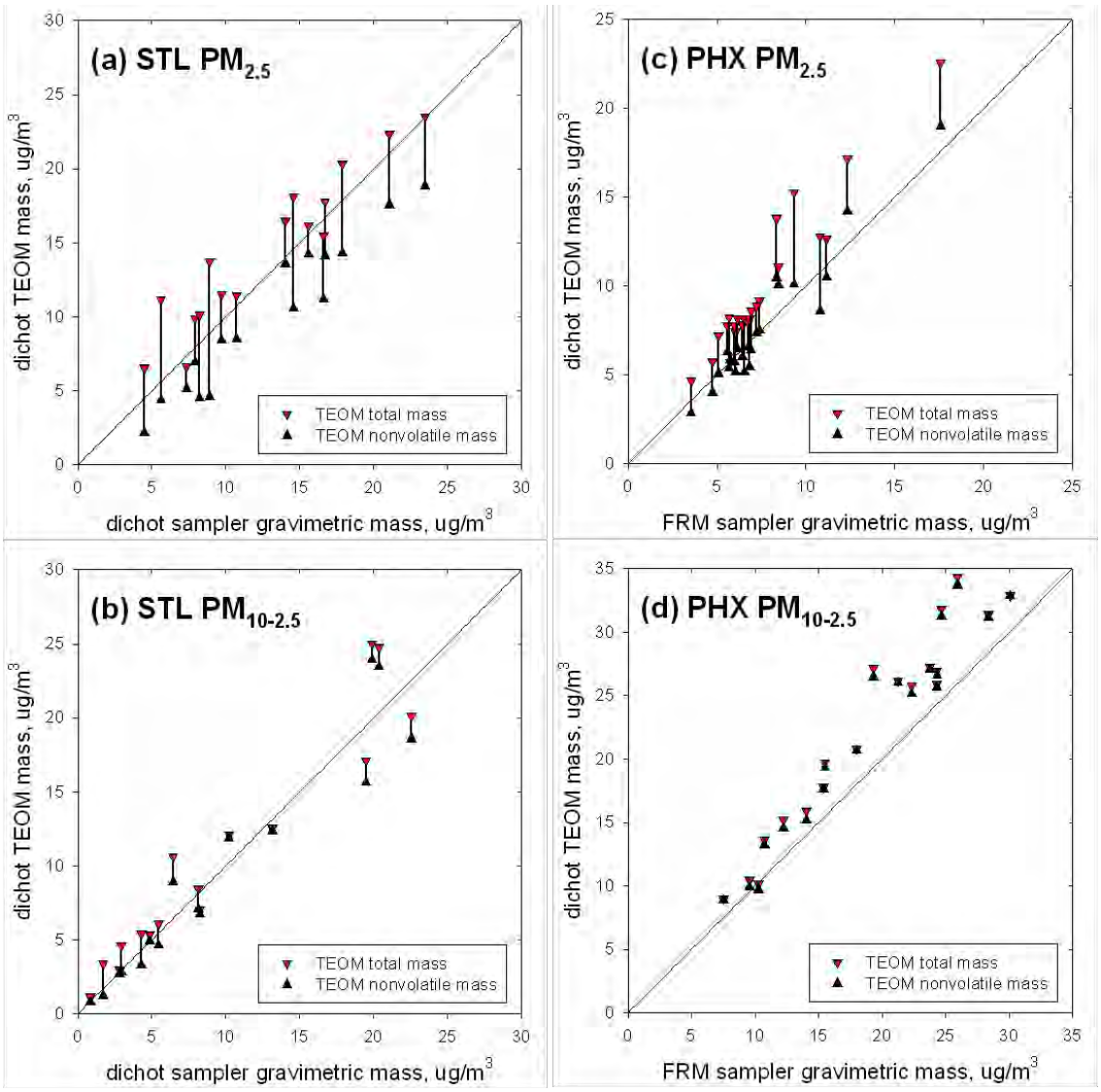

Figure 7-1. East St. Louis (left) and Phoenix (right) 24-hour average dichot TEOM total (red markers) and nonvolatile (black markers) PM mass concentrations versus the 24-hour integrated PM mass concentrations from filter-based samplers with gravimetric analysis on the Teflon filters: fine PM (top) and coarse PM (bottom). Lines connecting markers indicate corresponding data pairs. The diagonal line is the 1:1 relationship.

Figure 7-2 shows the time series for daily-average PM_{10} mass concentrations, stratified by fine and coarse PM contributions and presented as "stacked" graphs, at St. Louis (Figure 7-2a) and Phoenix (Figure 7-2b). At St. Louis, the fine PM mass is typically greater than the coarse PM mass (median $PM_{10-2.5}/PM_{2.5}$ ratio = 0.67), but there are periods with high coarse PM concentrations, such as mid-October. In contrast, at Phoenix, the coarse PM mass is much greater than the fine PM mass (median $PM_{10-2.5}/PM_{2.5}$ ratio = 2.8), but there are periods with relatively high fine particle mass, such as late January and early February. Overall, PM_{10} concentrations are much higher at Phoenix compared to St. Louis (note the twofold difference in the concentration scale ranges).

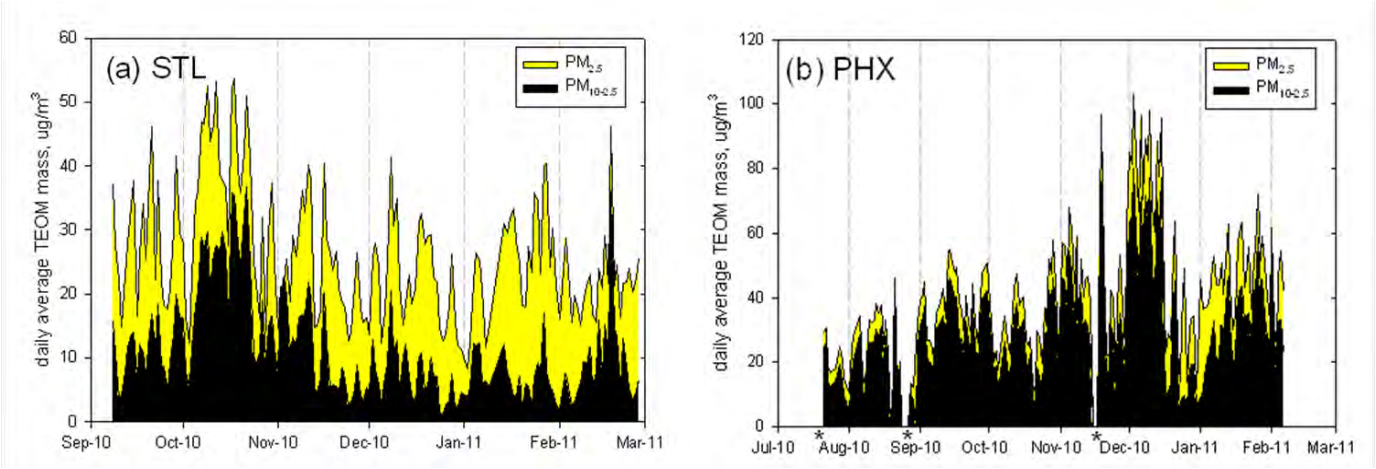

Figure 7-2. Daily-average dichot TEOM time series for fine PM (yellow) and coarse PM (black) at (a) East St. Louis, 9/2010-2/2011; and (b) Phoenix, 7/2010-2/2011. Note the concentration scale range differences (60 μg/m^3 for STL, 120 μg/m^3 for PHX). Asterisks below the x-axis in the PHX plot denote periods with three or more successive days of data removed.

Figure 7-3 shows the fine PM and coarse PM mass concentrations further stratified by FDMS volatility components. $PM_{2.5}$ volatile mass is appreciable at both St. Louis and Phoenix (Figure 7-3a,c), with median $PM_{2.5}$ volatile/total mass ratios of 0.30 and 0.21, respectively. In contrast, the $PM_{10-2.5}$ volatile mass at both sites (Figure 7-3b,d) is very small, with median $PM_{2.5}$ volatile/total mass ratios of 0.05 at St. Louis and 0.01 at Phoenix. The $PM_{10-2.5}$ mass concentrations for Phoenix are twice as high as those for St. Louis, as noted by the twofold scale range for Phoenix compared to St. Louis.

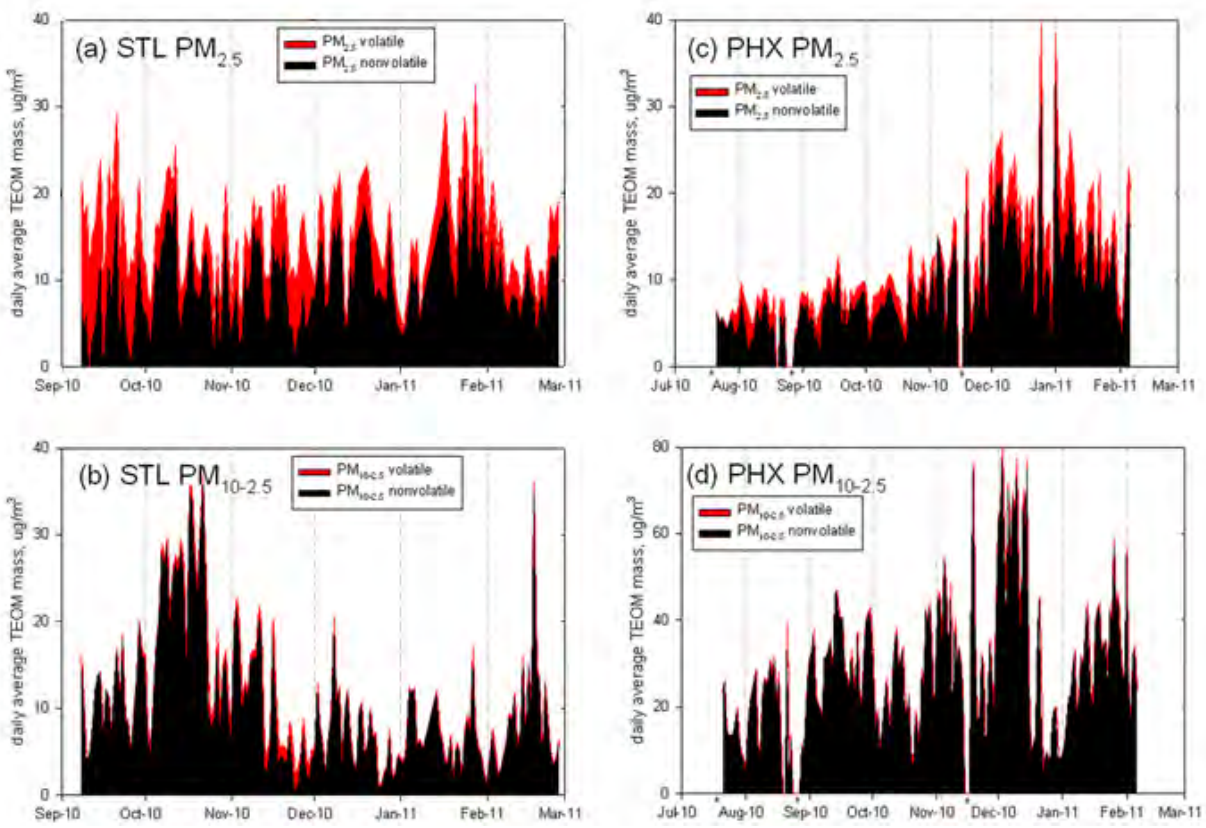

Figure 7-3. Daily-average dichot TEOM time series for fine PM (top) and coarse PM (bottom) at East St. Louis, 9/2010-2/2011 (left), and Phoenix, 7/2010-2/2011 (right). Daily average mass concentrations are partitioned into FDMS volatile (red) and nonvolatile (black) components. Note the concentration scale range is twice as high for Phoenix $PM_{10-2.5}$ (panel d). Asterisks below the x-axis in the Phoenix plots denote periods with three or more successive days of data removed.

Figure 7-4 shows diurnal profiles for $PM_{2.5}$ total (Figure 7-4a), nonvolatile (Figure 7-4b), and volatile (Figure 7-4c) mass at St. Louis and Phoenix. At St. Louis, there is a shallow midday minimum in both the total and nonvolatile mass that is consistent with dilution by daytime growth in the mixing layer depth. In contrast to the nonvolatile component, the volatile component exhibits a midday maximum. The data collected includes relatively low nitrate, so the volatile component is likely semivolatile organic aerosol. The midday maximum in the diurnal profile is consistent with the production of semivolatile organic aerosol by secondary processes in the atmosphere (Faveza et al., 2007). At Phoenix, total and nonvolatile mass increases in the early morning before rush hour, reaching a maximum at 0800 to 0900 local standard time (LST), followed by a deep midday minimum. Like St. Louis, the volatile component at Phoenix exhibits a midday maximum consistent with the secondary production of semivolatile organic aerosol.

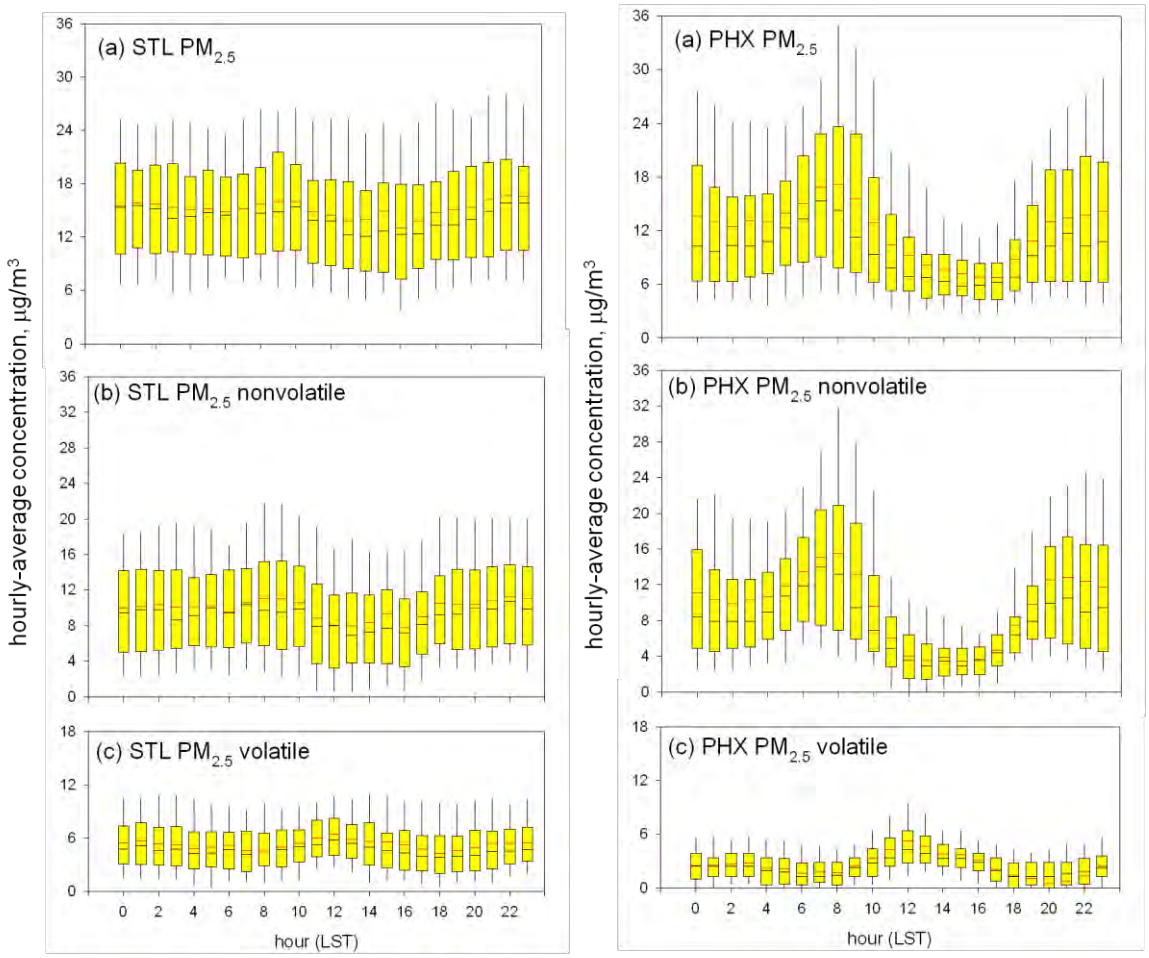

Figure 7-4. $PM_{2.5}$ diurnal profiles for East St. Louis, 9/2010 to 2/2011 (left) and Phoenix, 7/2010 to 2/2011 (right): (a) total TEOM mass; (b) nonvolatile TEOM mass; and (c) volatile TEOM mass. Whiskers are 10th and 90th percentiles, boxes are 25th and 75th percentiles, and the interior black and red lines are the median and arithmetic mean, respectively.

Figure 7-5 shows diurnal profiles for $PM_{10-2.5}$ total mass (Figure 7-5a) and volatile mass (Figure 7-5b) at St. Louis and Phoenix. Because of the extremely low concentrations, the volatile component concentrations have high uncertainty and therefore are not interpreted.

Because of the very low volatile mass in the coarse aerosol (Figure 7-5b), nonvolatile mass concentrations closely track the total mass; therefore, profiles are not shown for the nonvolatile mass concentrations. The $PM_{10-2.5}$ total mass diurnal profile at St. Louis exhibits a broad midday maximum, which is in contrast to the broad midday minimum exhibited for $PM_{2.5}$ total mass. The Phoenix $PM_{10-2.5}$ total mass diurnal profile closely tracks the $PM_{2.5}$ profile with an early morning maximum and a deep midday minimum.

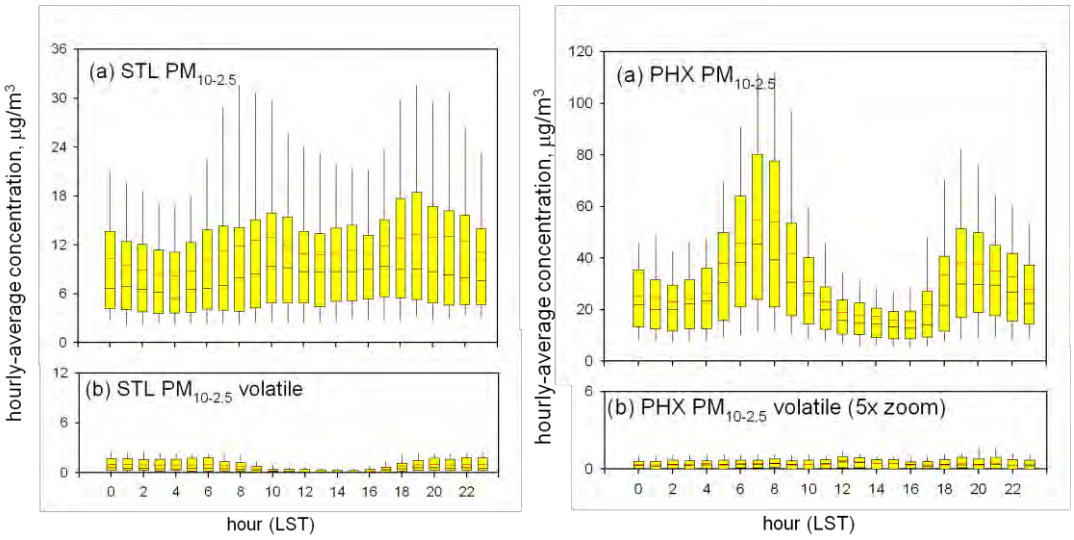

Figure 7-5. $PM_{10-2.5}$ diurnal profiles for East St. Louis, 9/2010 to 2/2011 (left) and Phoenix, 7/2010 to 2/2011 (right): (a) total TEOM mass and (b) volatile TEOM mass. Whiskers are 10th and 90th percentiles, boxes are 25th and 75th percentiles, and the interior black and red lines are the median and arithmetic mean, respectively.

To further examine these patterns, **Figure 7-6** shows $PM_{10-2.5}$ total mass diurnal profiles for weekdays (Figure 7-6a,b) and weekends (Figure 7-6c,d). For St. Louis, the broad midday maximum is observed on weekdays but not weekends. This suggests that the dominant driver for the elevated midday $PM_{10-2.5}$ concentrations at St. Louis is related to anthropogenic activities rather than windblown dust. For Phoenix, the early morning maximum is observed on weekdays but not weekends. This suggests that the elevated early morning $PM_{10-2.5}$ concentrations at Phoenix also arise from anthropogenic activities rather than windblown dust.

To further demonstrate the weekday excess $PM_{10-2.5}$ at both sites, **Figure 7-7** shows diurnal profiles for the difference between the median weekday mass and median weekend mass. The St. Louis weekday excess mass (green bars) is about 5 $\mu g/m^3$ from approximately 0700 to approximately 1900 LST. The weekday excess mass at Phoenix (red bars) is more than 5 $\mu g/m^3$ at 0500 LST, reaches a maximum of approximately 25 $\mu g/m^3$ at 0700 LST, and decays throughout the remainder of the morning hours. The weekday excess is about 4 $\mu g/m^3$ during the afternoon, and there is a local maximum at 1900 LST. Weekday versus weekday chemical speciation data should be examined for further insights into the origins of the weekday excess.

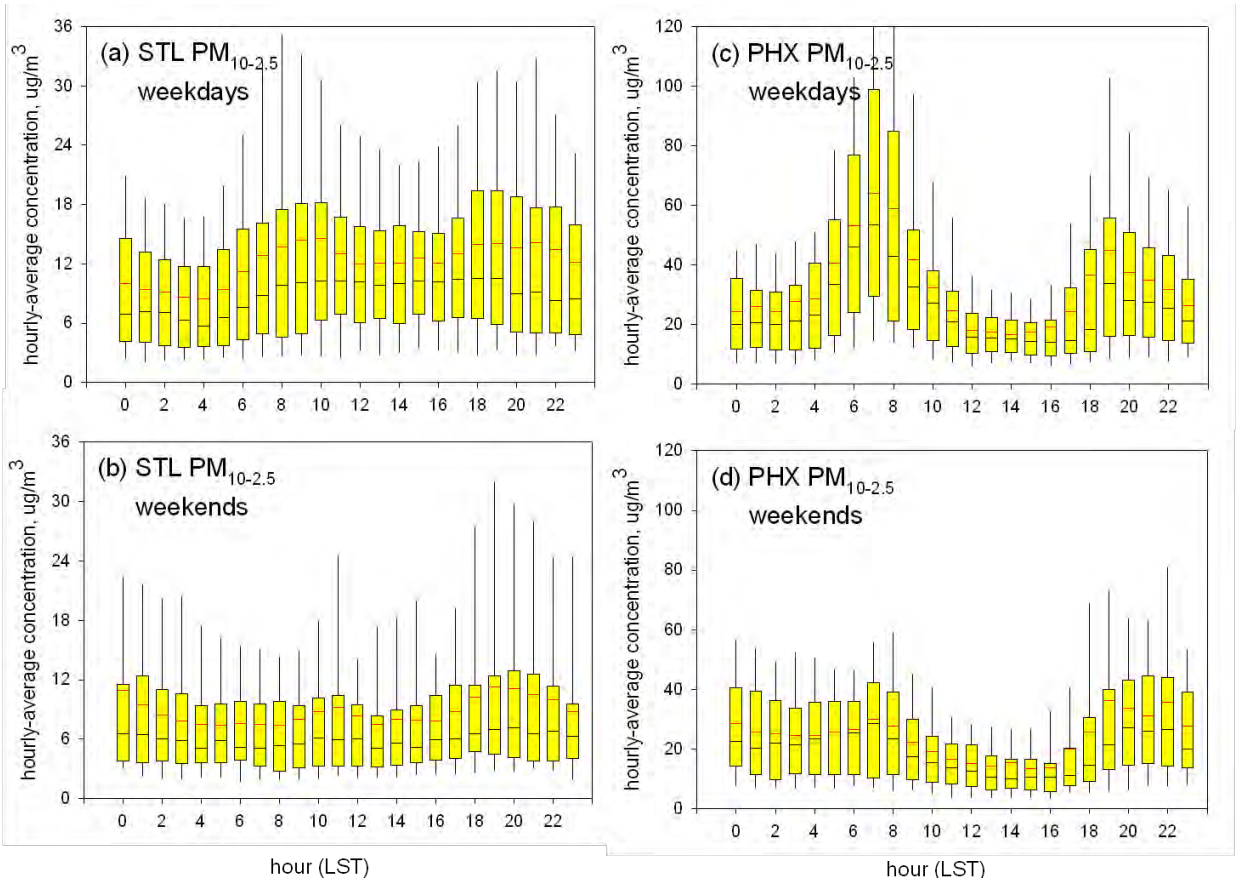

Figure 7-6. $PM_{10-2.5}$ weekday (top) and weekend (bottom) diurnal profiles for East St. Louis, 9/2010 to 2/2011 (left) and Phoenix, 7/2010 to 2/2011 (right). Whiskers are 10th and 90th percentiles, boxes are 25th and 75th percentiles, and the interior black and red lines are the median and arithmetic mean, respectively.

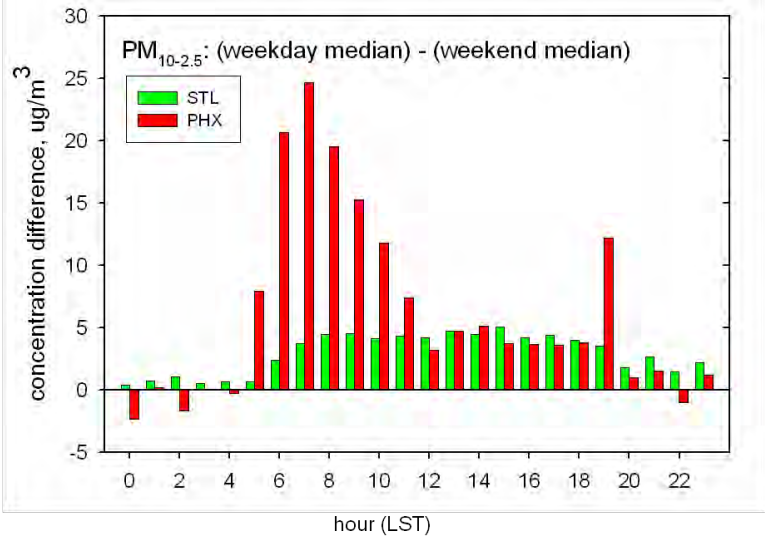

Figure 7-7. Diurnal profiles for the difference in weekday and weekend hourly median $PM_{10-2.5}$ concentrations for East St. Louis, 9/2010 to 2/2011 (green) and Phoenix, 7/2010 to 2/2011 (red).

7.2 FDMS TEOM-to-Dichot Summary

For the seven to eight months of dichot TEOM data collected in this study, the FDMS-defined volatile component of $PM_{2.5}$ at both St. Louis and Phoenix exhibits a midday maximum consistent with the production of semivolatile organic aerosol by secondary processes. The governing equation is presented in Equation 7-1 for calculating the FDMS-defined $PM_{10-2.5}$ volatility components from the minor and major flow data. At both sites, the $PM_{10-2.5}$ volatile component was relatively small. $PM_{10-2.5}$ total and nonvolatile mass is elevated on weekdays compared to weekends at both sites, albeit with different diurnal patterns for the weekday excess mass. Anthropogenic activities are the likely driver for this excess; more work exploring speciation data is needed to determine the precise nature of the contributing activities.

8. References

Ashbaugh L.L. and Eldred R.A. (2004) Loss of particle nitrate from Teflon sampling filters: Effects on measured gravimetric mass in California and in the IMPROVE network. *J. Air Waste Manage.*, 54(1), 93-104, Jan.

Bae M.S., Schauer J.J., and Turner J.R. (2006) Estimation of the monthly average ratios of organic mass to organic carbon for fine particulate matter at an urban site. *Aerosol Science & Technology*, 40, 1123-1139, September.

Chow J.C. and Watson J.G. (2002) $PM_{2.5}$ carbonate concentrations at regionally representative Interagency Monitoring of Protected Visual Environment sites. *Journal of Geophysical Research-Atmospheres*, 107(D21), Sep-Oct.

Dzubay T.G. and Stevens R.K. (1975) Ambient air analysis with dichotomous sampler and X-ray fluorescence spectrometer. *Environ. Sci. Technol.*, 9(7), July. Available at http://pubs.acs.org/doi/abs/10.1021/es60105a011.

Faveza O., Cachiera H., Sciarea J., and Moullec Y.L. (2007) Characterization and contribution to $PM_{2.5}$ of semi-volatile aerosols in Paris (France). *Atmos. Environ.*, 41(36), 7969-7976. Available at http://www.sciencedirect.com/science/article/pii/S1352231007008126.

Grover B.D., Kleinman M., Eatough N.L., Eatough D.J., Hopke P.K., Long R.W., Wilson W.E., Meyer M.B., and Ambs J.L. (2005) Measurement of total $PM_{2.5}$ mass (nonvolatile plus semivolatile) with the Filter Dynamic Measurement System tapered element oscillating microbalance monitor. *J. Geophys. Res.*, 110(D07S03), doi: 10.1029/2004JD004995. Available at http://www.agu.org/pubs/crossref/2005/2004JD004995.shtml.

Gutknecht W., Flanagan J., McWilliams A., Jayanty R.K., Kellogg R., Rice J., Duda P., and Sarver R.H. (2010) Harmonization of uncertainties of X-ray fluorescence data for $PM_{2.5}$ air filter analysis. *J. Air Waste Manage.*, 60(2), 184-194, (PubMed PMID: 20222531). Available at http://www.ncbi.nlm.nih.gov/pubmed/20222531.

Hyslop N.P. and White W.H. (2011) Identifying sources of uncertainty from the inter-species covariance of measurement errors. *Environ. Sci. Technol.*, 45(9), 4030-4037, doi: 10.1021/es102605x. Available at http://pubs.acs.org/doi/abs/10.1021/es102605x.

Lee T., Yu X-Y, Ayres B., Kreidenweis S.M., Malm W.C., and Collet J.L. (2008) Observations of fine and coarse particle nitrate at several rural locations in the United States. *Atmos. Environ.,* 42, 2720-2732.

Meyer M.B., Patashnick H., and Ambs J.L. (2002) Ongoing development of a continuous reference standard particulate matter mass monitor for ambient air. In *Proceedings from the Symposium on Air Quality Measurement Methods and Technology; A&WMA: Pittsburgh, PA*. Paper No. 53.

Simon H., Bhave P.V., Swall J.L., Frank N.H., and Malm W.C. (2011) Determining the spatial and seasonal variability in OM/OC ratios across the US using multiple regression. *Atmospheric Chemistry and Physics*, 11, 2933-2949, doi: 10.5194/acp-11-2933-2011. Available at http://www.atmos-chem-phys.net/11/2933/2011/acp-11-2933-2011.html.

Smith R.J. (2009) Use and misuse of the reduced major axis for line-fitting. *American Journal of Physical Anthropology*, 140, 476-486.

Tager I.B., Lurmann F.W., Haight T., Alcorn S., Penfold B., and Hammond S.K. (2010) Temporal and spatial patterns of ambient endotoxin concentrations in Fresno, California. *Environ. Health Persp.*, 118(10), 1490–1496, doi: 10.1289/ehp.0901602.

U.S. EPA (2001) Evaluation of PM2.5 chemical speciation samplers for use in the EPA national PM2.5 chemical speciation network. EPA-454/R-01-005, Office of Air Quality Planning and Standards, Research Triangle Park, NC 27711.

U.S.EPA (2010) $PM_{10-2.5}$ speciation pilot monitoring program, sample analysis, and data reporting: Quality Assurance Project Plan (QAPP). U.S. Environmental Protection Agency, March 2010. Available at http://epa.gov/ttn/amtic/pm10pilot.html.

U.S. EPA (2011) Field evaluation of the $PM_{2.5}$ federal reference method and development of a reference method method to measure and chemically speciate ambient coarse-mode aerosols. EPA/600/R-11/099, Office of Research and Development, National Exposure Research Laboratory, Reseach Triangle Park, NC 27711.

Appendix A: Summary Statistics

Table A-1. Summary of concentrations and MDLs by species and size fraction (PM_f or PM_c) at St. Louis for primary dichot, on Teflon and quartz filters; all species except OC and EC are from Teflon filter measurements. Two species, K and Na, were analyzed via XRF and IC; the latter analysis results are indicated by "_IC."

Species	Size	Avg Conc ($\mu g/m^3$)	Avg MDL ($\mu g/m^3$)	N	N > MDL	N > 3MDL	% > MDL	% > 3MDL	Avg Uncertainty ($\mu g/m^3$)
Ag_XRF	PM_c	0.0001	0.0145	31	0	0	0	0	N/A
Al_XRF	PM_c	0.2779	0.0098	31	30	29	97	94	0.0397
As_XRF	PM_c	0.0001	0.0010	31	0	0	0	0	N/A
Ba_XRF	PM_c	0.0142	0.0033	31	28	18	90	58	0.0025
Br_XRF	PM_c	0.0011	0.0009	31	12	3	39	10	0.0006
Ca_XRF	PM_c	1.1732	0.0017	31	31	31	100	100	0.1024
Cd_XRF	PM_c	0.0003	0.0089	31	0	0	0	0	N/A
Ce_XRF	PM_c	0.0000	0.0023	31	0	0	0	0	N/A
Cl_XRF	PM_c	0.2613	0.0019	31	31	31	100	100	0.0208
Co_XRF	PM_c	0.0008	0.0006	31	20	2	65	6	0.0005
Cr_XRF	PM_c	0.0017	0.0009	31	19	5	61	16	0.0005
Cs_XRF	PM_c	0.0004	0.0050	31	2	0	6	0	0.0029
Cu_XRF	PM_c	0.0050	0.0007	31	31	26	100	84	0.0006
Fe_XRF	PM_c	0.3109	0.0007	31	31	31	100	100	0.0227
In_XRF	PM_c	0.0004	0.0129	31	0	0	0	0	N/A
K_IC	PM_c	0.0376	0.0058	36	33	30	92	83	0.0040
K_XRF	PM_c	0.0921	0.0016	31	31	31	100	100	0.0082
Mass_Grav	PM_c	9.4453	0.3022	36	36	36	100	100	0.5661
Mg_XRF	PM_c	0.0740	0.0039	31	30	29	97	94	0.0139
Mn_XRF	PM_c	0.0071	0.0007	31	30	28	97	90	0.0007
Na_IC	PM_c	0.1974	0.0117	36	35	26	97	72	0.0337
Na_XRF	PM_c	0.2935	0.0113	31	29	24	94	77	0.0632
NH4_IC	PM_c	0.0083	0.0069	36	22	10	61	28	0.0250
Ni_XRF	PM_c	0.0003	0.0005	31	6	0	19	0	0.0002
NO3_IC	PM_c	0.4334	0.0028	36	36	36	100	100	0.0484
P_XRF	PM_c	0.0342	0.0037	31	22	22	71	71	0.0070
Pb_XRF	PM_c	0.0060	0.0018	31	15	5	48	16	0.0018
Rb_XRF	PM_c	0.0002	0.0010	31	1	0	3	0	0.0004
S_XRF	PM_c	0.1094	0.0026	31	31	31	100	100	0.0243
Sb_XRF	PM_c	0.0020	0.0206	31	1	0	3	0	0.0189
Se_XRF	PM_c	0.0001	0.0010	31	0	0	0	0	N/A

Species	Size	Avg Conc ($\mu g/m^3$)	Avg MDL ($\mu g/m^3$)	N	N > MDL	N > 3MDL	% > MDL	% > 3MDL	Avg Uncertainty ($\mu g/m^3$)
Si_XRF	PM_c	0.8686	0.0048	31	31	31	100	100	0.1180
Sn_XRF	PM_c	0.0016	0.0146	31	0	0	0	0	N/A
SO4_IC	PM_c	0.1959	0.0038	36	36	36	100	100	0.0590
Sr_XRF	PM_c	0.0024	0.0014	31	21	4	68	13	0.0007
Ti_XRF	PM_c	0.0118	0.0017	31	28	23	90	74	0.0016
V_XRF	PM_c	0.0004	0.0012	31	4	0	13	0	0.0008
Zn_XRF	PM_c	0.0663	0.0009	31	31	28	100	90	0.0051
Zr_XRF	PM_c	0.0022	0.0087	31	3	0	10	0	0.0048
Ag_XRF	PM_f	0.0002	0.0162	31	0	0	0	0	N/A
Al_XRF	PM_f	0.0406	0.0108	31	25	12	81	39	0.0073
As_XRF	PM_f	0.0005	0.0011	31	6	1	19	3	0.0009
Ba_XRF	PM_f	0.0029	0.0036	31	7	1	23	3	0.0024
Br_XRF	PM_f	0.0044	0.0010	31	30	19	97	61	0.0007
Ca_XRF	PM_f	0.0788	0.0019	31	31	31	100	100	0.0057
Cd_XRF	PM_f	0.0002	0.0099	31	0	0	0	0	N/A
Ce_XRF	PM_f	0.0000	0.0025	31	0	0	0	0	N/A
Cl_XRF	PM_f	0.0232	0.0021	31	31	27	100	87	0.0022
Co_XRF	PM_f	0.0004	0.0006	31	6	0	19	0	0.0004
Cr_XRF	PM_f	0.0010	0.0010	31	9	2	29	6	0.0005
Cs_XRF	PM_f	0.0007	0.0045	31	2	0	6	0	0.0028
Cu_XRF	PM_f	0.0046	0.0008	31	27	20	87	65	0.0006
Fe_XRF	PM_f	0.0831	0.0008	31	31	31	100	100	0.0060
In_XRF	PM_f	0.0007	0.0144	31	0	0	0	0	N/A
K_IC	PM_f	0.0577	0.0065	36	36	35	100	97	0.0045
K_XRF	PM_f	0.0626	0.0018	31	31	31	100	100	0.0045
Mass_Grav	PM_f	10.7419	0.3342	36	36	36	100	100	0.5517
Mg_XRF	PM_f	0.0068	0.0044	31	17	5	55	16	0.0025
Mn_XRF	PM_f	0.0025	0.0008	31	26	12	84	39	0.0004
Na_IC	PM_f	0.0505	0.0129	36	33	17	92	47	0.0252
Na_XRF	PM_f	0.0593	0.0119	31	30	17	97	55	0.0088
NH4_IC	PM_f	1.2044	0.0076	36	36	36	100	100	0.0853
Ni_XRF	PM_f	0.0002	0.0006	31	2	0	6	0	0.0003
NO3_IC	PM_f	1.0070	0.0031	36	36	36	100	100	0.0720
P_XRF	PM_f	0.0001	0.0040	31	0	0	0	0	N/A
Pb_XRF	PM_f	0.0070	0.0020	31	22	7	71	23	0.0016
Rb_XRF	PM_f	0.0001	0.0012	31	0	0	0	0	N/A

Species	Size	Avg Conc ($\mu g/m^3$)	Avg MDL ($\mu g/m^3$)	N	N > MDL	N > 3MDL	% > MDL	% > 3MDL	Avg Uncertainty ($\mu g/m^3$)
S_XRF	PM_f	0.8575	0.0028	31	31	31	100	100	0.0608
Sb_XRF	PM_f	0.0031	0.0228	31	0	0	0	0	N/A
Se_XRF	PM_f	0.0006	0.0011	31	5	0	16	0	0.0004
Si_XRF	PM_f	0.1005	0.0054	31	31	29	100	94	0.0092
Sn_XRF	PM_f	0.0008	0.0162	31	0	0	0	0	N/A
SO4_IC	PM_f	2.4379	0.0042	36	36	36	100	100	0.1734
Sr_XRF	PM_f	0.0004	0.0016	31	0	0	0	0	N/A
Ti_XRF	PM_f	0.0026	0.0019	31	12	3	39	10	0.0011
V_XRF	PM_f	0.0009	0.0013	31	9	1	29	3	0.0006
Zn_XRF	PM_f	0.0308	0.0010	31	31	31	100	100	0.0023
Zr_XRF	PM_f	0.0004	0.0097	31	0	0	0	0	N/A
EC_TOT	PM_c	0.3576	0.0640	41	29	25	71	61	N/A
OC_TOT	PM_c	2.0415	0.0640	41	40	40	98	98	N/A
EC_TOT	PM_f	0.5671	0.0640	41	40	37	98	90	N/A
OC_TOT	PM_f	3.1828	0.0640	41	41	41	100	100	N/A

Table A-2. Summary of concentrations and MDLs by species and size fraction (PM_f or PM_c) at St. Louis for FRM sampler, on Teflon and quartz filters; all species except OC and EC are from Teflon filter measurements. Two species, K and Na, were analyzed via XRF and IC; the latter analysis results are indicated by "_IC."

Species	Size	Avg Conc (µg/m^3)	Avg MDL (µg/m^3)	N	N > MDL	N > 3MDL	% > MDL	% > 3MDL	Avg Uncertainty (µg/m^3)
Ag_XRF	PM_c	0.0002	0.0136	38	0	0	0	0	N/A
Al_XRF	PM_c	0.3543	0.0094	38	38	38	100	100	0.0473
As_XRF	PM_c	0.0003	0.0010	38	6	2	16	5	0.0011
Ba_XRF	PM_c	0.0239	0.0034	38	37	32	97	84	0.0039
Br_XRF	PM_c	0.0019	0.0009	38	16	7	42	18	0.0013
Ca_XRF	PM_c	1.5866	0.0019	38	38	38	100	100	0.1361
Cd_XRF	PM_c	0.0007	0.0087	38	1	0	3	0	0.0083
Ce_XRF	PM_c	0.0024	0.0025	38	4	4	11	11	0.0035
Cl_XRF	PM_c	0.1622	0.0021	38	38	38	100	100	0.0138
Co_XRF	PM_c	0.0008	0.0006	38	25	3	66	8	0.0007
Cr_XRF	PM_c	0.0015	0.0009	38	25	7	66	18	0.0006
Cs_XRF	PM_c	-0.0001	0.0041	38	1	0	3	0	0.0042
Cu_XRF	PM_c	0.0071	0.0007	38	38	36	100	95	0.0011
Fe_XRF	PM_c	0.4297	0.0007	38	38	38	100	100	0.0380
In_XRF	PM_c	0.0001	0.0123	38	0	0	0	0	N/A
K_IC	PM_c	0.0391	0.0058	38	38	31	100	82	0.0091
K_XRF	PM_c	0.1274	0.0019	38	38	38	100	100	0.0164
Mass_Grav	PM_c	13.4626	0.3026	38	38	38	100	100	1.3528
Mg_XRF	PM_c	0.0908	0.0042	38	36	35	95	92	0.0162
Mn_XRF	PM_c	0.0104	0.0008	38	38	37	100	97	0.0012
Na_IC	PM_c	0.1445	0.0117	38	35	23	92	61	0.0376
Na_XRF	PM_c	0.1781	0.0116	38	37	26	97	68	0.0420
NH4_IC	PM_c	-0.0399	0.0069	38	10	5	26	13	0.1082
Ni_XRF	PM_c	0.0003	0.0005	38	14	0	37	0	0.0003
NO3_IC	PM_c	0.5952	0.0028	38	38	38	100	100	0.1253
P_XRF	PM_c	0.0526	0.0040	38	36	34	95	89	0.0067
Pb_XRF	PM_c	0.0048	0.0017	38	24	10	63	26	0.0026
Rb_XRF	PM_c	0.0002	0.0010	38	2	0	5	0	0.0006
S_XRF	PM_c	0.0661	0.0027	38	31	31	82	82	0.0787
Sb_XRF	PM_c	0.0000	0.0201	38	1	0	3	0	0.0201
Se_XRF	PM_c	0.0002	0.0009	38	3	0	8	0	0.0006
Si_XRF	PM_c	1.2516	0.0049	38	38	38	100	100	0.1676
Sn_XRF	PM_c	0.0007	0.0140	38	0	0	0	0	N/A

Species	Size	Avg Conc ($\mu g/m^3$)	Avg MDL ($\mu g/m^3$)	N	N > MDL	N > 3MDL	% > MDL	% > 3MDL	Avg Uncertainty ($\mu g/m^3$)
SO4_IC	PM_c	0.2262	0.0037	38	38	38	100	100	0.2505
Sr_XRF	PM_c	0.0031	0.0013	38	33	10	87	26	0.0014
Ti_XRF	PM_c	0.0179	0.0018	38	38	36	100	95	0.0022
V_XRF	PM_c	0.0013	0.0012	38	9	4	24	11	0.0012
Zn_XRF	PM_c	0.0326	0.0009	38	38	35	100	92	0.0043
Zr_XRF	PM_c	0.0017	0.0080	38	3	0	8	0	0.0070
Ag_XRF	PM_f	0.0001	0.0137	40	0	0	0	0	N/A
Al_XRF	PM_f	0.0387	0.0094	40	38	18	95	45	0.0064
As_XRF	PM_f	0.0006	0.0010	40	12	2	30	5	0.0008
Ba_XRF	PM_f	0.0042	0.0033	40	17	3	43	8	0.0023
Br_XRF	PM_f	0.0047	0.0009	40	40	31	100	78	0.0007
Ca_XRF	PM_f	0.0971	0.0018	40	40	40	100	100	0.0070
Cd_XRF	PM_f	0.0005	0.0087	40	1	0	3	0	0.0071
Ce_XRF	PM_f	0.0001	0.0024	40	0	0	0	0	N/A
Cl_XRF	PM_f	0.0167	0.0020	40	39	29	98	73	0.0017
Co_XRF	PM_f	0.0004	0.0006	40	9	0	23	0	0.0003
Cr_XRF	PM_f	0.0008	0.0009	40	12	2	30	5	0.0004
Cs_XRF	PM_f	0.0004	0.0040	40	0	0	0	0	N/A
Cu_XRF	PM_f	0.0052	0.0007	40	38	28	95	70	0.0005
Fe_XRF	PM_f	0.0956	0.0007	40	40	40	100	100	0.0068
In_XRF	PM_f	0.0009	0.0124	40	0	0	0	0	N/A
K_IC	PM_f	0.0632	0.0059	40	39	39	98	98	0.0050
K_XRF	PM_f	0.0717	0.0017	40	40	40	100	100	0.0052
Mass_Grav	PM_f	10.9770	0.3025	40	40	40	100	100	0.5600
Mg_XRF	PM_f	0.0088	0.0040	40	26	14	65	35	0.0024
Mn_XRF	PM_f	0.0029	0.0008	40	39	21	98	53	0.0004
Na_IC	PM_f	0.0433	0.0116	40	38	19	95	48	0.0207
Na_XRF	PM_f	0.0507	0.0110	40	40	24	100	60	0.0077
NH4_IC	PM_f	1.1790	0.0070	40	40	40	100	100	0.0836
Ni_XRF	PM_f	0.0002	0.0005	40	3	0	8	0	0.0002
NO3_IC	PM_f	0.8343	0.0028	40	40	40	100	100	0.0597
P_XRF	PM_f	0.0003	0.0039	40	1	0	3	0	0.0025
Pb_XRF	PM_f	0.0076	0.0018	40	35	17	88	43	0.0015
Rb_XRF	PM_f	0.0001	0.0010	40	1	0	3	0	0.0005
S_XRF	PM_f	0.8726	0.0027	40	40	40	100	100	0.0619
Sb_XRF	PM_f	0.0044	0.0202	40	2	0	5	0	0.0182
Se_XRF	PM_f	0.0006	0.0009	40	9	0	23	0	0.0004

Species	Size	Avg Conc ($\mu g/m^3$)	Avg MDL ($\mu g/m^3$)	N	N > MDL	N > 3MDL	% > MDL	% > 3MDL	Avg Uncertainty ($\mu g/m^3$)
Si_XRF	PM_f	0.1107	0.0047	40	40	40	100	100	0.0099
Sn_XRF	PM_f	0.0001	0.0140	40	0	0	0	0	N/A
SO4_IC	PM_f	2.4086	0.0036	40	40	40	100	100	0.1712
Sr_XRF	PM_f	0.0004	0.0013	40	2	0	5	0	0.0006
Ti_XRF	PM_f	0.0025	0.0017	40	19	2	48	5	0.0010
V_XRF	PM_f	0.0009	0.0012	40	10	2	25	5	0.0006
Zn_XRF	PM_f	0.0215	0.0009	40	40	40	100	100	0.0016
Zr_XRF	PM_f	0.0004	0.0081	40	0	0	0	0	N/A
EC_TOT	PM_c	0.3834	0.0640	26	24	20	92	77	N/A
OC_TOT	PM_c	1.8947	0.0640	26	24	24	92	92	N/A
EC_TOT	PM_f	0.5907	0.0640	29	29	27	100	93	N/A
OC_TOT	PM_f	3.3402	0.0640	29	29	29	100	100	N/A

Table A-3. Summary of concentrations and MDLs by species and size fraction (PM_f or PM_c) at Phoenix for primary dichot, on Teflon and quartz filters; all species except OC and EC are from Teflon filter measurements. Two species, K and Na, were analyzed via XRF and IC; the latter analysis results are indicated by "_IC."

Species	Size	Avg Conc ($\mu g/m^3$)	Avg MDL ($\mu g/m^3$)	N	N> MDL	N > 3MDL	% > MDL	% > 3MDL	Avg Uncertainty ($\mu g/m^3$)
Ag_XRF	PM_c	0.0001	0.0138	51	0	0	0	0	N/A
Al_XRF	PM_c	1.1182	0.0094	51	51	51	100	100	0.1420
As_XRF	PM_c	0.0003	0.0010	51	5	0	10	0	0.0007
Ba_XRF	PM_c	0.0281	0.0033	51	51	47	100	92	0.0037
Br_XRF	PM_c	0.0007	0.0009	51	22	1	43	2	0.0005
Ca_XRF	PM_c	1.1447	0.0019	51	51	51	100	100	0.0982
Cd_XRF	PM_c	0.0004	0.0087	51	0	0	0	0	N/A
Ce_XRF	PM_c	0.0010	0.0024	51	5	1	10	2	0.0024
Cl_XRF	PM_c	0.2680	0.0021	51	51	51	100	100	0.0216
Co_XRF	PM_c	0.0018	0.0006	51	44	27	86	53	0.0007
Cr_XRF	PM_c	0.0027	0.0009	51	47	21	92	41	0.0005
Cs_XRF	PM_c	0.0009	0.0043	51	7	0	14	0	0.0038
Cu_XRF	PM_c	0.0151	0.0007	51	51	51	100	100	0.0013
Fe_XRF	PM_c	0.7905	0.0007	51	51	51	100	100	0.0575
In_XRF	PM_c	0.0004	0.0124	51	0	0	0	0	N/A
K_IC	PM_c	0.0732	0.0057	61	61	61	100	100	0.0064
K_XRF	PM_c	0.3853	0.0018	51	51	51	100	100	0.0321
Mass_Grav	PM_c	18.7492	0.3013	61	61	61	100	100	0.9885
Mg_XRF	PM_c	0.1221	0.0040	51	51	51	100	100	0.0211
Mn_XRF	PM_c	0.0156	0.0008	51	51	51	100	100	0.0013
Na_IC	PM_c	0.2472	0.0120	61	61	61	100	100	0.0349
Na_XRF	PM_c	0.2731	0.0113	51	51	51	100	100	0.0547
NH4_IC	PM_c	0.0039	0.0068	61	29	6	48	10	0.0076
Ni_XRF	PM_c	0.0010	0.0005	51	40	10	78	20	0.0003
NO3_IC	PM_c	0.4154	0.0028	61	61	61	100	100	0.0368
P_XRF	PM_c	0.0414	0.0039	51	51	46	100	90	0.0063
Pb_XRF	PM_c	0.0026	0.0017	51	26	3	51	6	0.0013
Rb_XRF	PM_c	0.0012	0.0010	51	29	1	57	2	0.0005
S_XRF	PM_c	0.1274	0.0027	51	51	51	100	100	0.0151
Sb_XRF	PM_c	0.0036	0.0202	51	4	0	8	0	0.0187
Se_XRF	PM_c	0.0001	0.0009	51	0	0	0	0	N/A
Si_XRF	PM_c	3.3396	0.0048	51	51	51	100	100	0.4380

Species	Size	Avg Conc ($\mu g/m^3$)	Avg MDL ($\mu g/m^3$)	N	N> MDL	N > 3MDL	% > MDL	% > 3MDL	Avg Uncertainty ($\mu g/m^3$)
Sn_XRF	PM_c	0.0016	0.0140	51	0	0	0	0	N/A
SO4_IC	PM_c	0.2836	0.0036	61	61	61	100	100	0.0324
Sr_XRF	PM_c	0.0068	0.0013	51	47	39	92	76	0.0011
Ti_XRF	PM_c	0.0575	0.0018	51	51	51	100	100	0.0045
V_XRF	PM_c	0.0009	0.0012	51	12	2	24	4	0.0010
Zn_XRF	PM_c	0.0354	0.0009	51	51	51	100	100	0.0029
Zr_XRF	PM_c	0.0026	0.0081	51	3	0	6	0	0.0056
Ag_XRF	PM_f	0.0002	0.0153	51	0	0	0	0	N/A
Al_XRF	PM_f	0.1286	0.0105	51	51	51	100	100	0.0139
As_XRF	PM_f	0.0006	0.0011	51	12	1	24	2	0.0008
Ba_XRF	PM_f	0.0064	0.0037	51	29	11	57	22	0.0026
Br_XRF	PM_f	0.0034	0.0010	51	51	32	100	63	0.0006
Ca_XRF	PM_f	0.1543	0.0021	51	51	51	100	100	0.0114
Cd_XRF	PM_f	0.0007	0.0097	51	0	0	0	0	N/A
Ce_XRF	PM_f	0.0000	0.0027	51	0	0	0	0	N/A
Cl_XRF	PM_f	0.0792	0.0022	51	51	43	100	84	0.0060
Co_XRF	PM_f	0.0006	0.0006	51	20	1	39	2	0.0005
Cr_XRF	PM_f	0.0015	0.0010	51	29	4	57	8	0.0005
Cs_XRF	PM_f	0.0010	0.0043	51	5	0	10	0	0.0029
Cu_XRF	PM_f	0.0060	0.0008	51	51	43	100	84	0.0006
Fe_XRF	PM_f	0.1990	0.0008	51	51	51	100	100	0.0141
In_XRF	PM_f	0.0001	0.0138	51	0	0	0	0	N/A
K_IC	PM_f	0.0801	0.0063	61	57	56	93	92	0.0063
K_XRF	PM_f	0.1336	0.0019	51	51	51	100	100	0.0097
Mass_Grav	PM_f	7.6092	0.3325	61	61	61	100	100	0.3985
Mg_XRF	PM_f	0.0264	0.0044	51	46	37	90	73	0.0041
Mn_XRF	PM_f	0.0051	0.0008	51	49	43	96	84	0.0006
Na_IC	PM_f	0.1084	0.0133	61	61	51	100	84	0.0264
Na_XRF	PM_f	0.1013	0.0120	51	51	42	100	82	0.0130
NH4_IC	PM_f	0.3586	0.0075	61	61	61	100	100	0.0254
Ni_XRF	PM_f	0.0007	0.0006	51	20	3	39	6	0.0003
NO3_IC	PM_f	0.5000	0.0031	61	61	61	100	100	0.0361
P_XRF	PM_f	0.0005	0.0043	51	2	0	4	0	0.0032
Pb_XRF	PM_f	0.0041	0.0019	51	26	9	51	18	0.0015
Rb_XRF	PM_f	0.0002	0.0012	51	1	0	2	0	0.0006
S_XRF	PM_f	0.3052	0.0030	51	51	51	100	100	0.0221

Species	Size	Avg Conc ($\mu g/m^3$)	Avg MDL ($\mu g/m^3$)	N	N> MDL	N > 3MDL	% > MDL	% > 3MDL	Avg Uncertainty ($\mu g/m^3$)
Sb_XRF	PM_f	0.0036	0.0224	51	2	0	4	0	0.0206
Se_XRF	PM_f	0.0002	0.0010	51	2	0	4	0	0.0004
Si_XRF	PM_f	0.3880	0.0053	51	51	51	100	100	0.0363
Sn_XRF	PM_f	0.0013	0.0155	51	0	0	0	0	N/A
SO4_IC	PM_f	0.8465	0.0040	61	61	61	100	100	0.0608
Sr_XRF	PM_f	0.0012	0.0015	51	13	1	25	2	0.0010
Ti_XRF	PM_f	0.0083	0.0020	51	51	31	100	61	0.0013
V_XRF	PM_f	0.0004	0.0013	51	5	0	10	0	0.0007
Zn_XRF	PM_f	0.0227	0.0009	51	51	51	100	100	0.0017
Zr_XRF	PM_f	0.0009	0.0090	51	0	0	0	0	N/A
EC_TOT	PM_c	0.1919	0.0640	48	36	21	75	44	N/A
OC_TOT	PM_c	2.3576	0.0640	48	48	48	100	100	N/A
EC_TOT	PM_f	0.7180	0.0640	48	47	45	98	94	N/A
OC_TOT	PM_f	2.4693	0.0640	48	48	48	100	100	N/A

Table A-4. Summary of concentrations and MDLs by species and size fraction (PM_f or PM_c) at Phoenix for FRM sampler, on Teflon and quartz filters; all species except OC and EC are from Teflon filter measurements. Two species, K and Na, were analyzed via XRF and IC; the latter analysis results are indicated by "_IC."

Species	Size	Avg Conc ($\mu g/m^3$)	Avg MDL ($\mu g/m^3$)	N	N > MDL	N > 3MDL	% > MDL	% > 3MDL	Avg Uncertainty ($\mu g/m^3$)
Ag_XRF	PM_c	-0.0001	0.0136	44	0	0	0	0	N/A
Al_XRF	PM_c	1.3564	0.0094	44	44	44	100	100	0.1738
As_XRF	PM_c	0.0005	0.0010	44	13	1	30	2	0.0011
Ba_XRF	PM_c	0.0369	0.0034	44	44	43	100	98	0.0056
Br_XRF	PM_c	0.0012	0.0009	44	28	2	64	5	0.0009
Ca_XRF	PM_c	1.4398	0.0020	44	44	44	100	100	0.1339
Cd_XRF	PM_c	0.0005	0.0087	44	0	0	0	0	N/A
Ce_XRF	PM_c	0.0013	0.0025	44	4	2	9	5	0.0029
Cl_XRF	PM_c	0.2782	0.0022	44	44	44	100	100	0.0279
Co_XRF	PM_c	0.0019	0.0006	44	36	23	82	52	0.0010
Cr_XRF	PM_c	0.0030	0.0009	44	37	22	84	50	0.0008
Cs_XRF	PM_c	-0.0005	0.0042	44	4	1	9	2	0.0049
Cu_XRF	PM_c	0.0186	0.0007	44	44	44	100	100	0.0021
Fe_XRF	PM_c	0.9827	0.0007	44	44	44	100	100	0.0900
In_XRF	PM_c	0.0004	0.0123	44	0	0	0	0	N/A
K_IC	PM_c	0.0773	0.0059	44	44	43	100	98	0.0144
K_XRF	PM_c	0.4816	0.0020	44	44	44	100	100	0.0502
Mass_Grav	PM_c	22.6664	0.3032	44	44	44	100	100	1.6672
Mg_XRF	PM_c	0.1480	0.0043	44	44	44	100	100	0.0259
Mn_XRF	PM_c	0.0194	0.0008	44	44	44	100	100	0.0021
Na_IC	PM_c	0.2424	0.0116	44	44	44	100	100	0.0475
Na_XRF	PM_c	0.3140	0.0121	44	44	44	100	100	0.0695
NH4_IC	PM_c	0.0030	0.0070	44	21	14	48	32	0.0314
Ni_XRF	PM_c	0.0013	0.0005	44	37	16	84	36	0.0004
NO3_IC	PM_c	0.4946	0.0028	44	44	44	100	100	0.1030
P_XRF	PM_c	0.0593	0.0040	44	43	42	98	95	0.0071
Pb_XRF	PM_c	0.0036	0.0018	44	33	6	75	14	0.0021
Rb_XRF	PM_c	0.0017	0.0010	44	33	6	75	14	0.0007
S_XRF	PM_c	0.1212	0.0028	44	44	44	100	100	0.0375
Sb_XRF	PM_c	0.0003	0.0202	44	0	0	0	0	N/A
Se_XRF	PM_c	0.0001	0.0010	44	1	0	2	0	0.0006
Si_XRF	PM_c	4.3101	0.0050	44	44	44	100	100	0.5878
Sn_XRF	PM_c	-0.0014	0.0140	44	0	0	0	0	N/A

Species	Size	Avg Conc ($\mu g/m^3$)	Avg MDL ($\mu g/m^3$)	N	N > MDL	N > 3MDL	% > MDL	% > 3MDL	Avg Uncertainty ($\mu g/m^3$)
SO4_IC	PM_c	0.3097	0.0037	44	44	44	100	100	0.1026
Sr_XRF	PM_c	0.0092	0.0013	44	42	40	95	91	0.0016
Ti_XRF	PM_c	0.0728	0.0018	44	44	44	100	100	0.0065
V_XRF	PM_c	0.0014	0.0012	44	16	3	36	7	0.0013
Zn_XRF	PM_c	0.0530	0.0009	44	44	44	100	100	0.0053
Zr_XRF	PM_c	0.0032	0.0080	44	6	2	14	5	0.0067
Ag_XRF	PM_f	0.0003	0.0136	45	0	0	0	0	N/A
Al_XRF	PM_f	0.1526	0.0094	45	45	45	100	100	0.0144
As_XRF	PM_f	0.0005	0.0010	45	9	1	20	2	0.0008
Ba_XRF	PM_f	0.0106	0.0033	45	31	22	69	49	0.0028
Br_XRF	PM_f	0.0032	0.0009	45	44	25	98	56	0.0006
Ca_XRF	PM_f	0.2033	0.0018	45	45	45	100	100	0.0145
Cd_XRF	PM_f	0.0005	0.0087	45	1	0	2	0	0.0080
Ce_XRF	PM_f	0.0000	0.0024	45	0	0	0	0	N/A
Cl_XRF	PM_f	0.0827	0.0020	45	45	43	100	96	0.0061
Co_XRF	PM_f	0.0009	0.0006	45	29	3	64	7	0.0005
Cr_XRF	PM_f	0.0018	0.0009	45	29	10	64	22	0.0005
Cs_XRF	PM_f	0.0016	0.0041	45	9	0	20	0	0.0028
Cu_XRF	PM_f	0.0077	0.0007	45	45	43	100	96	0.0007
Fe_XRF	PM_f	0.2564	0.0007	45	45	45	100	100	0.0182
In_XRF	PM_f	0.0008	0.0123	45	0	0	0	0	N/A
K_IC	PM_f	0.0920	0.0059	45	43	42	96	93	0.0072
K_XRF	PM_f	0.1478	0.0017	45	45	45	100	100	0.0105
Mass_Grav	PM_f	9.0100	0.3024	45	45	45	100	100	0.4649
Mg_XRF	PM_f	0.0255	0.0040	45	43	35	96	78	0.0033
Mn_XRF	PM_f	0.0063	0.0008	45	44	42	98	93	0.0006
Na_IC	PM_f	0.1092	0.0116	45	45	42	100	93	0.0243
Na_XRF	PM_f	0.0962	0.0110	45	45	39	100	87	0.0110
NH4_IC	PM_f	0.4103	0.0069	45	45	45	100	100	0.0292
Ni_XRF	PM_f	0.0009	0.0005	45	23	5	51	11	0.0003
NO3_IC	PM_f	0.7160	0.0028	45	45	45	100	100	0.0513
P_XRF	PM_f	0.0017	0.0039	45	5	2	11	4	0.0032
Pb_XRF	PM_f	0.0047	0.0018	45	23	10	51	22	0.0015
Rb_XRF	PM_f	0.0002	0.0010	45	2	0	4	0	0.0005
S_XRF	PM_f	0.3032	0.0027	45	45	45	100	100	0.0216
Sb_XRF	PM_f	0.0021	0.0201	45	1	0	2	0	0.0156
Se_XRF	PM_f	0.0002	0.0009	45	1	0	2	0	0.0005

Species	Size	Avg Conc ($\mu g/m^3$)	Avg MDL ($\mu g/m^3$)	N	N > MDL	N > 3MDL	% > MDL	% > 3MDL	Avg Uncertainty ($\mu g/m^3$)
Si_XRF	PM_f	0.4651	0.0047	45	45	45	100	100	0.0388
Sn_XRF	PM_f	0.0017	0.0140	45	0	0	0	0	N/A
SO4_IC	PM_f	0.8495	0.0037	45	45	45	100	100	0.0609
Sr_XRF	PM_f	0.0017	0.0013	45	24	4	53	9	0.0007
Ti_XRF	PM_f	0.0117	0.0017	45	45	38	100	84	0.0014
V_XRF	PM_f	0.0004	0.0012	45	4	0	9	0	0.0007
Zn_XRF	PM_f	0.0173	0.0009	45	45	45	100	100	0.0013
Zr_XRF	PM_f	0.0013	0.0080	45	1	0	2	0	0.0047
EC_TOT	PM_c	0.2818	0.0640	29	24	17	83	59	N/A
OC_TOT	PM_c	2.1730	0.0640	29	28	27	97	93	N/A
EC_TOT	PM_f	0.6420	0.0640	30	28	25	93	83	N/A
OC_TOT	PM_f	2.3259	0.0640	30	30	30	100	100	N/A

Table A-5. Summary of concentrations by species and size fraction (PM_{10} or $PM_{2.5}$) at St. Louis for FRM sampler, on Teflon and quartz filters; all species except OC and EC are from Teflon filter measurements. Two species, K and Na, were analyzed via XRF and IC; the latter analysis results are indicated by "_IC."

Species	Avg $PM_{2.5}$ ($\mu g/m^3$)	Avg PM_{10} ($\mu g/m^3$)	Avg (PM_{10}/PM_{25}) ($\mu g/m^3$)	Avg $PM_{10-2.5}$ ($\mu g/m^3$)
EC_TOR	0.7776	1.244	1.8529	0.4664
OC_TOR	3.114	4.9257	1.7234	1.8117
Ag_XRF	0.0001	0.0003	0.6316	0.0002
Al_XRF	0.0389	0.3931	15.7212	0.3543
As_XRF	0.0006	0.0009	2.865	0.0003
Ba_XRF	0.0036	0.0275	8.5088	0.0239
Br_XRF	0.0047	0.0066	1.342	0.0019
Ca_XRF	0.0979	1.6845	17.6537	1.5866
Cd_XRF	0.0005	0.0012	0.7959	0.0007
Ce_XRF	0.0001	0.0025	10.0014	0.0024
Cl_XRF	0.0173	0.1795	9.2252	0.1622
Co_XRF	0.0003	0.0012	3.6365	0.0008
Cr_XRF	0.0008	0.0023	14.3764	0.0015
Cs_XRF	0.0004	0.0004	2.1755	-0.0001
Cu_XRF	0.0052	0.0123	2.6465	0.0071
Fe_XRF	0.0977	0.5273	5.7266	0.4297
In_XRF	0.0009	0.0011	0.8065	0.0001
K_IC	0.064	0.1031	1.7057	0.0391
K_XRF	0.0723	0.1997	2.9407	0.1274
Mass_Grav	10.9587	24.4213	2.3083	13.4626
Mg_XRF	0.0087	0.0995	24.7169	0.0908
Mn_XRF	0.003	0.0133	5.1863	0.0104
Na_IC	0.0444	0.1889	3.8968	0.1445
Na_XRF	0.0509	0.229	4.2644	0.1781
NH4_IC	1.1763	1.1363	0.9748	-0.0399
Ni_XRF	0.0002	0.0005	3.0465	0.0003
NO3_IC	0.8753	1.4705	5.5111	0.5952
P_XRF	0.0003	0.0529	360.3697	0.0526
Pb_XRF	0.0077	0.0125	1.713	0.0048
Rb_XRF	0.0001	0.0004	1.1014	0.0002
S_XRF	0.859	0.9252	1.1038	0.0661
Sb_XRF	0.0043	0.0043	1.7227	0
Se_XRF	0.0006	0.0008	1.4583	0.0002
Si_XRF	0.1107	1.3622	14.1381	1.2516

Species	Avg $PM_{2.5}$ ($\mu g/m^3$)	Avg PM_{10} ($\mu g/m^3$)	Avg (PM_{10}/PM_{25}) ($\mu g/m^3$)	Avg $PM_{10-2.5}$ ($\mu g/m^3$)
Sn_XRF	0.0001	0.0007	1.4	0.0007
SO4_IC	2.3774	2.6035	1.1025	0.2262
Sr_XRF	0.0004	0.0034	11.1222	0.0031
Ti_XRF	0.0025	0.0204	10.9788	0.0179
V_XRF	0.0009	0.0023	2.9389	0.0013
Zn_XRF	0.0222	0.0548	2.1138	0.0326
Zr_XRF	0.0004	0.0021	0.8464	0.0017

Table A-6. Summary of concentrations by species and size fraction (PM_{10} or $PM_{2.5}$) at Phoenix for FRM sampler, on Teflon and quartz filters; all species except OC and EC are from Teflon filter measurements. Two species, K and Na, were analyzed via XRF and IC; the latter analysis results are indicated by "_IC."

Species	Avg $PM_{2.5}$ ($\mu g/m^3$)	Avg PM_{10} ($\mu g/m^3$)	Avg (PM_{10}/PM_{25}) ($\mu g/m^3$)	Avg $PM_{10-2.5}$ ($\mu g/m^3$)
EC_TOR	0.705	0.9455	1.5653	0.2405
OC_TOR	2.2175	4.4318	2.0787	2.2143
Ag_XRF	0.0003	0.0002	0	-0.0001
Al_XRF	0.1548	1.5112	12.3484	1.3564
As_XRF	0.0004	0.0009	2.3656	0.0005
Ba_XRF	0.0105	0.0475	6.8446	0.0369
Br_XRF	0.0032	0.0044	1.5075	0.0012
Ca_XRF	0.2067	1.6465	9.2552	1.4398
Cd_XRF	0.0005	0.001	1.2469	0.0005
Ce_XRF	0	0.0014	0	0.0013
Cl_XRF	0.0841	0.3623	7.2231	0.2782
Co_XRF	0.0009	0.0028	9.68	0.0019
Cr_XRF	0.0019	0.0048	5.2488	0.003
Cs_XRF	0.0016	0.0011	1.5787	-0.0005
Cu_XRF	0.0078	0.0263	3.7401	0.0185
Fe_XRF	0.2592	1.2418	5.5261	0.9827
In_XRF	0.0009	0.0012	1.0127	0.0004
K_IC	0.0927	0.17	2.4991	0.0773
K_XRF	0.1492	0.6308	5.6951	0.4816
Mass_Grav	9.0859	31.7523	3.9565	22.6664
Mg_XRF	0.026	0.174	12.627	0.148
Mn_XRF	0.0063	0.0258	5.1943	0.0194
Na_IC	0.1105	0.3529	3.5033	0.2424
Na_XRF	0.0974	0.4115	4.8287	0.314
NH4_IC	0.4099	0.4128	1.0612	0.003
Ni_XRF	0.0009	0.0022	4.3738	0.0013
NO3_IC	0.7237	1.2184	2.8001	0.4946
P_XRF	0.0017	0.061	29.5247	0.0593
Pb_XRF	0.0048	0.0084	3.6215	0.0036
Rb_XRF	0.0002	0.002	6.657	0.0017
S_XRF	0.3023	0.4234	1.5213	0.1212
Sb_XRF	0.0021	0.0025	2.4151	0.0003
Se_XRF	0.0002	0.0002	1.5455	0

Species	Avg $PM_{2.5}$ ($\mu g/m^3$)	Avg PM_{10} ($\mu g/m^3$)	Avg (PM_{10}/PM_{25}) ($\mu g/m^3$)	Avg $PM_{10-2.5}$ ($\mu g/m^3$)
Si_XRF	0.4725	4.7826	11.8616	4.3101
Sn_XRF	0.0018	0.0004	0.018	-0.0014
SO4_IC	0.8447	1.1544	1.4591	0.3097
Sr_XRF	0.0017	0.0109	8.7813	0.0092
Ti_XRF	0.0118	0.0846	8.6226	0.0728
V_XRF	0.0004	0.0018	4.2143	0.0014
Zn_XRF	0.0175	0.0705	5.1821	0.053
Zr_XRF	0.0013	0.0045	2.8155	0.0032

Appendix B: Summary Ratios of Collocated Dichot Measurements

Table B-1. Dichot B-to-Dichot A concentration ratios were calculated for each sample and the means and medians of these distributions by species and size fraction (PM_f or PM_c) at Phoenix and St. Louis on Teflon and quartz filters are reported below; all species except OC and EC are from Teflon filter measurements. Two species, K and Na, were analyzed via XRF and IC; the latter analysis results are indicated by "_IC." Species that have at least 25% of samples above MDL are indicated in the last two columns.

Site ID	Size	Species	N > MDL	Avg (DichotB/ DichotA)	Med (DichotB/ DichotA)	%>MDL (Dichot A)	%>MDL (Dichot B)
PHX	PM_c	EC_TOT	5	0.95	0.68	68	75
PHX	PM_c	OC_TOT	14	1.22	1.20	100	100
PHX	PM_c	Al_XRF	22	0.95	0.94	100	100
PHX	PM_c	As_XRF	1	0.50	0.50		
PHX	PM_c	Ba_XRF	22	0.94	0.93	100	100
PHX	PM_c	Br_XRF	3	0.92	0.95	43	
PHX	PM_c	Ca_XRF	22	0.96	0.95	100	100
PHX	PM_c	Ce_XRF	2	1.03	1.03		
PHX	PM_c	Cl_XRF	22	0.94	0.93	100	100
PHX	PM_c	Co_XRF	18	1.18	0.86	86	78
PHX	PM_c	Cr_XRF	19	0.99	1.00	92	88
PHX	PM_c	Cs_XRF	1	1.34	1.34		
PHX	PM_c	Cu_XRF	22	0.95	0.95	100	100
PHX	PM_c	Fe_XRF	22	0.96	0.97	100	100
PHX	PM_c	K_IC	31	0.98	0.98	100	100
PHX	PM_c	K_XRF	22	0.96	0.96	100	100
PHX	PM_c	Mass_Grav	31	0.97	0.95	100	100
PHX	PM_c	Mg_XRF	22	0.97	1.01	100	100
PHX	PM_c	Mn_XRF	22	0.96	0.97	100	100
PHX	PM_c	Na_IC	31	1.01	0.95	100	100
PHX	PM_c	Na_XRF	22	0.92	0.86	100	100
PHX	PM_c	NH4_IC	6	1.05	1.11	48	32
PHX	PM_c	Ni_XRF	14	0.81	0.83	78	75
PHX	PM_c	NO3_IC	31	0.96	0.95	100	100
PHX	PM_c	P_XRF	20	0.91	0.93	100	91
PHX	PM_c	Pb_XRF	8	1.11	1.08	51	59
PHX	PM_c	Rb_XRF	8	1.14	1.11	57	53
PHX	PM_c	S_XRF	22	0.96	0.95	100	100
PHX	PM_c	Si_XRF	22	0.96	0.96	100	100

Site ID	Size	Species	N > MDL	Avg (DichotB/ DichotA)	Med (DichotB/ DichotA)	%>MDL (Dichot A)	%>MDL (Dichot B)
PHX	PM_c	SO4_IC	31	0.99	0.94	100	100
PHX	PM_c	Sr_XRF	20	0.94	0.94	92	91
PHX	PM_c	Ti_XRF	22	0.97	0.95	100	100
PHX	PM_c	V_XRF	3	1.04	1.11		28
PHX	PM_c	Zn_XRF	22	0.98	0.98	100	100
PHX	PM_f	Na_IC	3	1.21	1.28		
PHX	PM_f	NH4_IC	19	0.98	0.99	56	62
PHX	PM_f	NO3_IC	31	0.96	0.98	100	100
PHX	PM_f	SO4_IC	27	1.07	0.98	87	90
PHX	PM_f	EC_TOT	13	1.18	1.07	93	98
PHX	PM_f	OC_TOT	14	1.04	1.01	100	100
PHX	PM_f	Al_XRF	22	1.13	1.08	100	97
PHX	PM_f	As_XRF	2	0.89	0.89		
PHX	PM_f	Ba_XRF	11	1.03	0.85	57	62
PHX	PM_f	Br_XRF	21	1.07	1.07	100	94
PHX	PM_f	Ca_XRF	22	1.14	1.11	100	100
PHX	PM_f	Cl_XRF	22	1.11	1.09	100	97
PHX	PM_f	Co_XRF	6	0.88	0.81	39	44
PHX	PM_f	Cr_XRF	9	0.89	0.81	57	50
PHX	PM_f	Cs_XRF	1	1.25	1.25		
PHX	PM_f	Cu_XRF	22	1.08	1.04	100	97
PHX	PM_f	Fe_XRF	22	1.08	1.07	100	100
PHX	PM_f	K_IC	28	1.00	1.00	93	93
PHX	PM_f	K_XRF	22	1.07	1.07	100	100
PHX	PM_f	Mass_Grav	31	1.06	1.01	100	100
PHX	PM_f	Mg_XRF	18	1.15	1.04	90	88
PHX	PM_f	Mn_XRF	21	1.11	1.13	96	94
PHX	PM_f	Na_IC	31	1.04	1.02	100	100
PHX	PM_f	Na_XRF	22	1.13	1.13	100	100
PHX	PM_f	NH4_IC	31	0.99	0.98	100	100
PHX	PM_f	Ni_XRF	8	1.13	1.13	39	38
PHX	PM_f	NO3_IC	31	1.05	1.03	100	100
PHX	PM_f	Pb_XRF	9	1.21	1.13	51	56
PHX	PM_f	S_XRF	22	1.00	1.00	100	100
PHX	PM_f	Si_XRF	22	1.12	1.12	100	100
PHX	PM_f	SO4_IC	31	1.00	0.99	100	100
PHX	PM_f	Sr_XRF	5	1.30	1.17	25	47

Site ID	Size	Species	N > MDL	Avg (DichotB/ DichotA)	Med (DichotB/ DichotA)	%>MDL (Dichot A)	%>MDL (Dichot B)
PHX	PM_f	Ti_XRF	21	1.29	1.23	100	94
PHX	PM_f	Zn_XRF	22	1.08	1.05	100	100
STL	PM_c	EC_TOT	7	0.77	0.62	88	71
STL	PM_c	OC_TOT	13	0.97	0.90	100	98
STL	PM_c	Al_XRF	11	0.81	0.83	97	100
STL	PM_c	Ba_XRF	11	0.93	0.94	90	93
STL	PM_c	Br_XRF	4	1.19	1.15	39	36
STL	PM_c	Ca_XRF	11	0.90	0.92	100	100
STL	PM_c	Cl_XRF	11	0.84	0.85	100	100
STL	PM_c	Co_XRF	4	1.27	0.98	65	61
STL	PM_c	Cr_XRF	4	1.06	1.05	61	68
STL	PM_c	Cu_XRF	11	0.85	0.86	100	100
STL	PM_c	Fe_XRF	11	0.88	0.91	100	100
STL	PM_c	K_IC	8	0.89	0.93	92	90
STL	PM_c	K_XRF	11	0.88	0.87	100	100
STL	PM_c	Mass_Grav	11	0.84	0.89	100	100
STL	PM_c	Mg_XRF	11	0.78	0.88	97	100
STL	PM_c	Mn_XRF	10	0.90	0.89	97	100
STL	PM_c	Na_IC	11	0.91	0.87	97	97
STL	PM_c	Na_XRF	10	0.92	0.81	94	82
STL	PM_c	NH4_IC	3	0.54	0.63	61	45
STL	PM_c	Ni_XRF	1	1.10	1.10		
STL	PM_c	NO3_IC	11	0.97	0.94	100	100
STL	PM_c	P_XRF	8	0.83	0.85	71	82
STL	PM_c	Pb_XRF	5	0.88	0.92	48	54
STL	PM_c	S_XRF	11	0.92	0.86	100	100
STL	PM_c	Si_XRF	11	0.90	0.91	100	100
STL	PM_c	SO4_IC	11	0.86	0.83	100	100
STL	PM_c	Sr_XRF	6	0.83	0.82	68	64
STL	PM_c	Ti_XRF	10	0.86	0.87	90	100
STL	PM_c	V_XRF	1	1.10	1.10		
STL	PM_c	Zn_XRF	11	0.92	0.88	100	100
STL	PM_f	Na_IC	1	1.08	1.08		
STL	PM_f	NH4_IC	9	1.10	1.09	83	87
STL	PM_f	NO3_IC	11	1.02	1.01	100	100
STL	PM_f	SO4_IC	11	1.27	1.08	100	97
STL	PM_f	EC_TOT	13	0.82	0.80	100	98

Site ID	Size	Species	N > MDL	Avg (DichotB/ DichotA)	Med (DichotB/ DichotA)	%>MDL (Dichot A)	%>MDL (Dichot B)
STL	PM_f	OC_TOT	13	0.87	0.89	100	100
STL	PM_f	Al_XRF	8	1.14	1.08	81	82
STL	PM_f	As_XRF	1	1.90	1.90		29
STL	PM_f	Ba_XRF	2	1.20	1.20		39
STL	PM_f	Br_XRF	10	1.00	1.08	97	100
STL	PM_f	Ca_XRF	11	1.23	1.15	100	100
STL	PM_f	Cl_XRF	11	0.91	0.94	100	96
STL	PM_f	Cr_XRF	2	0.44	0.45	29	39
STL	PM_f	Cs_XRF	1	1.28	1.28		
STL	PM_f	Cu_XRF	10	1.51	1.30	87	96
STL	PM_f	Fe_XRF	11	1.11	1.04	100	100
STL	PM_f	K_IC	11	0.98	0.99	100	97
STL	PM_f	K_XRF	11	1.00	1.00	100	100
STL	PM_f	Mass_Grav	11	1.00	1.02	100	100
STL	PM_f	Mg_XRF	4	0.89	0.79	55	64
STL	PM_f	Mn_XRF	7	1.05	1.02	84	86
STL	PM_f	Na_IC	10	1.06	1.07	92	93
STL	PM_f	Na_XRF	10	1.24	1.21	97	100
STL	PM_f	NH4_IC	11	0.96	0.96	100	100
STL	PM_f	NO3_IC	11	0.93	0.96	100	100
STL	PM_f	Pb_XRF	6	0.96	0.89	71	82
STL	PM_f	S_XRF	11	0.96	0.97	100	100
STL	PM_f	Si_XRF	11	1.18	1.15	100	100
STL	PM_f	SO4_IC	11	0.98	0.98	100	100
STL	PM_f	Ti_XRF	3	1.40	1.10	39	50
STL	PM_f	V_XRF	1	0.74	0.74	29	
STL	PM_f	Zn_XRF	11	1.15	1.03	100	100

Appendix C: Summary of Dichot-to-FRM Comparisons

Table C-1. Dichot-to-FRM concentration ratios were calculated for each sample and the means and medians of these distributions by species and size fraction (PM_f or PM_c) at Phoenix and St. Louis on Teflon and quartz filters are reported below; all species except OC and EC are from Teflon filter measurements. Two species, K and Na, were analyzed via XRF and IC; the latter analysis results are indicated by "_IC." Species that have at least 25% of samples above MDL are indicated in the last two columns. Elements were analyzed by XRF, and ions were analyzed by IC. Potassium and sodium were analyzed by both methods.

Sampler_ID	Size	Species	N > MDL	Avg (Dichot/ FRM)	Med (Dichot/ FRM)	% > MDL (FRM)	% > MDL (Dichot)
PHX-Dichot_A	PM_c	EC_TOT	13	0.92	0.86	83	68
PHX-Dichot_A	PM_c	OC_TOT	20	1.13	0.98	97	100
PHX-Dichot_A	PM_c	Al_XRF	35	0.90	0.93	100	100
PHX-Dichot_A	PM_c	As_XRF	2	0.86	0.87	30	
PHX-Dichot_A	PM_c	Ba_XRF	35	0.85	0.80	100	100
PHX-Dichot_A	PM_c	Br_XRF	8	0.74	0.63	64	43
PHX-Dichot_A	PM_c	Ca_XRF	35	0.86	0.87	100	100
PHX-Dichot_A	PM_c	Ce_XRF	3	0.78	0.86		
PHX-Dichot_A	PM_c	Cl_XRF	35	0.92	0.94	100	100
PHX-Dichot_A	PM_c	Co_XRF	28	1.06	0.93	82	86
PHX-Dichot_A	PM_c	Cr_XRF	29	0.99	0.96	84	92
PHX-Dichot_A	PM_c	Cs_XRF	2	0.80	0.81		
PHX-Dichot_A	PM_c	Cu_XRF	35	0.99	0.93	100	100
PHX-Dichot_A	PM_c	Fe_XRF	35	0.85	0.85	100	100
PHX-Dichot_A	PM_c	K_IC	35	1.01	0.86	100	100
PHX-Dichot_A	PM_c	K_XRF	35	0.83	0.82	100	100
PHX-Dichot_A	PM_c	Mass_Grav	35	0.83	0.85	100	100
PHX-Dichot_A	PM_c	Mg_XRF	35	0.91	0.90	100	100
PHX-Dichot_A	PM_c	Mn_XRF	35	0.84	0.84	100	100
PHX-Dichot_A	PM_c	Na_IC	35	0.90	0.93	100	100
PHX-Dichot_A	PM_c	Na_XRF	35	0.87	0.89	100	100
PHX-Dichot_A	PM_c	NH4_IC	11	0.56	0.59	48	48
PHX-Dichot_A	PM_c	Ni_XRF	24	0.85	0.82	84	78
PHX-Dichot_A	PM_c	NO3_IC	35	0.83	0.83	100	100
PHX-Dichot_A	PM_c	P_XRF	34	0.68	0.66	98	100
PHX-Dichot_A	PM_c	Pb_XRF	18	0.84	0.71	75	51
PHX-Dichot_A	PM_c	Rb_XRF	15	0.75	0.69	75	57

Sampler_ID	Size	Species	N > MDL	Avg (Dichot/ FRM)	Med (Dichot/ FRM)	% > MDL (FRM)	% > MDL (Dichot)
PHX-Dichot_A	PM_c	S_XRF	35	1.17	1.08	100	100
PHX-Dichot_A	PM_c	Si_XRF	35	0.85	0.87	100	100
PHX-Dichot_A	PM_c	SO4_IC	35	0.93	0.93	100	100
PHX-Dichot_A	PM_c	Sr_XRF	33	0.76	0.77	95	92
PHX-Dichot_A	PM_c	Ti_XRF	35	0.85	0.86	100	100
PHX-Dichot_A	PM_c	V_XRF	7	0.92	0.71	36	
PHX-Dichot_A	PM_c	Zn_XRF	35	0.83	0.77	100	100
PHX-Dichot_A	PM_c	Zr_XRF	1	1.47	1.47		
PHX-Dichot_A	PM_f	Na_IC	1	0.98	0.98		
PHX-Dichot_A	PM_f	NH4_IC	22	1.00	0.99	60	56
PHX-Dichot_A	PM_f	NO3_IC	36	1.03	1.03	100	100
PHX-Dichot_A	PM_f	SO4_IC	22	1.49	1.36	73	87
PHX-Dichot_A	PM_f	EC_TOT	18	1.06	0.96	93	93
PHX-Dichot_A	PM_f	OC_TOT	21	1.03	0.99	100	100
PHX-Dichot_A	PM_f	Al_XRF	36	0.94	0.93	100	100
PHX-Dichot_A	PM_f	As_XRF	2	0.90	0.90		
PHX-Dichot_A	PM_f	Ba_XRF	18	0.88	0.98	69	57
PHX-Dichot_A	PM_f	Br_XRF	35	1.07	1.09	98	100
PHX-Dichot_A	PM_f	Ca_XRF	36	0.89	0.89	100	100
PHX-Dichot_A	PM_f	Cl_XRF	36	0.94	0.87	100	100
PHX-Dichot_A	PM_f	Co_XRF	12	0.99	0.83	64	39
PHX-Dichot_A	PM_f	Cr_XRF	18	0.87	0.90	64	57
PHX-Dichot_A	PM_f	Cs_XRF	1	0.93	0.93		
PHX-Dichot_A	PM_f	Cu_XRF	36	0.87	0.85	100	100
PHX-Dichot_A	PM_f	Fe_XRF	36	0.89	0.91	100	100
PHX-Dichot_A	PM_f	K_IC	34	1.00	1.00	96	93
PHX-Dichot_A	PM_f	K_XRF	36	0.93	0.94	100	100
PHX-Dichot_A	PM_f	Mass_Grav	36	0.92	0.94	100	100
PHX-Dichot_A	PM_f	Mg_XRF	30	1.48	0.98	96	90
PHX-Dichot_A	PM_f	Mn_XRF	34	0.91	0.94	98	96
PHX-Dichot_A	PM_f	Na_IC	36	0.89	0.85	100	100
PHX-Dichot_A	PM_f	Na_XRF	36	0.97	0.88	100	100
PHX-Dichot_A	PM_f	NH4_IC	36	0.97	0.99	100	100
PHX-Dichot_A	PM_f	Ni_XRF	12	0.92	0.88	51	39
PHX-Dichot_A	PM_f	NO3_IC	36	0.94	0.93	100	100

Sampler_ID	Size	Species	N > MDL	Avg (Dichot/ FRM)	Med (Dichot/ FRM)	% > MDL (FRM)	% > MDL (Dichot)
PHX-Dichot_A	PM_f	P_XRF	1	0.79	0.79		
PHX-Dichot_A	PM_f	Pb_XRF	14	0.91	0.87	51	51
PHX-Dichot_A	PM_f	Rb_XRF	1	1.27	1.27		
PHX-Dichot_A	PM_f	S_XRF	36	1.00	1.02	100	100
PHX-Dichot_A	PM_f	Si_XRF	36	0.92	0.89	100	100
PHX-Dichot_A	PM_f	SO4_IC	36	0.97	0.99	100	100
PHX-Dichot_A	PM_f	Sr_XRF	8	1.12	1.09	53	25
PHX-Dichot_A	PM_f	Ti_XRF	36	0.84	0.81	100	100
PHX-Dichot_A	PM_f	V_XRF	2	1.43	1.43		
PHX-Dichot_A	PM_f	Zn_XRF	36	1.01	0.97	100	100
PHX-Dichot_B	PM_c	EC_TOT	11	1.18	0.63	83	75
PHX-Dichot_B	PM_c	OC_TOT	22	1.40	1.13	97	100
PHX-Dichot_B	PM_c	Al_XRF	25	0.84	0.87	100	100
PHX-Dichot_B	PM_c	As_XRF	4	0.96	0.95	30	
PHX-Dichot_B	PM_c	Ba_XRF	25	0.79	0.76	100	100
PHX-Dichot_B	PM_c	Br_XRF	4	0.84	0.74	64	
PHX-Dichot_B	PM_c	Ca_XRF	25	0.81	0.82	100	100
PHX-Dichot_B	PM_c	Ce_XRF	3	0.70	0.64		
PHX-Dichot_B	PM_c	Cl_XRF	25	0.89	0.88	100	100
PHX-Dichot_B	PM_c	Co_XRF	17	1.07	0.84	82	78
PHX-Dichot_B	PM_c	Cr_XRF	18	0.81	0.84	84	88
PHX-Dichot_B	PM_c	Cs_XRF	1	0.83	0.83		
PHX-Dichot_B	PM_c	Cu_XRF	25	0.90	0.89	100	100
PHX-Dichot_B	PM_c	Fe_XRF	25	0.80	0.81	100	100
PHX-Dichot_B	PM_c	K_IC	25	1.02	0.92	100	100
PHX-Dichot_B	PM_c	K_XRF	25	0.79	0.78	100	100
PHX-Dichot_B	PM_c	Mass_Grav	25	0.81	0.83	100	100
PHX-Dichot_B	PM_c	Mg_XRF	25	0.87	0.93	100	100
PHX-Dichot_B	PM_c	Mn_XRF	25	0.81	0.82	100	100
PHX-Dichot_B	PM_c	Na_IC	25	0.88	0.89	100	100
PHX-Dichot_B	PM_c	Na_XRF	25	0.76	0.85	100	100
PHX-Dichot_B	PM_c	NH4_IC	7	0.44	0.42	48	32
PHX-Dichot_B	PM_c	Ni_XRF	16	0.75	0.71	84	75
PHX-Dichot_B	PM_c	NO3_IC	25	0.80	0.76	100	100
PHX-Dichot_B	PM_c	P_XRF	23	0.65	0.63	98	91

Sampler_ID	Size	Species	N > MDL	Avg (Dichot/ FRM)	Med (Dichot/ FRM)	% > MDL (FRM)	% > MDL (Dichot)
PHX-Dichot_B	PM_c	Pb_XRF	11	0.71	0.54	75	59
PHX-Dichot_B	PM_c	Rb_XRF	12	0.87	0.87	75	53
PHX-Dichot_B	PM_c	S_XRF	25	1.11	0.96	100	100
PHX-Dichot_B	PM_c	Si_XRF	25	0.79	0.82	100	100
PHX-Dichot_B	PM_c	SO4_IC	25	0.89	0.90	100	100
PHX-Dichot_B	PM_c	Sr_XRF	23	0.84	0.81	95	91
PHX-Dichot_B	PM_c	Ti_XRF	25	0.79	0.80	100	100
PHX-Dichot_B	PM_c	V_XRF	5	0.78	0.64	36	28
PHX-Dichot_B	PM_c	Zn_XRF	25	0.80	0.80	100	100
PHX-Dichot_B	PM_f	NH4_IC	14	1.01	1.05	60	62
PHX-Dichot_B	PM_f	NO3_IC	25	1.04	1.04	100	100
PHX-Dichot_B	PM_f	SO4_IC	18	1.32	1.14	73	90
PHX-Dichot_B	PM_f	EC_TOT	20	1.14	1.05	93	98
PHX-Dichot_B	PM_f	OC_TOT	22	1.05	1.03	100	100
PHX-Dichot_B	PM_f	Al_XRF	25	0.99	0.94	100	97
PHX-Dichot_B	PM_f	As_XRF	3	1.44	0.82		
PHX-Dichot_B	PM_f	Ba_XRF	13	0.73	0.66	69	62
PHX-Dichot_B	PM_f	Br_XRF	24	1.09	1.04	98	94
PHX-Dichot_B	PM_f	Ca_XRF	25	0.89	0.91	100	100
PHX-Dichot_B	PM_f	Cl_XRF	25	0.93	0.89	100	97
PHX-Dichot_B	PM_f	Co_XRF	9	1.01	1.03	64	44
PHX-Dichot_B	PM_f	Cr_XRF	11	0.90	0.72	64	50
PHX-Dichot_B	PM_f	Cs_XRF	2	0.84	0.84		
PHX-Dichot_B	PM_f	Cu_XRF	25	0.82	0.82	100	97
PHX-Dichot_B	PM_f	Fe_XRF	25	0.88	0.89	100	100
PHX-Dichot_B	PM_f	K_IC	23	0.99	0.98	96	93
PHX-Dichot_B	PM_f	K_XRF	25	0.91	0.93	100	100
PHX-Dichot_B	PM_f	Mass_Grav	25	0.92	0.95	100	100
PHX-Dichot_B	PM_f	Mg_XRF	22	1.07	0.96	96	88
PHX-Dichot_B	PM_f	Mn_XRF	24	0.86	0.86	98	94
PHX-Dichot_B	PM_f	Na_IC	25	0.91	0.87	100	100
PHX-Dichot_B	PM_f	Na_XRF	25	1.08	0.95	100	100
PHX-Dichot_B	PM_f	NH4_IC	25	0.94	0.97	100	100
PHX-Dichot_B	PM_f	Ni_XRF	9	0.85	0.76	51	38
PHX-Dichot_B	PM_f	NO3_IC	25	0.91	0.89	100	100

Sampler_ID	Size	Species	N > MDL	Avg (Dichot/ FRM)	Med (Dichot/ FRM)	% > MDL (FRM)	% > MDL (Dichot)
PHX-Dichot_B	PM_f	Pb_XRF	12	1.00	0.94	51	56
PHX-Dichot_B	PM_f	Rb_XRF	1	1.25	1.25		
PHX-Dichot_B	PM_f	S_XRF	25	0.96	0.95	100	100
PHX-Dichot_B	PM_f	Se_XRF	1	1.09	1.09		
PHX-Dichot_B	PM_f	Si_XRF	25	0.92	0.92	100	100
PHX-Dichot_B	PM_f	SO4_IC	25	0.95	0.97	100	100
PHX-Dichot_B	PM_f	Sr_XRF	9	1.00	1.06	53	47
PHX-Dichot_B	PM_f	Ti_XRF	24	0.91	0.86	100	94
PHX-Dichot_B	PM_f	Zn_XRF	25	1.03	0.97	100	100
STL-Dichot_A	PM_c	EC_TOT	10	0.91	0.56	92	88
STL-Dichot_A	PM_c	OC_TOT	11	1.08	1.04	92	100
STL-Dichot_A	PM_c	Al_XRF	18	0.99	0.98	100	97
STL-Dichot_A	PM_c	Ba_XRF	16	0.85	0.76	97	90
STL-Dichot_A	PM_c	Br_XRF	5	0.77	0.86	42	39
STL-Dichot_A	PM_c	Ca_XRF	18	0.97	0.96	100	100
STL-Dichot_A	PM_c	Cl_XRF	18	1.04	1.03	100	100
STL-Dichot_A	PM_c	Co_XRF	10	0.97	0.99	66	65
STL-Dichot_A	PM_c	Cr_XRF	9	1.38	1.14	66	61
STL-Dichot_A	PM_c	Cu_XRF	18	1.05	0.99	100	100
STL-Dichot_A	PM_c	Fe_XRF	18	0.94	0.90	100	100
STL-Dichot_A	PM_c	K_IC	18	1.46	1.15	100	92
STL-Dichot_A	PM_c	K_XRF	18	0.90	0.88	100	100
STL-Dichot_A	PM_c	Mass_Grav	18	0.90	0.93	100	100
STL-Dichot_A	PM_c	Mg_XRF	16	1.04	0.97	95	97
STL-Dichot_A	PM_c	Mn_XRF	18	0.96	0.91	100	97
STL-Dichot_A	PM_c	Na_IC	17	0.99	0.94	92	97
STL-Dichot_A	PM_c	Na_XRF	16	0.94	0.88	97	94
STL-Dichot_A	PM_c	NH4_IC	2	0.16	0.16	26	61
STL-Dichot_A	PM_c	Ni_XRF	1	0.95	0.95	37	
STL-Dichot_A	PM_c	NO3_IC	18	0.82	0.86	100	100
STL-Dichot_A	PM_c	P_XRF	14	0.86	0.91	95	71
STL-Dichot_A	PM_c	Pb_XRF	6	1.23	0.93	63	48
STL-Dichot_A	PM_c	S_XRF	15	1.12	0.89	82	100
STL-Dichot_A	PM_c	Si_XRF	18	0.96	0.96	100	100
STL-Dichot_A	PM_c	SO4_IC	18	0.77	0.74	100	100

Sampler_ID	Size	Species	N > MDL	Avg (Dichot/ FRM)	Med (Dichot/ FRM)	% > MDL (FRM)	% > MDL (Dichot)
STL-Dichot_A	PM_c	Sr_XRF	13	1.01	0.87	87	68
STL-Dichot_A	PM_c	Ti_XRF	17	0.95	0.93	100	90
STL-Dichot_A	PM_c	V_XRF	2	0.78	0.79		
STL-Dichot_A	PM_c	Zn_XRF	18	1.01	0.99	100	100
STL-Dichot_A	PM_c	Zr_XRF	2	1.00	1.01		
STL-Dichot_A	PM_f	Na_IC	2	1.15	1.16		
STL-Dichot_A	PM_f	NH4_IC	14	1.05	0.96	85	83
STL-Dichot_A	PM_f	NO3_IC	19	1.06	1.02	100	100
STL-Dichot_A	PM_f	SO4_IC	18	1.96	1.36	88	100
STL-Dichot_A	PM_f	EC_TOT	16	1.17	1.16	100	100
STL-Dichot_A	PM_f	OC_TOT	16	1.11	1.11	100	100
STL-Dichot_A	PM_f	Al_XRF	14	1.15	1.12	95	81
STL-Dichot_A	PM_f	Ba_XRF	5	1.05	1.06	42	
STL-Dichot_A	PM_f	Br_XRF	18	0.98	1.01	100	97
STL-Dichot_A	PM_f	Ca_XRF	19	1.07	0.99	100	100
STL-Dichot_A	PM_f	Cl_XRF	18	1.29	1.02	98	100
STL-Dichot_A	PM_f	Co_XRF	1	0.89	0.89		
STL-Dichot_A	PM_f	Cr_XRF	3	1.05	1.20	30	29
STL-Dichot_A	PM_f	Cu_XRF	15	1.16	1.21	95	87
STL-Dichot_A	PM_f	Fe_XRF	19	1.05	1.02	100	100
STL-Dichot_A	PM_f	K_IC	19	1.04	1.01	98	100
STL-Dichot_A	PM_f	K_XRF	19	1.00	1.02	100	100
STL-Dichot_A	PM_f	Mass_Grav	19	1.01	1.00	100	100
STL-Dichot_A	PM_f	Mg_XRF	7	1.38	1.02	65	55
STL-Dichot_A	PM_f	Mn_XRF	15	1.04	1.01	98	84
STL-Dichot_A	PM_f	Na_IC	18	1.01	0.99	95	92
STL-Dichot_A	PM_f	Na_XRF	19	0.88	0.83	100	97
STL-Dichot_A	PM_f	NH4_IC	19	0.98	0.98	100	100
STL-Dichot_A	PM_f	Ni_XRF	1	1.98	1.98		
STL-Dichot_A	PM_f	NO3_IC	19	1.01	1.00	100	100
STL-Dichot_A	PM_f	Pb_XRF	13	1.06	1.12	88	71
STL-Dichot_A	PM_f	S_XRF	19	0.99	1.01	100	100
STL-Dichot_A	PM_f	Se_XRF	2	1.21	1.21		
STL-Dichot_A	PM_f	Si_XRF	19	1.02	0.98	100	100
STL-Dichot_A	PM_f	SO4_IC	19	1.01	1.00	100	100

Sampler_ID	Size	Species	N > MDL	Avg (Dichot/ FRM)	Med (Dichot/ FRM)	% > MDL (FRM)	% > MDL (Dichot)
STL-Dichot_A	PM_f	Ti_XRF	3	0.80	0.82	48	39
STL-Dichot_A	PM_f	V_XRF	5	0.98	0.93		29
STL-Dichot_A	PM_f	Zn_XRF	19	0.99	0.94	100	100
STL-Dichot_B	PM_c	EC_TOT	10	0.99	0.92	92	71
STL-Dichot_B	PM_c	OC_TOT	15	1.11	1.10	92	98
STL-Dichot_B	PM_c	Al_XRF	21	0.86	0.84	100	100
STL-Dichot_B	PM_c	Ba_XRF	19	0.84	0.71	97	93
STL-Dichot_B	PM_c	Br_XRF	4	1.49	1.15	42	36
STL-Dichot_B	PM_c	Ca_XRF	21	0.88	0.90	100	100
STL-Dichot_B	PM_c	Ce_XRF	2	0.69	0.69		
STL-Dichot_B	PM_c	Cl_XRF	21	1.10	0.90	100	100
STL-Dichot_B	PM_c	Co_XRF	7	1.45	1.77	66	61
STL-Dichot_B	PM_c	Cr_XRF	8	1.17	1.12	66	68
STL-Dichot_B	PM_c	Cu_XRF	21	0.81	0.86	100	100
STL-Dichot_B	PM_c	Fe_XRF	21	0.85	0.82	100	100
STL-Dichot_B	PM_c	K_IC	20	1.08	0.93	100	90
STL-Dichot_B	PM_c	K_XRF	21	0.84	0.83	100	100
STL-Dichot_B	PM_c	Mass_Grav	21	0.80	0.79	100	100
STL-Dichot_B	PM_c	Mg_XRF	21	0.93	0.85	95	100
STL-Dichot_B	PM_c	Mn_XRF	21	0.85	0.83	100	100
STL-Dichot_B	PM_c	Na_IC	20	0.90	0.86	92	97
STL-Dichot_B	PM_c	Na_XRF	16	0.76	0.75	97	82
STL-Dichot_B	PM_c	NH4_IC	3	1.33	0.97	26	45
STL-Dichot_B	PM_c	Ni_XRF	3	1.10	1.10	37	
STL-Dichot_B	PM_c	NO3_IC	21	0.69	0.80	100	100
STL-Dichot_B	PM_c	P_XRF	18	0.77	0.80	95	82
STL-Dichot_B	PM_c	Pb_XRF	11	0.96	0.86	63	54
STL-Dichot_B	PM_c	S_XRF	17	1.75	1.17	82	100
STL-Dichot_B	PM_c	Si_XRF	21	0.86	0.85	100	100
STL-Dichot_B	PM_c	SO4_IC	21	0.73	0.69	100	100
STL-Dichot_B	PM_c	Sr_XRF	13	0.79	0.74	87	64
STL-Dichot_B	PM_c	Ti_XRF	21	0.85	0.82	100	100
STL-Dichot_B	PM_c	V_XRF	2	0.57	0.57		
STL-Dichot_B	PM_c	Zn_XRF	21	0.97	0.90	100	100
STL-Dichot_B	PM_f	Na_IC	2	1.06	1.07		

Sampler_ID	Size	Species	N > MDL	Avg (Dichot/ FRM)	Med (Dichot/ FRM)	% > MDL (FRM)	% > MDL (Dichot)
STL-Dichot_B	PM_f	NH4_IC	18	1.00	0.97	85	87
STL-Dichot_B	PM_f	NO3_IC	21	1.05	1.02	100	100
STL-Dichot_B	PM_f	SO4_IC	18	2.33	1.79	88	97
STL-Dichot_B	PM_f	EC_TOT	19	0.96	0.98	100	98
STL-Dichot_B	PM_f	OC_TOT	19	0.98	1.05	100	100
STL-Dichot_B	PM_f	Al_XRF	17	1.34	1.11	95	82
STL-Dichot_B	PM_f	As_XRF	5	1.37	1.53	30	29
STL-Dichot_B	PM_f	Ba_XRF	8	1.40	1.46	42	39
STL-Dichot_B	PM_f	Br_XRF	21	0.93	0.94	100	100
STL-Dichot_B	PM_f	Ca_XRF	21	1.17	1.17	100	100
STL-Dichot_B	PM_f	Cl_XRF	20	1.04	1.03	98	96
STL-Dichot_B	PM_f	Co_XRF	3	1.41	1.32		
STL-Dichot_B	PM_f	Cr_XRF	3	1.04	0.86	30	39
STL-Dichot_B	PM_f	Cu_XRF	20	1.26	1.02	95	96
STL-Dichot_B	PM_f	Fe_XRF	21	1.08	1.09	100	100
STL-Dichot_B	PM_f	K_IC	20	1.02	1.03	98	97
STL-Dichot_B	PM_f	K_XRF	21	0.99	0.99	100	100
STL-Dichot_B	PM_f	Mass_Grav	21	1.01	1.01	100	100
STL-Dichot_B	PM_f	Mg_XRF	13	1.02	0.90	65	64
STL-Dichot_B	PM_f	Mn_XRF	18	1.17	1.15	98	86
STL-Dichot_B	PM_f	Na_IC	20	1.06	1.02	95	93
STL-Dichot_B	PM_f	Na_XRF	21	0.99	0.94	100	100
STL-Dichot_B	PM_f	NH4_IC	21	0.96	0.96	100	100
STL-Dichot_B	PM_f	NO3_IC	21	1.18	1.08	100	100
STL-Dichot_B	PM_f	Pb_XRF	15	0.96	0.83	88	82
STL-Dichot_B	PM_f	S_XRF	21	0.97	0.96	100	100
STL-Dichot_B	PM_f	Se_XRF	1	0.91	0.91		
STL-Dichot_B	PM_f	Si_XRF	21	1.14	1.12	100	100
STL-Dichot_B	PM_f	SO4_IC	21	0.99	0.99	100	100
STL-Dichot_B	PM_f	Ti_XRF	7	0.94	0.90	48	50
STL-Dichot_B	PM_f	V_XRF	3	1.07	0.81		
STL-Dichot_B	PM_f	Zn_XRF	21	1.06	1.00	100	100

Appendix D: Quartz Fiber Filter Carbon Blanks

Seven sets of trip blanks and field blanks (collected in May, July, September, and November 2010, and January, April, and May 2011) were analyzed by thermal optical reflectance (TOR) using the IMPROVE_A thermal-optical analysis (TOA) method. Each set included two to four trip blank filters and four to twelve field blank filters per site. OC loadings on these trip blanks and field blanks filters provide a context for characterizing and interpreting OC on the front and backup filters. The OC minimum detection limit (MDL) for the IMPROVE_A method is 2.03 µg/filter. As summarized in this section, the trip blanks and field blanks data can be used to estimate the lower quantifiable limits (LQL) for particulate matter OC. LQL is a metric that complements the MDL estimate and aids in data interpretation.

Figure D-1 shows the mean and standard deviation of OC mass loadings for each trip blank and field blank collection event at each site. For the trip blanks (Figure D-1a), the OC mass loadings were highest for the first collection event (May 2010) and relatively low and consistent during the remainder of the study. Exceptions were the April and May 2011 samples for St. Louis, for which the trip blank mass loadings exhibited relatively high mean values. At St. Louis a single sample (mass loading 34 µg/filter) was responsible for the high mean value in April 2011; by excluding this sample, the April 2011 mean loading decreased from 10 µg/filter to 2 µg/filter. In contrast, the May 2011 mean loading of 10 µg/filter at St. Louis included two high samples (16 and 12 µg/filter), and two low samples (6 and 5 µg/filter).

The field blanks (Figure D-1b) initially decreased with each event, exhibited nearly constant values from November 2010 to April 2011, and increased in May 2011.

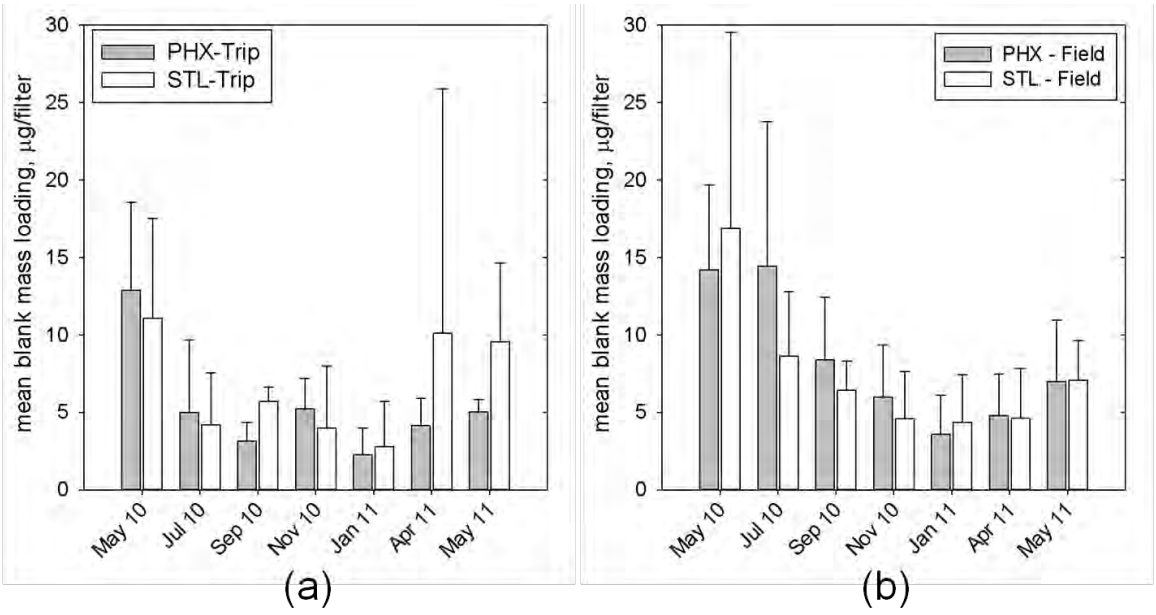

Figure D-1. Mean and standard deviation of OC (a) trip blanks data and (b) field blanks data. Data are stratified by site and by the seven collection events between May 2010 and May 2011.

Statistical analyses were performed separately for the trip blanks and field blanks data sets. In each case, unbalanced two-way analysis of variance (ANOVA) was performed on log-transformed OC with site and date as factors. All hypothesis testing was conducted for the 95% confidence level. For the trip blank data, site had an insignificant effect ($p = 0.62$), whereas date had a significant effect ($p < 0.01$) on the OC mass loadings. Trip blank mass loading values measured in May 2010, the first month of the study, were relatively high compared to subsequent months. ANOVA with the May 2010 data excluded resulted in insignificant effects for both the site and date ($p = 0.51$ and $p = 0.18$, respectively). Pooling all the trip blanks data (but excluding the May 2010 samples) yields mean and median OC mass loadings of 5.4 ± 5.7 µg/filter and 4.2 µg/filter, respectively ($N = 44$).

The same statistical analyses were performed for the seven sets of field blanks, which were collected at the same times as the trip blanks. Each set included four to twelve filters per site, with the maximum case being front and back filters in the $PM_{2.5}$ FRM, PM_{10} FRM, and both channels of both dichot samplers. While in principle the sampler type and filter position (front versus back) could be treated as additional factors, their effects were deemed insignificant, and samples pooled across these factors were treated as pseudo-replicates. Site had an insignificant effect ($p = 0.28$), whereas date had a significant effect ($p < 0.01$). After removing the May 2010 data, site still had an insignificant effect ($p = 0.21$) and date a significant effect ($p < 0.01$) on the OC mass loadings. Pooling all the field blanks data (but excluding the May 2010 samples) yields mean and median OC mass loadings of 6.6 ± 5.0 and 5.2 µg/filter, respectively ($N = 130$).

The trip and field blanks ANOVA analyses demonstrated statistically insignificant dependencies on site. Therefore, the Phoenix and St. Louis data were pooled. **Figure D-2** shows the mean and standard deviation of OC mass loadings for each trip and field blanks collection event. ANOVA on the site pooled data yielded significant effects ($p < 0.01$) for both date and blanks type (trip versus field). This result was obtained both including and excluding the May 2010 samples.

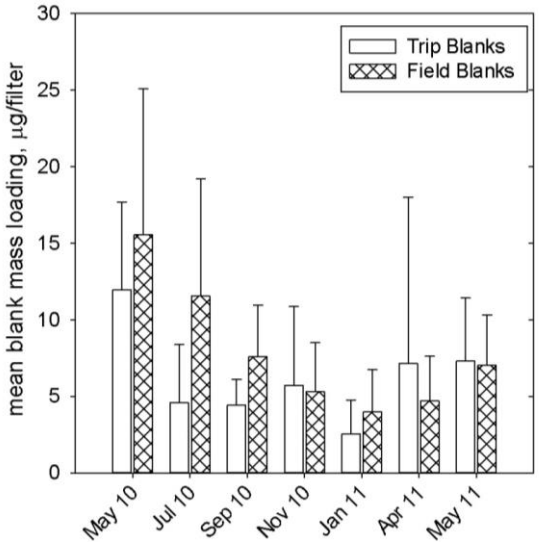

Figure D-2. Mean and standard deviation of OC trip and field blanks data stratified by date and combined across the Phoenix and St. Louis sites.

In summary, one year of data is too short a time series to conclusively interpret the trip and field blank trends. ANOVA analysis suggests that date has an insignificant effect on the values. However, the high trip blank values observed in the first month of the study (May 2010) may be the driver for the high field blank values observed during that collection event. For subsequent months, it is not clear whether the field blanks exhibit an intrinsic seasonal behavior or are significantly influenced by the trip blanks. Large differences between trip and field blank values in July 2010 suggest some decoupling, but the higher field blank values towards the end of the study coincided with higher trip blank values.

The possibility of temporal behavior in blank loadings confounds using the 95th percentile OC mass loading as a robust estimate of the LQL, but it can be used as a conservative estimate. The 95th percentile trip blank and field blanks mass loadings are each 19 μg/filter for all samples and 15 μg/filter excluding the May 2010 samples.

Appendix E: Nitrate Correlations with Other Species

Nitrate (NO_3) can be difficult to accurately measure, since much of it can be volatilized off of the Teflon filter. Lee et al., (2008) found that it was not uncommon at rural locations to find a significant fraction of particulate NO_3 present in forms other than ammonium nitrate. In order to explore whether nitrate was associated with species other than ammonium, correlations between PMf and PMc nitrate and the other measured species were evaluated.

Tables E-1 and E-2 display the correlation between NO_3 (Table E-1 for Teflon filter NO_3 and Table E-2 for Teflon/nylon filter NO_3) and a subset of species that are primarily above minimum detection limit (MDL) for the primary dichotomous sampler (Dichot A). No consistently high correlations were observed between NO_3 and the other parameters at either St. Louis or Phoenix, except for ammonium in the PMf fraction. Moderate correlations (around 0.6) were found for some elements in St. Louis for the PMc fraction. Visual inspection of scatter plot matrices showed that there were no outliers biasing the correlation coefficients low, and confirmed the correlation coefficients reported in Tables E-1 and E-2.

Table E-1. Correlation between Teflon filter NO_3 and a subset of species that are primarily above MDL for the primary dichotomous sampler (A) in PHX and STL. Correlations are colored from high (red) to low (green).

Correlation with Species	PHX NO_3 PM_c	PHX NO_3 PM_f	STL NO_3 PM_c	STL NO_3 PM_f
SO_4	0.50	-0.15	0.56	0.13
K_IC	0.25	0.27	0.32	0.21
Na_IC	0.29	-0.12	0.34	-0.07
NH_4	0.33	0.84	0.22	0.80
Al	0.50	-0.15	0.59	-0.24
Ba	0.40	0.37	0.46	0.15
Br	0.22	0.35	0.11	0.31
Ca	0.44	-0.11	0.56	-0.12
Cl	0.15	0.21	0.13	0.49
Co	0.18	-0.09	0.52	-0.02
Cr	0.38	0.05	0.15	0.10
Cu	-0.11	0.54	0.25	0.11
Fe	0.33	0.02	0.54	0.05
K	0.47	0.23	0.60	-0.19
Mg	0.53	-0.10	0.65	-0.36
Mn	0.41	0.10	0.47	0.27
Na	0.29	-0.12	0.38	-0.13
Ni	0.21	-0.01	0.15	-0.26
P	0.42	-0.07	0.40	-0.11
Pb	-0.02	0.12	0.12	-0.04
Rb	0.31	-0.02	0.15	-0.18
S	0.54	-0.13	0.58	0.12
Si	0.48	-0.15	0.66	-0.33
Sr	0.24	0.47	0.56	0.08
Ti	0.37	-0.06	0.60	-0.23
Zn	-0.14	0.02	0.08	-0.05
Gravimetric Mass	0.36	0.69	0.64	0.60

Table E-2. Correlation between Teflon/nylon filter NO_3 and a subset of species that are primarily above MDL for the primary dichotomous sampler (A) in PHX and STL. Correlations are colored from high (red) to low (green).

Correlation with Species	PHX NO_3 PM_c	PHX NO_3 PM_f	STL NO_3 PM_c	STL NO_3 PM_f
SO_4	0.37	-0.24	0.55	0.15
K_IC	0.14	0.22	0.31	0.25
Na_IC	0.10	-0.26	0.30	-0.07
NH_4	0.25	0.91	0.22	0.82
Al	0.37	-0.18	0.60	-0.25
Ba	0.36	0.35	0.49	0.17
Br	0.13	0.34	0.13	0.41
Ca	0.36	-0.14	0.57	-0.10
Cl	-0.01	0.07	0.09	0.51
Co	0.10	-0.07	0.53	0.01
Cr	0.32	0.10	0.17	0.10
Cu	-0.12	0.47	0.28	0.13
Fe	0.26	0.05	0.56	0.04
K	0.35	0.18	0.60	-0.14
Mg	0.40	-0.21	0.65	-0.35
Mn	0.34	0.18	0.48	0.26
Na	0.14	-0.26	0.34	-0.09
Ni	0.15	-0.03	0.16	-0.26
P	0.31	-0.06	0.41	-0.12
Pb	-0.06	0.10	0.11	0.03
Rb	0.26	-0.06	0.14	-0.16
S	0.43	-0.22	0.63	0.12
Si	0.36	-0.15	0.67	-0.34
Sr	0.16	0.37	0.57	0.08
Ti	0.30	-0.07	0.61	-0.26
Zn	-0.14	-0.01	0.08	0.03
Gravimetric Mass	0.29	0.63	0.64	0.62

United States
Environmental Protection
Agency

Office of Air Quality Planning and Standards
Air Quality Assessment Division
Research Triangle Park, NC

Publication No. EPA-454/R-15-001
February 2015